وزارة التعليم العالي والبحث العلمي

Ministry of Higher Education and Scientific Research

HIGHER SCHOOL OF INDUSTRIAL TECHNOLOGIES

المدرسة العليا للتكنولوجيات الصناعية – عنابة –

Year / 2020

THESIS FOR THE DEGREE OF ELECTRICAL ENGINEER

Design of advanced MPPT techniques for photovoltaic power system under dynamic weather conditions

By

CHABANA Hadjer

MERAH Soumia

Submitted to the Department of Engineering

In partial fulfillment of the requirements for

the Degree of Electrical Engineer

option Electricity Generation & Renewable Energy

At the

Higher School of Industrial Technologies – Annaba, Algeria

September 2020

Advisor:		
AFGHOUL Hamza	Assistant Professor	ESTI Annaba
	Committee Member:	
Président :		
HOUABES Mourad	Pr.	ESTI Annaba
Examiners:		
	MCB	ESTI Annaba
	MCB	ESTI Annaba

وزارة التعليم العالي والبحث العلمي
Ministère de l'Enseignement Supérieur et de la Recherche Scientifique

ÉCOLE SUPERIEURE DE TECHNOLOGIES INDUSTRIELLES - ANNABA -

المدرسة العليا للتكنولوجيات الصناعية – عنابة –

Année / 2020

DEPARTEMENT DU SECOND CYCLE

FILIÈRE

ELECTROTECHNIQUE

MEMOIRE

Présenté en vue de l'obtention du diplôme d'Ingénieur d'État

Conception de techniques MPPT avancées pour système d'alimentation photovoltaïque dans des conditions météorologiques dynamiques

Spécialité

Production Electrique et Energie Renouvelables

Par

CHABANA Hadjer

MERAH Soumia

Sous la direction de :	Grade	Établissement d'affiliation
AFGHOUL Hamza	Maître assistant	ESTI Annaba
	Devant le jury	
Président :		
HOUABES Mourad	Pr.	ESTI Annaba
Examinateurs :		
	MCB	ESTI Annaba
	MCB	ESTI Annaba

Dedication

To our beloved parents

Who always teach us to trust in Allah, and believe in hard work

Thank you for your patient, encouragement and sacrifices

To our wonderful families

Who believed in us

Thank you for your support and your endless love

To our dearest friends

Thank you for being there whenever we need a support

Acknowledgements

First and foremost, all praise and thanks be to almighty ALLAH for giving us health, wisdom, and patient, without him nothing of our work would have been done.

We would like to express our sincere gratitude to our supervisor Dr. Afghoul Hamza for his, suggestions, valuable directions, and constructive criticism throughout our research study. We are not only learned the technical knowledge but also acquired the attitude and spirit of research.

We would also like to thank my English teacher Boumaaza Hadjer, for her advices and for helping us to correct the grammatical mistakes.

Our deepest gratitude goes out to our beloved parents and families who have always supported, encouraged, and believed in us. We are greatly indebted to their understanding, patient and love through thewhole period of our study.

Abstract: Recently, the Photovoltaic (PV) system becomes the most promising energy resource among the different renewable energy resources. However, there are some limitations that prevent the PV generator to operate at the Maximum Power Point (MPP) such as its nonlinear characteristics and the dynamic weather conditions. In order to drive the operating point to the MPP, many Maximum Power Point Techniques (MPPT) have been proposed to control the duty cycle of the DC-DC converter which interfaces the load and the PV generator. This thesis investigates the different MPPT controllers. The conventional P&O and InC algorithms are discussed due to their simplicity and low implementation cost, then a variable step P&O method is introduced for better tracking performance. Furthermore, Fuzzy Logic Controller and Artificial Neural Network which are basically Artificial Intelligence techniques are discussed to improve the performance of the conventional MPPT algorithms by offering high accuracy, stability, and flexibility. In order to introduce more efficiency and accuracy to the previous MPPT controllers, hybrid MPPT controllers including Artificial Neuro-Fuzzy Inference System and Adaptive Fuzzy P&O techniques are presented. The PV generator is simulated by using MATLAB/Simulink software to extract I-V and P-V curve characteristics. Moreover, the previous MPPT controllers are implemented using the same software and tested under the same weather conditions to evaluate and compare their performance with each other. The simulation results show that variable step P&O technique eliminates the drawbacks in the conventional P&O and InC techniques. The results confirm that FLC and ANN techniques provide fast and accurate response compared to the conventional techniques. Furthermore, ANFIS technique offers the highest tracking performance in comparison with the AI-based MPPT controllers and the conventional techniques.

Résumé: Récemment, le système photovoltaïque (PV) est devenu la ressource énergétique la plus prometteuse parmi les différentes sources d'énergie renouvelable. Cependant, certaines limitations empêchent le générateur PV de fonctionner au point de puissance maximale (MPP), telles que ses caractéristiques non linéaires et les conditions météorologiques dynamiques. Afin d'attirer le point de fonctionnement vers le MPP, de nombreuses techniques de point de puissance maximale (MPPT) ont été proposées pour contrôler le rapport cyclique du convertisseur DC-DC qui relie la charge et le générateur PV. Cette thèse étudie les différents contrôleurs MPPT. Les algorithmes P&O et InC conventionnels sont discutés en raison de leur simplicité et de leur faible coût de mise en œuvre, puis une méthode P&O à pas variables est introduite pour de meilleures performances de suivi. En outre, le contrôleur de la logique floue et les réseaux de neurone artificiel, qui sont essentiellement des techniques d'intelligence artificielle. Ces derniers sont discutés pour améliorer les performances des algorithmes MPPT conventionnels en offrant une précision, stabilité et une flexibilité élevées. Afin d'introduire plus d'efficacité et de précision aux contrôleurs MPPT précédents, des contrôleurs MPPT hybrides, y compris le système d'inférence neuro-floue artificielle et la technique adaptative Fuzzy P&O sont présentés. Le générateur PV est simulé à l'aide du logiciel MATLAB / Simulink pour extraire les caractéristiques des courbes I-V et P-V. De plus, les contrôleurs MPPT précédents sont implémentés à l'aide du même logiciel et testés dans les mêmes conditions météorologiques pour évaluer et comparer leurs performances les uns avec les autres. Les résultats de la simulation montrent que la technique P&O àpas variable élimine les inconvénients des techniques P&O et InC conventionnelles. Les résultats confirment que les techniques FLC et ANN fournissent une réponse rapide et précise par rapport aux techniques conventionnelles. En outre, la technique ANFIS offre les performances de suivi les plus élevées par rapport aux contrôleurs MPPT basés sur l'IA et aux techniques conventionnelles.

ملخص: في الآونة الأخيرة، أصبح نظام الطاقة الكهروضوئية أكثر موارد الطاقة الواعدة بين موارد الطاقة المتجددة المختلفة. ومع ذلك، هناك بعض القيود التي تمنع المولد الكهروضوئي من العمل عند أقصى نقطة للطاقة مثل خصائصه غير الخطية وظروف الطقس الديناميكية. من أجل دفع نقطة التشغيل إلى نقطة الاستطاعة العظمى، تم اقتراح العديد من تقنيات للتحكم في دورة عمل محول الطاقة الذي يمثل واجهة ربط تتوسط المولد الكهروضوئي والحمل. تتناول هذه الرسالة تقنيات التحكم المختلفة. حيث تتم مناقشة الخوارزميات التقليدية نظرًا لبساطتها وتكلفة تنفيذها المنخفضة، ثم يتم تقديم طريقة P&O ذات الخطوة المتغيرة لتحسين أداء التتبع لدى تقنية P&O. علاوة على ذلك، تتم مناقشة الشبكة العصبية الاصطناعية والمنطق الضبابي التي تعد في الأساس تقنيات ذكاء اصطناعي لتحسين أداء الخوارزميات التقليدية من خلال تقديم دقة عالية واستقرار ومرونة. من أجل إضافة المزيد من الكفاءة والدقة لتقنيات التحكم السابقة، يتم تقديم تقنيات التحكم الهجينة بما في ذلك نظام الاستدلال العصبي الضبابي الاصطناعي وتقنيات Adaptive Fuzzy P&O. يتم محاكاة المولد الكهروضوئي باستخدام برنامج MATLAB / Simulink لاستخراج خصائص منحنى التيار-التوتر والاستطاعة-التوتر. علاوة على ذلك، يتم تنفيذ تقنيات التحكم السابقة باستخدام نفس البرنامج واختبارها في ظل نفس الظروف الجوية لتقييم ومقارنة أدائها مع بعضها البعض. تظهر نتائج المحاكاة أن تقنية الخطوة المتغيرة P&O تزيل سلبيات تقنيات P&O وInC التقليدية. تؤكد النتائج أن تقنيات FLC وANN توفر استجابة سريعة ودقيقة مقارنة بالتقنيات التقليدية. علاوة على ذلك، تقدم تقنية ANFIS أعلى أداء تتبع مقارنة بتقنيات التحكم القائمة على الذكاء الاصطناعي والتقنيات التقليدية.

Table of Contents

List of Figure

List of Tables

List of Acronyms

1M3P	Single Mechanism Three Parameters.
1M4P	Single Mechanism Four Parameters.
1M5P	Single Mechanism FiveParameters.
2M5P	Double Mechanism Five Parameters.
2M6P	Single Mechanism six Parameters.
2M7P	Double Mechanism Seven Parameters.
ANFIS	Adaptive-Neuro Fuzzy Inference system
AI	Artificial Intelligence
ANN	Artificial Neural Network
BP	Back-Propagation
COA	Centroid of Area
COG	CenterOf Gravity
FL	Fuzzy Logic
FLC	Fuzzy Logic Controller
GMPP	Global maximum power point
GPV	Photovoltaic Generator
INC	Incremental Conductance
I-V	Current-Voltage
LSE	Least Square Estimation
MOM	Mean Of Maximum
MPP	Maximum Power Point
MPPT	Maximum Power Point Technique
P&O	Perturb and Observe
PV	Photovoltaic
P-V	Power -Voltage
PWM	Pulse Width Modulation
STC	Standard Test Conditions
TSK	Takagi-Sugeno_Kang
VLSI V	Very-large-scale integration

List of Symbols

α	Diode ideality factor.
μ	Membership function
a_i, b_i, c_i	Parameters set
D	Duty cycle
D_k	Duty cycle of the current iteration.
D_{k-1}	Duty cycle of the previous iteration
Eg	Energy band (eV)
G	Solar irradiance (W/m2).
G_r	Reference irradiance (1000 W/m2).
I_{C1}	Current through the first capacitor
I_{C2}	Current through the second capacitor
I_D	Diode curent
Iph	Photocurrent
I_{PV}	Photovoltaic array output current (A)
Irs	The reverse saturation current
I_s	Shunt resistance
I_{sc}	Short circuit current (A), Short circuit current
K	Boltzmann's constant (1.380653 × 10□23 (J/K))
O^1_i	Membership value for the crisp value
O_{Pj}	The measured output of the outputs
q :	Electron charge (1.06217646 × 10e-19 (C)).
Rs	Series resistance
R_{sh}	Shunt resistance
T	Cell's temperature (K).
t_{Pj}	Desired output of the output neurons.
Tref	Temperature at STC (25°C)
V_D	Diode voltage, : Diode voltage.
V_i	Input voltage of DC-DC converter
V_L	Inductor voltage

V_o	Output voltage of DC-DC converter
V_{oc}	Open circuit voltage (V), Open circuit voltage (V)
V_{PV}	Photovoltaic array output voltage (V)
V_T	Thermal voltage

General Introduction

General Introduction

According to the United Nations, the current world population estimated at around 7.7 billion people, this dramatic growth causes a huge increase in energy demand, which leads to remarkable growth in primary energy consumption especially fossil fuels which accounted for about 84.32 percent of global energy consumption by the end of 2019. This overdependence on fossil fuels is a major reason for concerns about their depletion andtheir environmental impacts such as global warming, climate changes, CO_2 emission, greenhouse gases, and environmental pollution.

Research during the last decades has focused on developing clean and sustainable energy sources such as sun, wind, water, biomass ...etc., due to their provision of abundance, reliable, and safe energy, besides, their capability to manage microgrids, energy storage, and low environmental effect. Among all of these renewable energies, the photovoltaic (PV) system is the most promising energy generator according to its low operational and maintenance costs, free energy source, high availability, moreover, it converts the sunlight directly to electricity without noise or environmental pollution.

Over the years many mathematical models based on Shockley diode equation have been introduced to literature aiming to describe the nonlinear behaviour of the PV cell which represents the basic device of the PV system, these models are distinguished from each other by the degree of complexity and accuracy, starting by the ideal single diode model which is the simplest approach and ending by 2M7P approach which is the most accurate and complicated model.

Since the nonlinear I-V and P-V characteristics of PV generator are depending on solar irradiance and cell temperature, the operating point can be located away from the maximum power point (MPP) especially in the case of direct connection with the load, which affects the efficiency of PV panel and leads to high power losses. In order to overcome this problema DC-DC boost converter is used as an interface device matching between the PV generator and the load, where the duty cycle is controlled by Maximum Power Point Technique (MPPT).

Many MPPT algorithms have been introduced to extract maximum power from the PV generator such as Perturb and Observe (P&O), Incremental Conductance (INC), Fuzzy Logic Controller (FLC), Artificial Neural Network (ANN), Artificial Neuro-

Fuzzy Inference System (ANFIS), these techniques differ in simplicity, accuracy, tracking speed, ease of implementation, steady-state stability, tracking efficiency and cost.

The most widely MPPT controllers used are the conventional MPPT algorithms including Perturb and Observe (P&O) and Incremental Conductance (InC) techniques due to their simplicity, ease of implementation and low cost, however, these on-line techniques exhibit several drawbacks such as the oscillation around the MPP, slow tracking speed and mistracking of the MPP during a rapid change in weather conditions. Moreover, these techniques suffer to offer a trade-off between dynamic response and steady-state stability due to their fixed step size, hence a variable step (P&O) and (InC) algorithms have been proposed to overcome this limitation by offering a fast and stable tracking performance.

Recently, artificial intelligence (AI) is successfully used in several fields due to its ability to make a decision the same way the human reason is performing, besides its ability to deal with nonlinear systems, therefore the AI-based controllers such as Artificial Neural Network (ANN) and Fuzzy Logic Controller (FLC) are developing for MPPT application as a powerful alternative for conventional MPPT methods to eliminate their limitations and enhance the tracking performance. Despite their drawbacks, FLC and ANN track the MPP effectively better than the conventional MPPT controllers by offering flexible, fast, and accurate tracking performance with a stable steady-state even though under challenging weather conditions.

Since advanced and conventional MPPT techniques provide several advantages and disadvantages during the tracking process, hybrid MPPT methods have been proposed to combine the benefits of these individual MPPT methods and to overcome their drawbacks to offer a new MPPT controller with fast and accurate tracking performance under different weather conditions. The adaptive fuzzy-P&O algorithm is a hybrid MPPT method that combines the simplicity and ease of implementation of the P&O technique and the speed and accuracy of FLC under a rapid change in the environmental conditions to offer a fast convergence time without providing oscillation around the MPP. Moreover, the ANFIS technique incorporates the benefits of two AI techniques ANN and FL, this controller predicts the output accurately without the need for neither an accurate mathematical model nor prior knowledge about PV system.

General Introduction

This thesis is organized into five chapters

The first chapter introduces a general review on PV cell and PV generator, then the equivalent circuits and mathematical equations of single and double diode models are presented. Finally, this chapter highlights the effect of the equivalent model parameters and the environmental factors on PV curve characteristics.

In the second chapter, the DC-DC boost converter, its equivalent circuit, and its operating modes are described in detail. Then the conventional P&O and InC techniques are discussed. Finally, the variable step P&O technique is introduced as a solution to overcome the drawbacks exhibited by P&O algorithm.

The third chapter introduces two artificial intelligence techniques fuzzy Logic and Artificial Neural Network and their application for MPPT system.

The fourth chapter investigates other MPPT approaches reported in the literature, Artificial Neuro-Fuzzy Inference System and Adaptive Fuzzy-P&O approaches which are considered as hybrid MPPT controllers.

Finally, the fifth chapter presents the analysis and discussions of the simulation results.

Chapter 01

1 Chapter 01: Photovoltaic System

1.1 Introduction

Solar cell converts directly the sun lights to electricity based on a specific mechanism. Photovoltaic cells are connected to each other in series to generate a certain value of voltage and or in parallel to generate a certain value of current forming a photovoltaic generator.

In order to recognize the photovoltaic cell performances and determine their non-linear I-V characteristics, several models have been introduced to literature. Each one of them has an equivalent circuit model, an equivalent mathematical equation, a specified number of unknown parameters and a certain range of accuracy and complexity.

The different parameters specified in the datasheet of the photovoltaic panel are given under STC (Standard Test Conditions), but it is necessary to determine the behaviour of the PV cell under different weather conditions and understand their impact at the output I-V characteristics of the PV module.

The photovoltaic module could have been performed up to 20 years. During this period, the values of series resistance and shunt resistance can be changed either in a slight or a significant ways. Hence, it is necessary to study the output I-V characteristics in several values of Rs and Rsh in order to recognize how this variation affects the photovoltaic module's performance and leads to a degradation.

1.2 Photovoltaic Cell and Photovoltaic Generator

1.2.1 Photovoltaic Cell

The solar cell is the basic unit of a photovoltaic system, and the responsible element of converting the sunrays into electricity [1, 2, 3, 4]. The PV cell is made from a semiconductor material. As its shown in Figure 1.1, it consists of two stratums; the first one is n-layer charged negatively and the second one is p-layer charged positively. These two layers form the p-n junction area, which acts as a diode when the PV cell is exposed to the sunlight's [1, 2, 5, 6, 7]

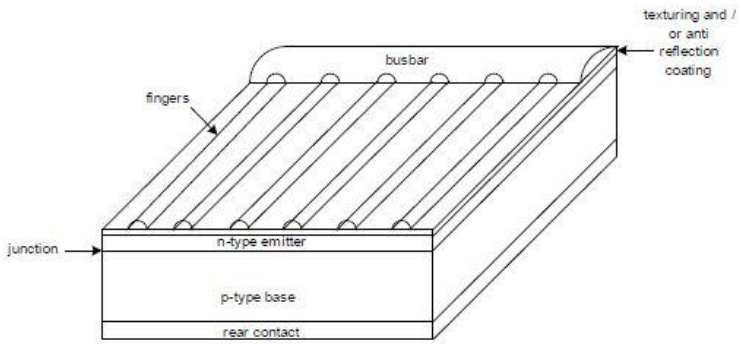

Figure 1.1. Schematic diagram of solar cell physical structure.

1.2.2 Photovoltaic Generator

In order to reach to the required values of current and voltage, photovoltaic cells are connected in parallel series forming a photovoltaic generator. [8, 9, 10].

1.3 Modelling of Photovoltaic Cell

Many electrical circuit models have been introduced to describe the non-linear I-V characteristics of the photovoltaic cell under different weather conditions. Each model has a certain range of simplicity and accuracy. These models can be mathematically presented based on Shockley diode equation [2, 3, 11, 12,].

1.3.1 Single-Diode Model

1.3.1.1 Ideal Single-Diode Model

The basic model of the photovoltaic cell is represented as a current source in parallel to a diode which is also known as 1M3P (Single Mechanism Three Parameters) [12, 13, 14, 15]. This is clearly shown in Figure 1.2.

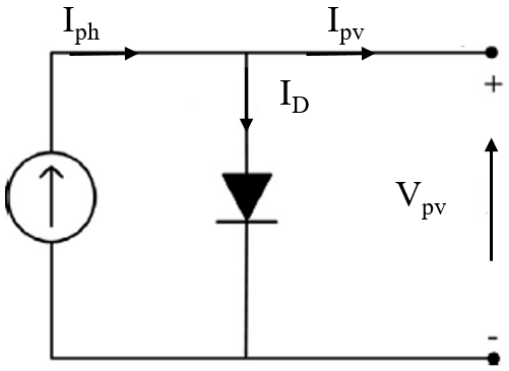

Figure 1.2. Ideal Single-Diode Model

However, this model is not the most accurate approach but it gives the basic nonlinear I-V characteristics of the PV cell. The latter acts as a p-n junction diode in the darknessand can be mathematically represented by Shockley‘s equation (1.1) [3, 11, 12, 14]

$$I_D = I_S\left[\exp\left(\frac{V_D}{\alpha V_T}\right)-1\right] \qquad (1.1)$$

Where V_T is the thermal voltage and its value can be obtained by a function of temperature as displayed in equation (1.2)

$$V_T = \frac{K \times T}{q} \qquad (1.2)$$

Where :

V_D: Diode voltage.

α : Diode ideality factor.

K : Boltzmann’s constant (1.380653×10^{-23} (J/K)).

q : Electron charge ($1.06217646 \times 10^{-19}$ (C)).

T : Cell’s temperature (K).

I_s denotes the saturation current of the diode which varies with the cell’s temperature as described in the equation (1.3).

$$I_S = I_{rs}\left(\frac{T}{T_{ref}}\right)^3 \times \exp\left[\frac{q \times E_g\left(\left(\frac{1}{T_{ref}}\right) - \frac{1}{T}\right)}{\alpha \times K}\right] \quad (1.3)$$

Where:

Eg: Energy band (eV).

Tref: Temperature at STC (25°C).

Moreover,Irs is the reverse saturation current at STC (Standard Test Conditions) (Tref =25°C K and G0 = 1000 W/m2).

$$I_{rs} = \frac{I_{sc}}{\exp\left(\frac{q \times V_{oc}}{\alpha \times K \times T_{ref}}\right) - 1} \quad (1.4)$$

Where:

I_{sc}: Short circuit current (A).

V_{oc}: Open circuit voltage (V).

Hence, the output current is given based on Kirchhoff law, in the following equation:

$$I_{PV} = I_{ph} - I_S\left[\exp\left(\frac{V_D}{\alpha \times V_T}\right) - 1\right] \quad (1.5)$$

Where Iph represents the photocurrent generated at STC. It is directly proportional to the cell's temperature and sun irradiation as shown in the following equation:

$$I_{ph} = \frac{G}{G_r}\left[I_{sc} + K_i\left(T - T_{ref}\right)\right] \quad (1.6)$$

Where :

G : Solar irradiance (W/m^2).

G_r: Reference irradiance(1000 W/m^2).

1.3.1.2 Single-Diode Model with Four Parameters

The single diode model with series resistance shows a high range of accuracy as compared to the 1M3P model. This approach which is also called 1M4P describes the losses related to the contact resistance between the semiconductor and the metal grid, the top and the base metal contacts and the flow of current through the solar emitter.[13, 14, 15, 16]. The equivalent circuit of the model is shown in Figure 1.3.

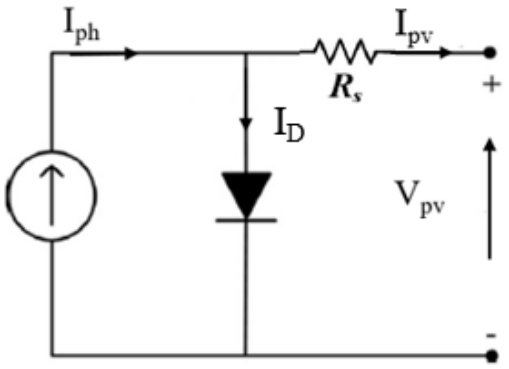

Figure 1.3. Single-diode model with series resistance

Therefore, the relationship between I_{pv} and V_{pv} can be written as

$$I_{PV} = I_{ph} - I_s \left[\exp\left(\frac{V_{PV} + I_{PV} R_s}{\alpha V_T} \right) - 1 \right] \qquad (1.7)$$

I_{PV}: Photovoltaic array output current (A)

V_{PV} : Photovoltaic array output voltage (V)

1.3.1.3 Single-Diode Model with five parameters

The 1M4P approach proved its simplicity and efficiency. However, it is still not realistic enough especially in serious temperature variation. Therefore, more accuracy can be introduced to this model by adding a shunt resistance which is due to the leakage current to the ground [12, 13, 14, 15, 16, 17].

The equivalent model of the R_{sh}-model, which is also called 1M5P, can be represented as demonstrated in Figure 1.4.

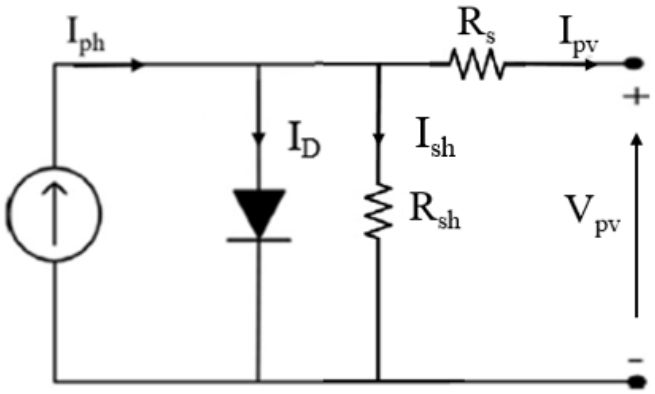

Figure 1.4. Single-diode model with five parameters

The I-V characteristic equation based on this equivalent circuit is

$$I_{PV} = I_{ph} - I_s \left[\exp\left(\frac{V_{PV} + I_{PV} R_s}{\alpha V_T} \right) \right] - \frac{V_{PV} + I_{PV} R_s}{R_{sh}} \qquad (1.8)$$

1.3.2 Double-Diode Model

A more sophisticated model of photovoltaic cell has been proposed in the literature. It includes a second diode in parallel with the first one. This approach shows more accuracy in weather conditions variation mainly at low levels of irradiation and temperature [6, 11, 12].

Two additional unknown parameters are added to the previous model (single-diode model)which are the ideality factor of the second diode α_2 and the reverse saturation current I_{s2}.This latter represents the recombination current loss in the junction region (space-charge region) particularly at low values of voltage. [11, 12, 14, 18, 19]

However, the increase in the number of the unknown parameters makes this model more complex in computation than the single diode model [2, 6].

1.3.2.1 Ideal Double-Diode Model

The 2M5P model is used to extract the fundamental non-linear I-V characteristics as well as the single-diode model [17].

Figure 1.5 displays the model as a current source in parallel with two diodes without taking into consideration the effect of RS and Rsh.

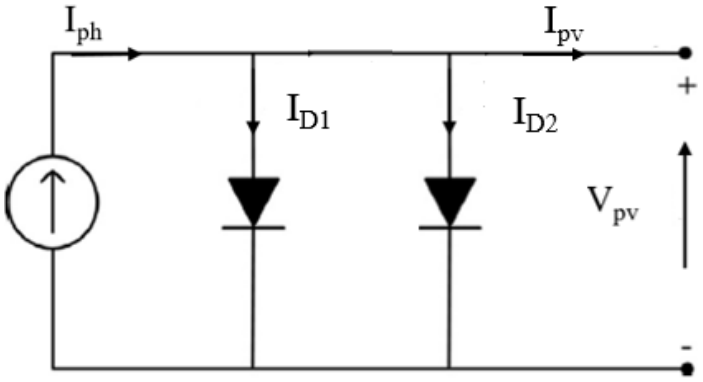

Figure 1.5. Double-diode model with five parameters

The mathematical current-voltage relationship is given in the following expressionV_{D1}

$$I_{PV} = I_{ph} - I_{s_1}\left[\exp\left(\frac{V_{D_1}}{\alpha_1 V_T}\right)-1\right] - I_{s_2}\left[\exp\left(\frac{V_{D_2}}{\alpha_2 V_T}\right)-1\right] \qquad (1.9)$$

1.3.2.2 Double-Diode model with six parameters

In the 2M6P approach, a series resistance is introduced to the previous model which increases the number of the unknown parameters to six parameters. Figure 1.6 illustrates the equivalent circuit [6, 11, 20].

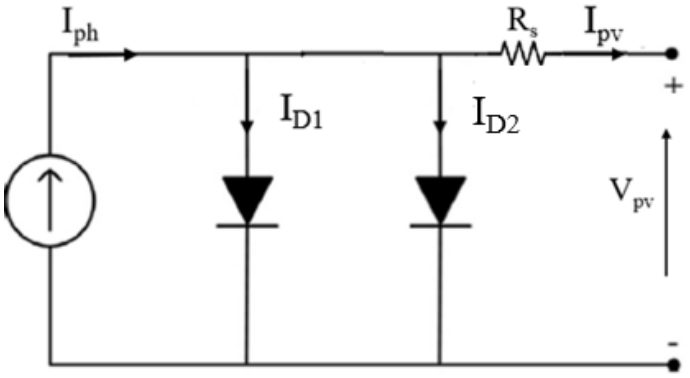

Figure 1.6. Double-diode model with six parameters

The I-V characteristics is mathematically represented as

$$I_{PV} = I_{ph} - I_{s_1}\left[\exp\left(\frac{V_{PV} + I_{PV} \times R_s}{\alpha_1 V_T}\right) - 1\right] - I_{s_2}\left[\exp\left(\frac{V_{PV} + I_{PV} \times R_s}{\alpha_2 V_T}\right) - 1\right] \qquad (1.10)$$

1.3.2.3 Double Diode Model With Seven Paramerters

In this model which called also 2M7P, as revealed in Figure 1.7, an extra resistance is put in parallel with the two diodes. This makes this model more accurate but also more complex [2, 17].

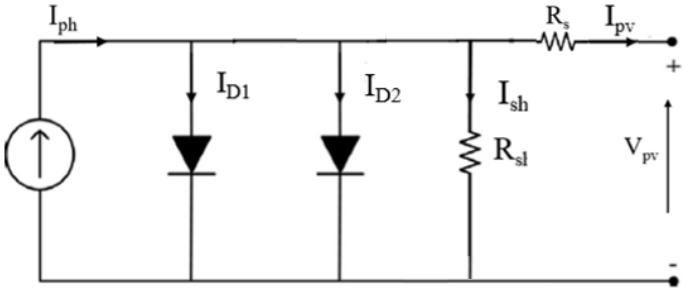

Figure 1.7. Double-diode model with seven parameters

The output current equation for this model can be written as follows :

$$I_{PV} = I_{ph} - I_{s_1}\left[\exp\left(\frac{V_{PV} + I_{PV} \times R_s}{\alpha_1 V_T}\right) - 1\right] - I_{s_2}\left[\exp\left(\frac{V_{PV} + I_{PV} \times R_s}{\alpha_2 V_T}\right) - 1\right] - \frac{V_{PV} + I_{PV} \times R_s}{R_{sh}} \quad (1.11)$$

1.4 Electrical I-V and P-V Curves Characteristics

It is essential to define the non-linear I-V and P-V characteristics in order to recognize the performance of a GPV.

Figure 1.8 shows the I-V characteristic of a typical solar cell, where the current generated is given by the equation (1.8) under constant irradiation and temperature conditions. While Figure 1.9 illustrates its PV curve characteristic.

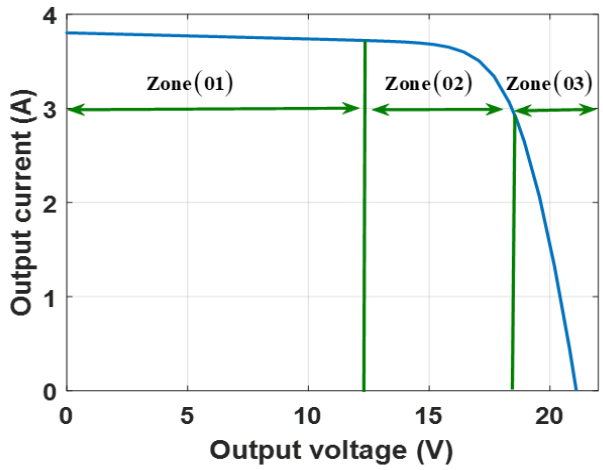

Figure 1.8. The I-V characteristic of a typical solar cell.

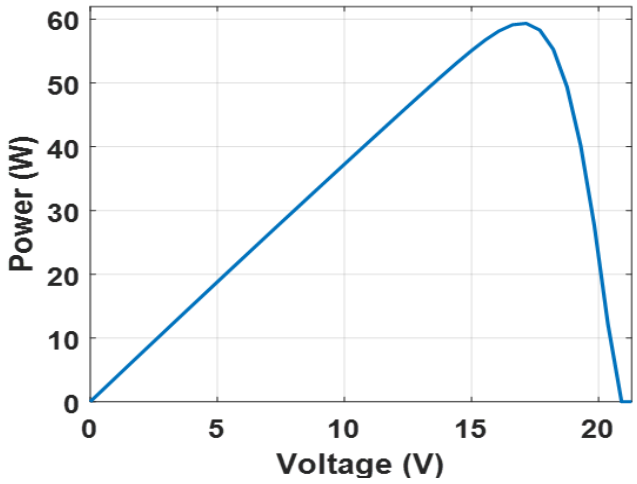

9

Figure 1.9. The P-V characteristic of a typical solar cell

The standard irradiation adopted to measure the response of photovoltaic modules is a radiant intensity of 1000 W/m2 and a temperature of 25°C.The operation of the module is essentially characterized by three zones.

Zone (1): the cell behaves like a current generator (the current is practically constant with a value close to Isc).

Zone (2): in this area, the operation of the cell is characterized by maximum power

Zone (3): the cell behaves like a voltage generator (despite the variation in the value of output current, the output voltage remains stable with a value close to Voc).

1.5 Effects of Equivalent Model Parameters on PV Curve Characteristics

1.5.1 Effects of Rs on PV Curve Characteristics

The series resistance Rs represents the internal losses due to current flow. The effect of varying $R_s$on the I-V and P-V curves characteristics is displayed in Figures 1.10 and Figure 1.11. We notice that the increase in the $R_s$causes a decrease in the curve when the cell behaves like a voltage generator against the short circuit current I_{sc} and the open circuit voltage V_{oc}remains stable. The influence of the series resistance also leads to the decrease in the slope of the power curve. [11,21].

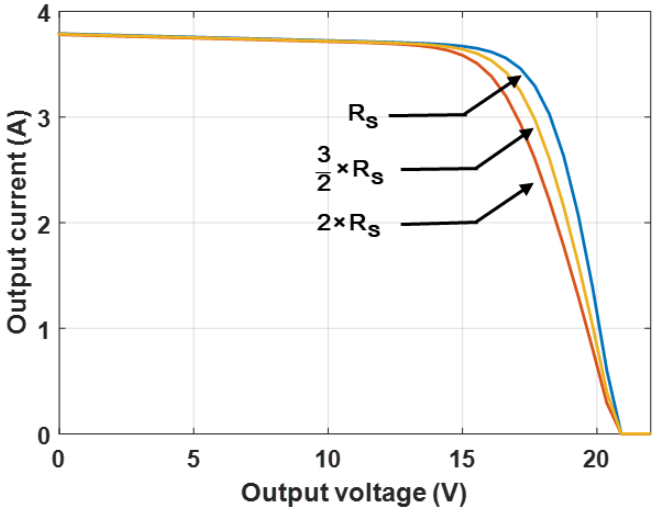

Figure 1.10. Effect of an increase in Rs on the I–V characteristics

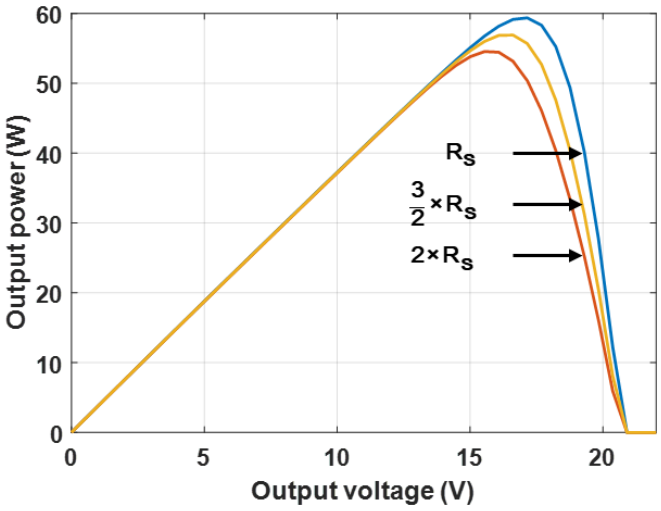

Figure 1.11. Effect of an increase in Rs on the P–V characteristics

1.5.2 Effects of R_{sh}on PV Curve Characteristics

The shunt resistance characterizes the leakage currents due to the solar cell p-n junction or on the cell edges. The effect of varying Rsh on the I-V and P-V curves characteristics are shown in Figure 1.12 and Figure 1.13.The result reveals a significant change in the PV curve when the change is considerable in Rsh [11, 22].

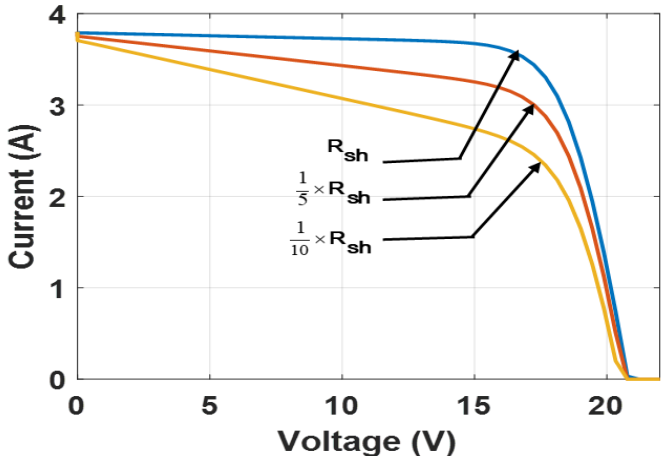

Figure 1.12. Effect of a decrease in Rsh on the I–V characteristics

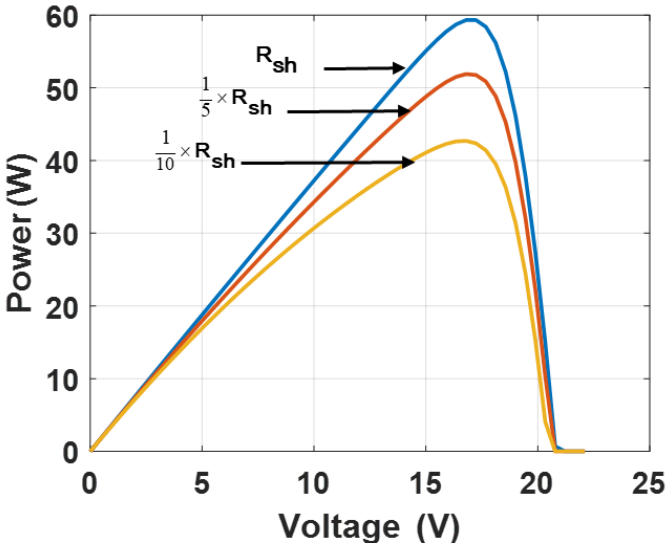

Figure 1.13. Effect of a decrease in Rsh on the P–V characteristics

1.5.3 Effects of the Quality Factor of Diode on PV Curve Characteristics

The diode ideality factor (n) is an adjustment constant factor used to correct for discrepancies between the practical behaviours of diode with the theoretical ideal behaviour. The typical I-V and P-V curves, for various diode ideality factors are illustrated in Figures 1.14 and 1.15 It is clear that there are a proportional relation between the factor n and the maximum voltage. This therefore, leads to change the Voc. [21, 23]

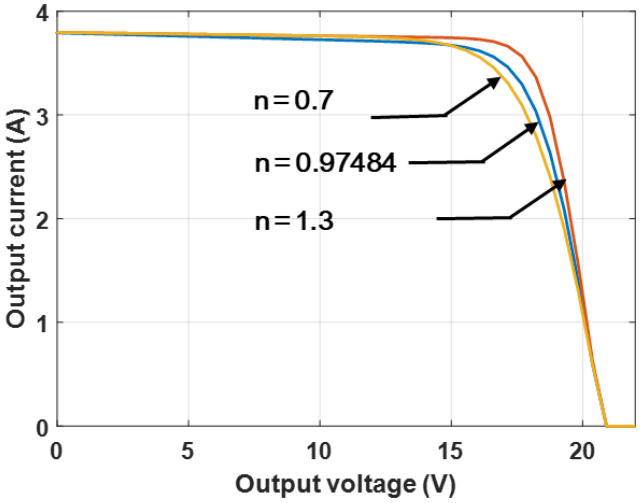

Figure 1.14. I-V curves, for various diode Ideality factors

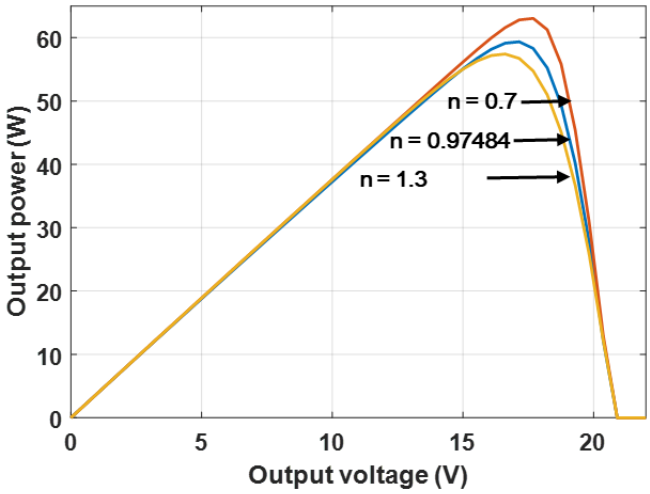

Figure 1.15.P-V curves, for various diode Ideality factors

1.6 Effect of Environmental Influences on PV Curves Characteristics

1.6.1 Effect of irradiance level on PV curves characteristics

Figures 1.15, 1.17 demonstrates the I-V and P-V characteristics of a photovoltaic cell for a range of irradiance with a step of 200 W/m2at 25oC. The current generated by a photovoltaic device is proportional to the photon flux, which explains the proportionality between both short circuit current (Isc), power output of a

solar panel and the irradiance, whereas the open circuit voltage (Voc) stays approximately constant [24, 9].

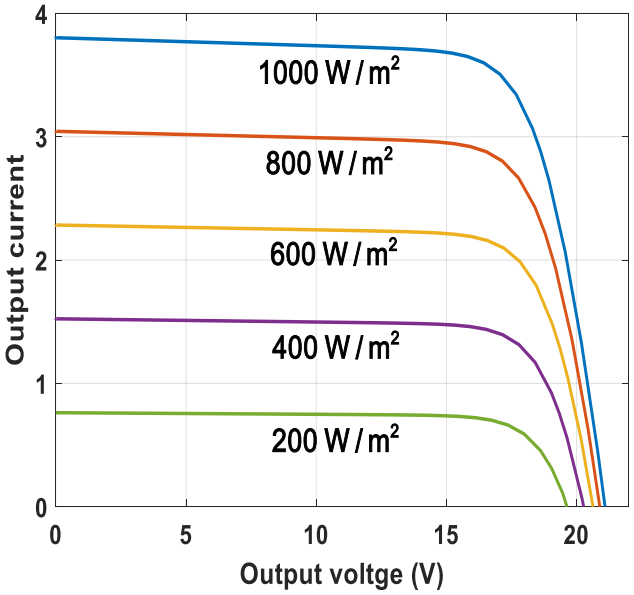

Figure 1.16. I-V characteristics of a photovoltaic cell array for a range of irradiance S at 25 oC

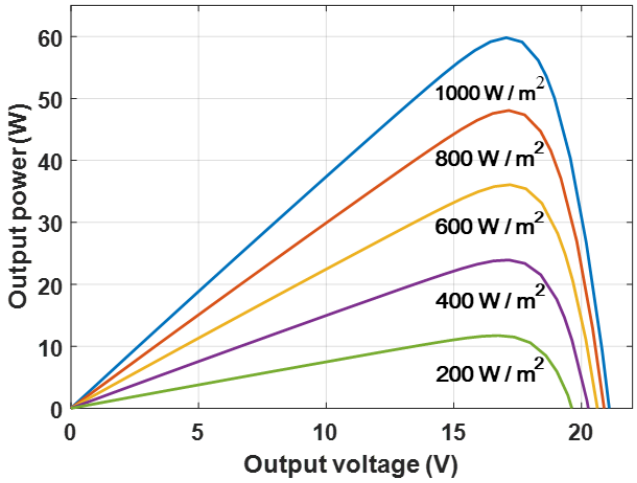

Figure 1.17. P-V characteristics of a photovoltaic cell array for a range of irradiance G at 25°C.

1.6.2 The Effect of Temperature Level on PV Curves characteristics

Figure 1.18 and Figure 1.19 reveal the variation of the I-V and P-V characteristics of a photovoltaic cell for a range of temperatures with a step of 25ºC at a fixed irradiance.

The rise up in temperature leads to lowering in band gap of the semiconductor material. The most influenced parameter is the open-circuit voltage due to its reliance on saturation current. [25].

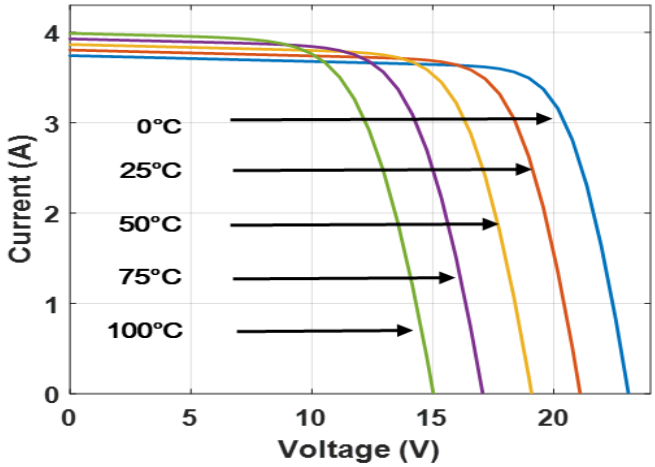

Figure 1-18. I-V characteristics of a photovoltaic array for a range of temperatures at an irradiance of 1000 W/m2

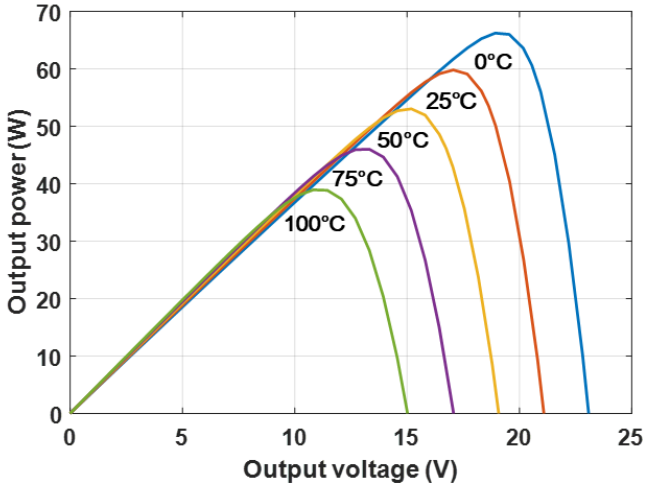

Figure 1.18. P-V characteristics of a photovoltaic cell array for various values of temperature T at an irradiance of 1000 W/m2

1.7 Conclusion

This chapter offered a general approach on photovoltaic systems. We first focused on modeling of photovoltaic cells using the equivalent circuit of single and double-diode model. The points chosen for the parameter determination are the short circuit current point (0, Isc), and open circuit voltage point (Voc, 0).Then the simulation results, which show the influence of the equivalent model parameters and the environmental influence on PV curve characteristics, have been presented.

Chapter 02

2 Chapter 2 : DC-DC Boost Converter and Conventional MPPT Algorithms

2.1 Introduction

The main aim of an efficient PV system is satisfying the load's demands and maximizing the return of the investment, this would not be achieved with a direct connection between the PV panel and the load, where the PV generator is performing away from the MPP (Maximum Power Point).

In order to drive the operating point towards the MPP, a DC-DC converter is placed between the load and the PV panel. The DC–DC boost converter is used for stepping-up the PV array terminal voltage by adjusting the duty cycle, this latter is controlling by MPPT (Maximum Power Point Tracking) controller.

Many MPPT algorithms have been introduced, Perturb and Observe (P&O) and Incremental Conductance (INC) are the most widely used which proved their simplicity, efficiency, and accuracy especially in stable weather conditions. However, these techniques exhibit several limitations during a rapid change in environmental conditions.

Since P&O technique with fixed step provides several limitations which leads to high power losses, variable step-size P&O algorithm has been proposed in order to make a trade off between steady-state stability and convergence time especially under dynamic weather conditions.

2.2 Load Effect in Operating Point of PV Solar Panels Curves

Two fundamental types of load can be fed by a photovoltaic system; a constant voltage load, such as batteries and resistive load. The intersection between the characteristics of the load and the I-V curve characteristics of the PV panel defines a point known as the operating point as shown in Figure 2.1-2. In the case of direct connection between the PV panel and the load, this point would located away from the (MPP). This means that the PV panel does not deliver the maximum power [4,9].

This kind of connection strongly affects the efficiency of the PV system power extraction as well as the investment cost.

Figure 2.1 and Figure 2.2 show I-V curve characteristic with resistive load and constant voltage load respectively.

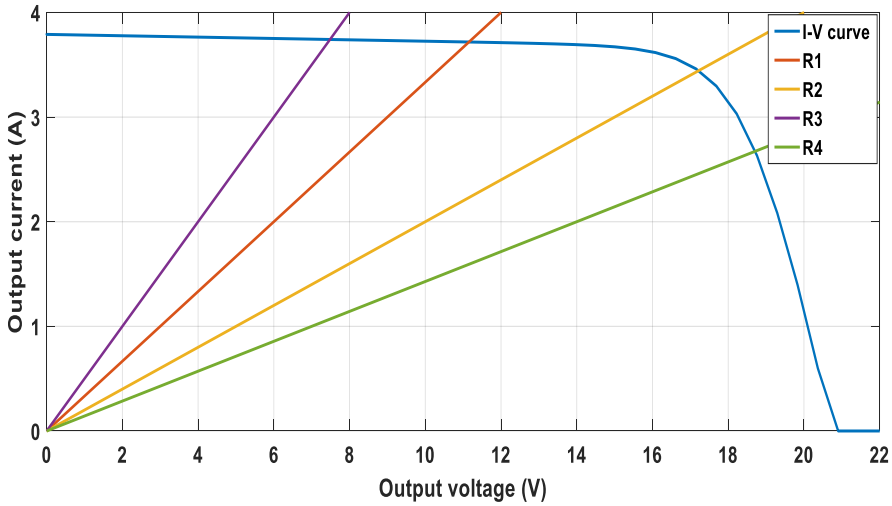

Figure 2.1. I-V Curve Characteristic with Resistive Load

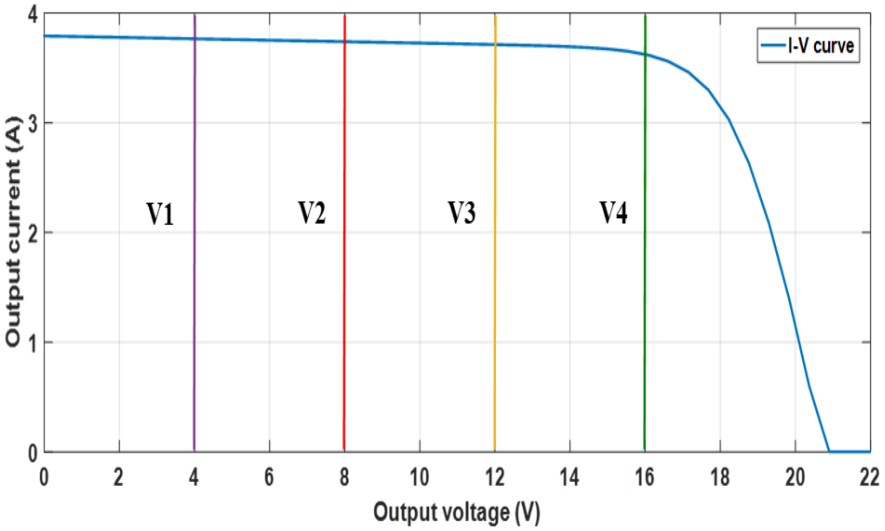

Figure 2.2. I-V Curve Characteristic with Constant Voltage Load

2.3 DC-DC Converter

A DC-DC converter is used as an interface device connecting the PV panel and the load in order to extract the maximum power from the PV generator whatever the weather's conditions or the type of the load [4, 9, 26, 27].As it is shown in Figure 2.3.

Furthermore, the DC-DC converter acts as impedance, which varies the duty ratio adjusted by MPPT controller, to drive the operating point towards the MPP. It converts the unregulated input power ($P_{PV}=I_{PV} * V_{PV}$) into a controlled output power ($P = I * V$), required by the load, and matches the impedance of the PV panel with the one of the load [4, 9, 27, 28].

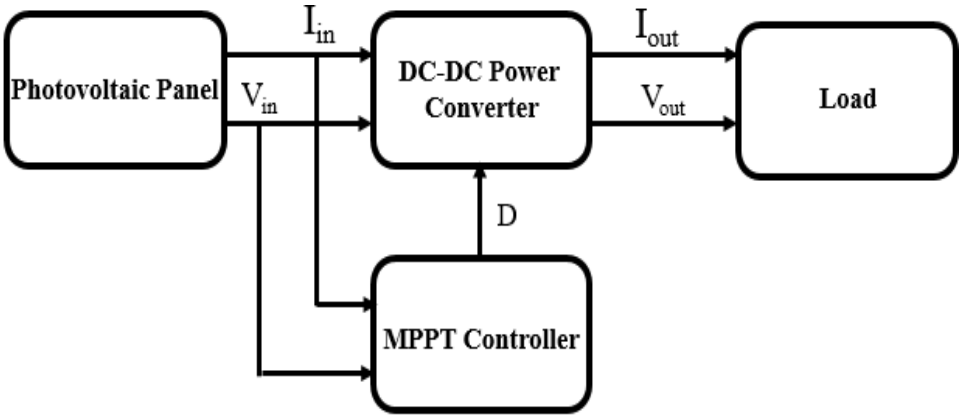

Figure 2.3. PV Panel with DC-DC Converter and MPPT Controller

2.4 DC-DC Boost Converter

The DC-DC boost converter, which is also known as step-up converter, is a non-isolated power stage topology converting a low input voltage to a high output voltage. The following equation describes the relation between the input voltage and the output voltage [49, 26, 27, 28, 29].

$$V_O = \frac{1}{1-D} V_i \qquad (2.1)$$

Where :

V_i : Input voltage

V_o : Output voltage

D : Duty cycle

As it is shown in Figure 2.4, the general structure of a DC-DC boost converter consists of an input voltage (source), output voltage (load), and a power electronic

switch such as MOSFET or IGBT in parallel with a diode. It also contains an inductor to filter the output current and a capacitor to filter the output voltage [5, 28, 29, 30].

In the case of a photovoltaic system, the DC-DC step-up converter is used on maximum power tacking where the duty cycle is controlled by the MPPT controller [26, 27].

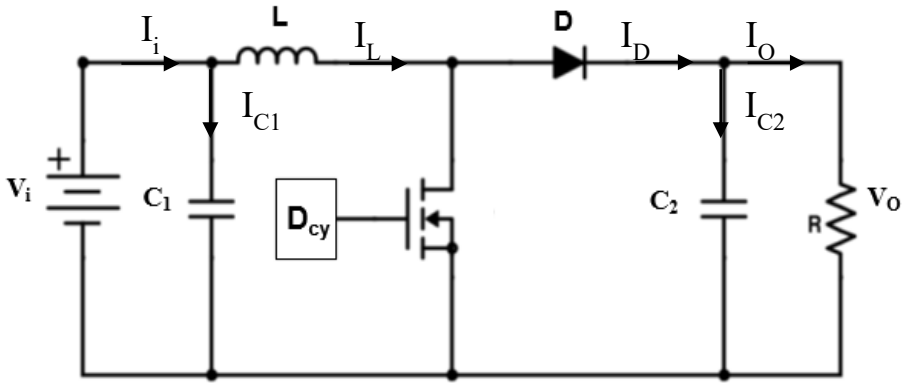

Figure 2.4. General Structure of DC-DC Boost Converter

2.5 Analysis of Operating Modes of DC/DC Boost Converter

2.5.1 Switching ON Mode

When the switch turns on, the energy generated by the source is stored in the inductor and the current through it increases from a minimum value to a maximum value, and the diode is reverse biased (the diode is OFF) [4,5, 9, 27, 28, 30].

Figure 2.5 displays the equivalent electrical circuit of this operating mode

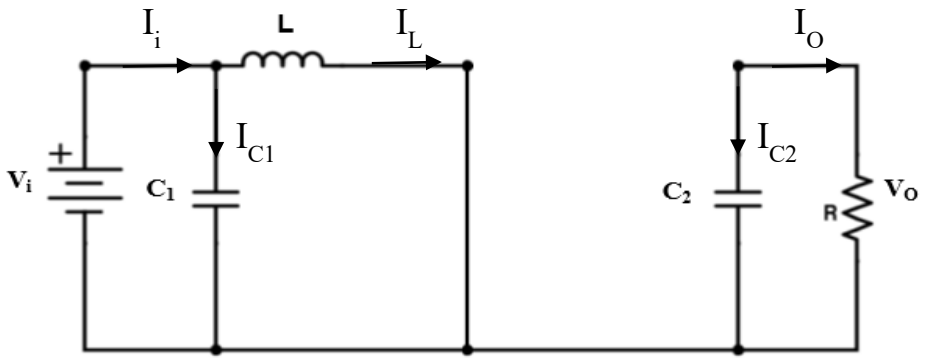

Figure 2.5. Step-UP Boost Converter Switch Closed.

During the interval **(0< t ≤ DT)**

$$\begin{cases} I_{C_1} = C_1 \dfrac{dV_i}{dt} = I_i - I_L \\ I_{C_2} = C_2 \dfrac{dV_O}{dt} = -I_O \\ V_L = L \dfrac{dI_L}{dt} = V_i \\ V_D = -V_O \\ I_D = 0 \end{cases} \qquad (2.2)$$

I_{C1} : Current through the first capacitor

I_{C2} : Current through the second capacitor

I_L : Current through the inductor

V_L : Inductor voltage

V_D : Diode voltage

I_D : Diode curent

2.5.2 Switching OFF Mode

During the second interval, the switch is OFF and the diode is ON. Both of the source and the inductor deliver their energy to the load. Therefore, the current stored in the inductor, decreases from a high level to a low level. In this operating mode, the filter capacitor is used to minimize the output ripple voltage [4, 5, 9, 27, 28, 30].

The equivalent circuit of the switching OFF mode is clearly shown in Figure 2.6.

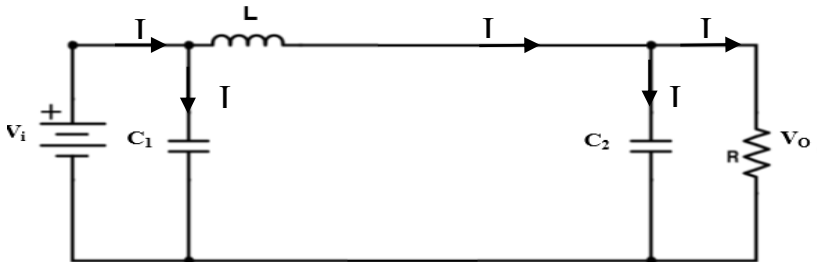

Figure 2.6. Step-UP Boost Converter Switch Opened

During the interval **(DT <t ≤ T)**

$$\left\{\begin{array}{l} I_{C_1} = C_1 \dfrac{dV_i}{dt} = I_i - I_L \\ I_{C_2} = C_2 \dfrac{dV_O}{dt} = I_L - I_O \\ V_L = L \dfrac{dI_L}{dt} = V_i \\ V_D = -V_O \\ I_D = I_O \end{array}\right\} \qquad (2.3)$$

2.6 Maximum Power Point Tracking Algorithms

The main purpose of a PV system is generating the amount of power required by the load, whatever the nature of the load or the atmospheric conditions which effect the I-V curve characteristics of the PV panel, and, therefore, affecting the position of the MPP [4, 5, 9, 28].

Many MPPT algorithms have been introduced aiming to ensure that the PV panel is operating at or near to the MPP, and to extract the maximum power by matching the internal impedance of the PV panel and the load impedance. This would happen by adjusting the duty cycle of the DC-DC converter. These algorithms can be categorised in conventional and advanced techniques [4, 5, 9, 28].

The main characteristics that can make the difference between the several MPPT techniques are [4, 5, 9, 28, 30].

- Simplicity
- Stability
- Cost
- Range of efficiency under environmental conditionsvariation.
- Speed of convergence towards the MPP.
- Adaptation with different types of DC-DC converter and load.

2.7 Conventional MPPT Algorithms

2.7.1 Perturb and observe (P&O) algorithm

Perturb and observe (P&O) algorithm is classified as the most commonly used algorithm compared to the other MPPT algorithms because of its simple feedback structure, the ease of implementation and the reduced number of their parameters [4, 5 9, 30, 31]. As shown in Figure 2.7 this method is based on periodically perturbing the operating point towards the MPP by incrementing or decrementing the operating voltage [4, 5, 9, 30, 32,]. During each stage, the output power Pn is calculated by multiplying the measured output voltage and the output current, then this value is compared with the previous perturbation Pn+1, if the output power is increased than the perturbation keep the same direction, otherwise it will be on the opposite direction. Once the MPP is reached (Pn = Pn+1), the operating point starts to oscillate around the MPP [4, 5, 9, 30, 31, 32].

However, P&O method has several limitations such as:

- The increase of the power losses as a result of the oscillation around the MPP in the steady state condition especially in the case of large step [4, 5, 9, 32,]
- During a speed change condition in the irradiation levels, the (P&O) algorithm is inaccurate and slow especially in the case of small step size [4, 5, 30, 31, 32].
- Besides the high number of iterations, this method requires to measure the current and the voltage in each stage, this strongly affects the efficiency of (P&O) algorithm and leads to more losses in the power [9, 31].

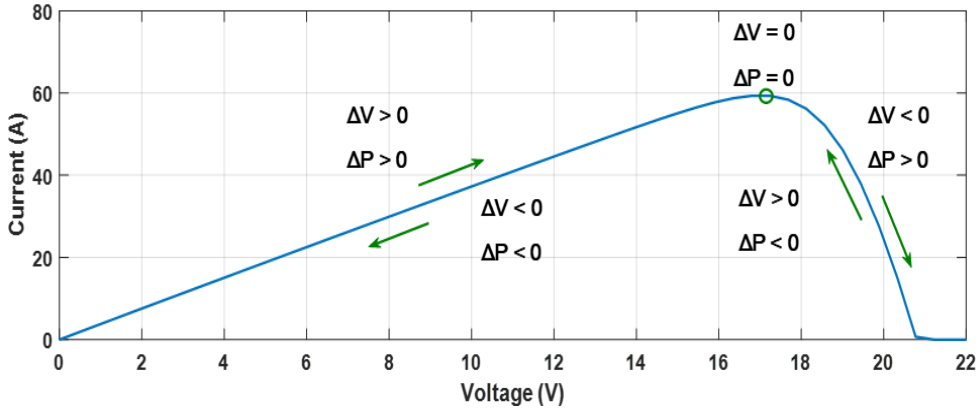

Figure 2.7. Perturb and observe method

The flowchart of the (P&O) algorithm is shown in the Figure 2.8.

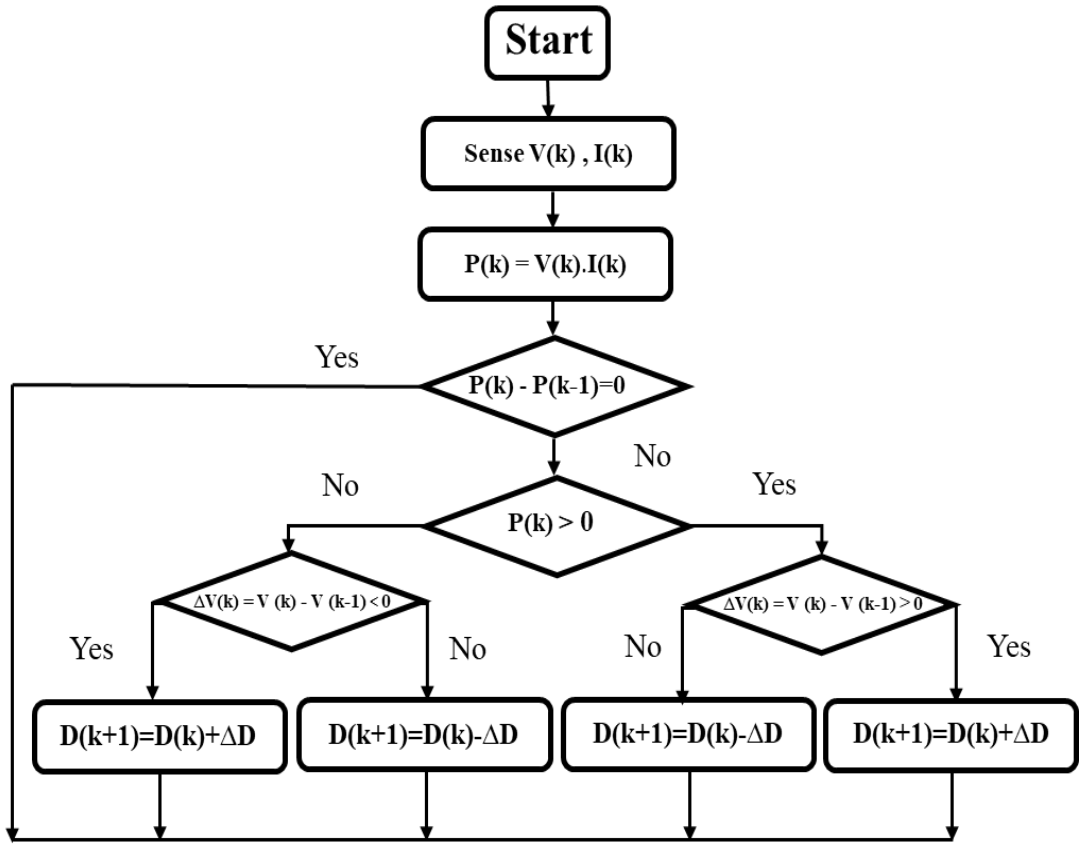

Figure 2.8. Flowchart of Perturb and observe algorithm

2.7.1.1 Incremental conductance (INC) algorithm

Incremental conductance (INC) algorithm is also widely used, it is introduced to defeat the limitations of (P&O) algorithm and improve its performances [30, 31, 33]. During each stage this method compares the instantaneous conductance (I/V) and the incremental conductance (ΔI/ΔV). If the slope of P-V curve (ΔP/ΔV) is negative which means that the operating point is on right of the MPP, than the PV array terminal voltage is decreased. In the case of positive slope, the operating point is on left of the MPP and the PV array terminal voltage is increased, otherwise the slope is equal to zero which means that the instantaneous conductance and the incremental conductance are equal and the MPP is reached [4, 5, 9, 30, 33].

The following equations clearly explain how the (INC) algorithm works:

$$\frac{dP}{dV} = \frac{d\left(I \times V\right)}{dV} = V\frac{dI}{dV} + I\frac{dV}{dV} + I \qquad (2.4)$$

$$\begin{cases} \dfrac{dP}{dV} < 0 \Rightarrow \dfrac{dI}{dV} < -\dfrac{I}{V} \\ \dfrac{dP}{dV} > 0 \Rightarrow \dfrac{dI}{dV} > -\dfrac{I}{V} \\ \dfrac{dP}{dV} = 0 \Rightarrow \dfrac{dI}{dV} = -\dfrac{I}{V} \end{cases} \qquad (2.5)$$

Despite its accuracy during rapid change environmental conditions, the (INC) algorithm exhibits some limitations such as :

- The oscillation around the MPP which leads to power losses [5, 9, 30].
- This method needs to continually measure the current and the voltage which leads to a slow tracking speed [4, 9].
- The inefficiency of (INC) algorithm under partial shading conditions [5, 34]
- The incremental conductance algorithm exhibits a high computational complexity in comparison with (P&O) method [4, 9, 31, 35]

Figure 2.9 shows sign of the (ΔP/ΔV) at different positions on the P-V curve characteristic

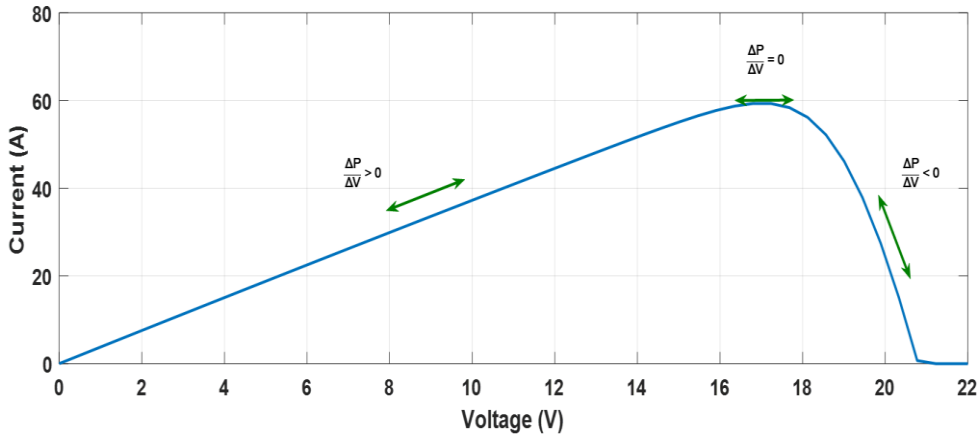

Figure 2.9. Basic Idea of Incremental Conductance Algorithm

The flowchart of the (INC) algorithm is shown in the Figure 2.10.

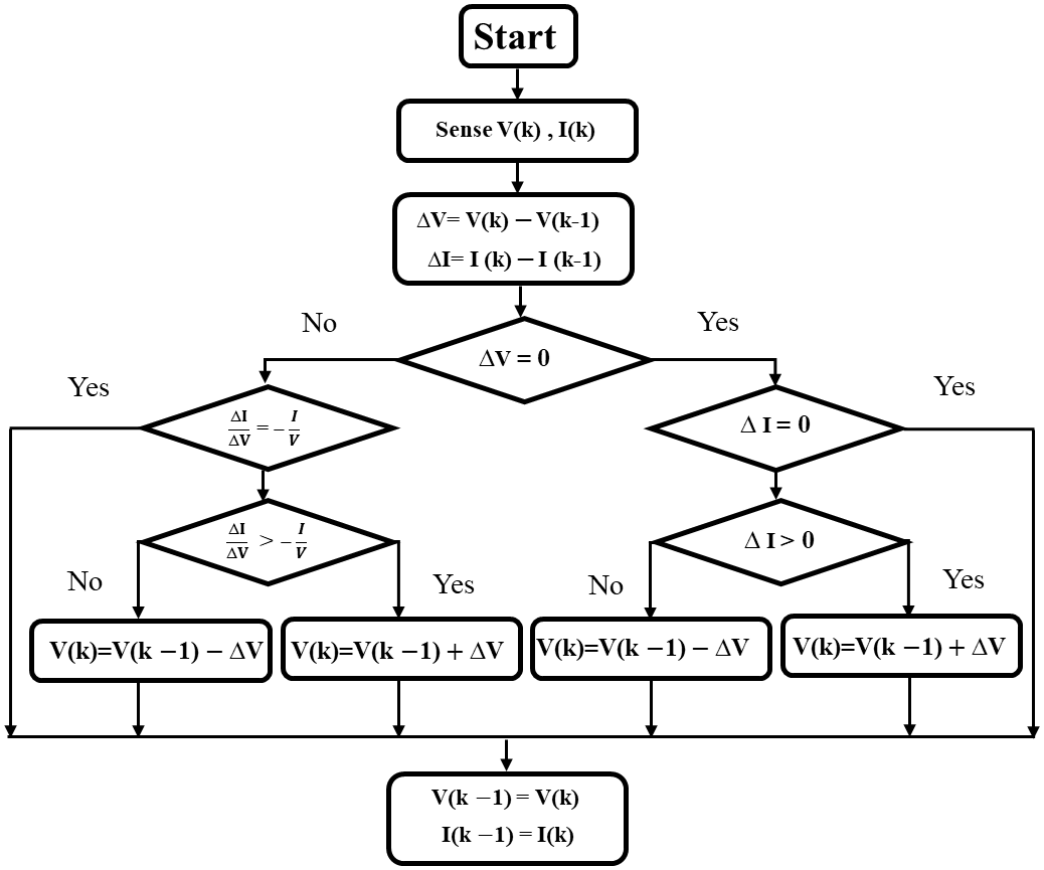

Figure 2.10. Flowchart of Incremental conductance algorithm

2.7.1.2 Variable step-size P&O algorithm

Variable step-size P&O method is proposed as a solution to overcome the drawbacks caused by the fixed step-size of the conventional P&O algorithm by making a compromise between the steady-state oscillation and the time of response under dynamic weather conditions [36, 37, 38].As it is shown in the flowchart represented in Figure 2.11, the duty cycle is automatically adjusted against the irradiance change according to the position of the operating point. During the tracking process, this technique applies a large step size if the operating point is located far from the MPP, however, a small step size is applied if the operating point is near to the MPP, when the MPP is reached the duty cycle keeps the same value, this latter is obtained according to the following equation [39, 40, 41, 42]

$$D_k = D_{k-1} \pm \frac{\Delta P}{\Delta V} \qquad (2.6)$$

D_k : Duty cycle of the current iteration.

D_{k-1} : Duty cycle of the previous iteration.

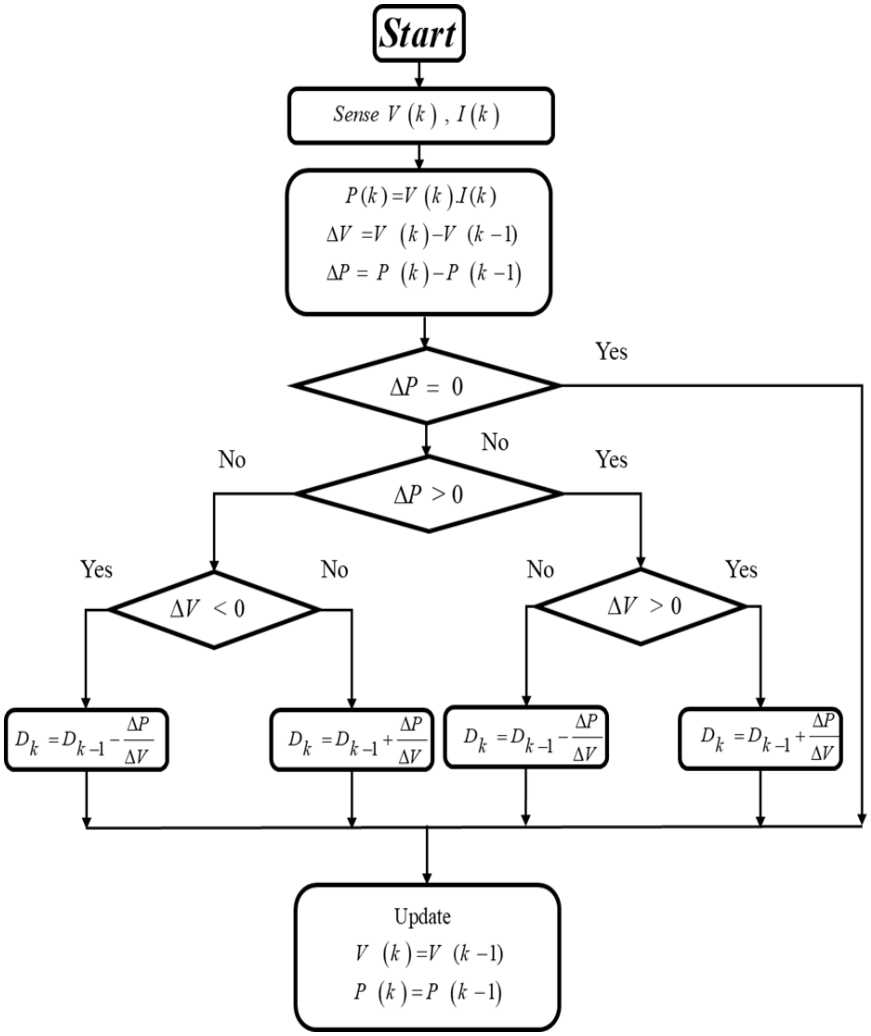

Figure 2.11. Flowchart of Variable step-size P&O algorithm

2.8 Conclusion

This chapter is highlighting the issue of the direct connection between the PV panel and the load. It presents also the equivalent electrical circuit of the power electronic interface device (DC-DC converter) and its operating modes. Finally, this chapter gives an overview of some of the conventional approaches that have been implemented in the MPPT system.

Chapter 03

3 Chapter 3: MPPT Based Artificial Intelligence Techniques

3.1 Introduction

Over the last decade, many researchers have concentrated on various MPP methods to track the maximum power of photovoltaic generator. These algorithms differ in many ways, such as simplicity, required sensors, cost, range of performance, convergence speed, correct tracking during irradiation and/or temperature shift, hardware needed for implementation, and popularity. Conventional MPPT methods are commonly used because they are usually simple and inexpensive. However, the usefulness of such methods is limited due to steady-state oscillation, diverging tracking path and may not even be able to define the global optimum power point under certain special conditions, such as sudden changes in irradiance due to shading.

To overcome these limitations, several MPPT techniques based on Artificial Intelligence (AI) have been introduced, such as Fuzzy Logic Controller (FLC), Artificial Neural Networks (ANN), fuzzy Inference System (ANFIS), and Genetic Algorithms (GA). These techniques exhibit more flexibility in the case of rapid change in the weather's conditions, fast tracking speed and large range of accuracy in comparison with P&O and InC algorithms.

In this chapter, the advanced concepts of MPPT algorithm such as fuzzy logic controllers (FLC) and artificial neural network (ANN) are described and analyzed.

3.2 Artificial Intelligence (AI)

The artificial intelligence (AI) technique is a system that makes decisions like humans' beings by adapting to the situations and coming with adequate decisions automatically for future similar situations [43, 44]. The AI systems are proposed to solve the limitations of traditional techniques and improve the steady and dynamic states [44].

In this section, we propose an MPPT control system based on fuzzy logic and neural networks to improve the efficiency of PV energy system. The fuzzy and the neural

network algorithms are applied to the control a DC-DC converter Boost for maximum power point tracking.

3.2.1 Fuzzy logic

The concept of fuzzy logic (FL) first became known 40 years ago, since Zadeh introduced the fundamental theory in 1965[45, 46]. However, FL's principle was not applied to the control system until ten years later, due to inadequate small machine technology before that time. The theory started to show results in the early 1970's when it was applied in a practical application to regulate Mamdani's automatic steam engine in 1974[47]. In 1986,Togai and Watanabe created the first special-purpose Very-large-scale integration (VLSI) chip for performing fuzzy logic inferences [48]. These VLSI chips can boost the performance of fuzzy rule-based systems for real time applications. Several companies were founded (e.g., APTRONIX, INFORM) to market hardware and software tools for the development of Fuzzy systems. Furthermore, vendors of traditional control design tools began to implement add-on toolbox for the design of fuzzy systems. In 1994, the Fuzzy Logic Toolbox for MATLAB was introduced as a component add-on to MATLAB [49].

Fuzzy logic is based on a mathematical model that deals with uncertainty and imprecision, confusion, noise or lack of input information. It compares the analog input signal to the default logic variable membership or fuzzy set, which corresponds to values in the range 0 and 1. Fuzzy logic is applied in a control system to mimic guided human-like decisions. Due to its heuristic nature associated with simplicity and efficacy for both linear and nonlinear systems, FL techniques have been widely used in a wide range of engineering applications [50]. It can be implemented in a combination of all software, hardware. Fuzzy sets are called the Fuzzy control system's brain which, in effect, is responsible for converting analog input values to a scale of 0 to 1[51-52].

3.2.1.1 Fuzzy Logic Controller Structure

A fuzzy logic controller's (FLC) fundamental function is to provide input-output relationships in terms of fuzzy rules. FLC consists of four different stages in real-time:

Fuzzification, knowledge base, interface engine, and defuzzification [53-54], as shown in Figure 3.1.

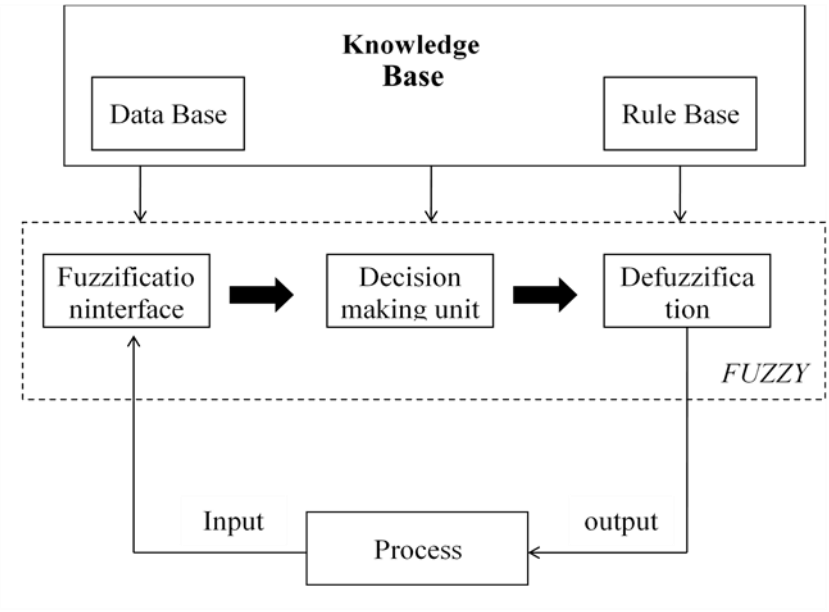

Figure 3.1. General structure of fuzzy interface system

The main five construction operations of fuzzy rules based system can express as follow [55, 56]:

- A database that describes the Fuzzy Sets membership functions used in the Fuzzy Rules.
- A fuzzification interface that converts the crisp inputs into corresponding degrees with linguistic values.
- A rule base that contains a number of fuzzy if-then rules.
- A decision-making unit that performs the operations of inference on the rules.
- A defuzzification interface that converts the fuzzy results of the inference into a crisp output.

Every fuzzy set can be defined by its function of membership. The form of membership function depends on the application and can be monotonic, triangular, trapezoidal, gaussian, bell-shaped, sigmoidal or S-curve. Some popular waveforms of the membership functions as shown in Figure 3.2 [57].

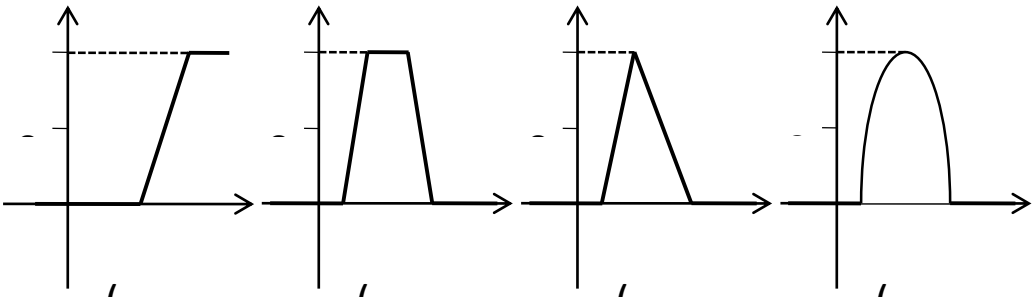

Figure 3.2. Different graphs of membership functions (a) monotonic (b) trapezoidal (c) triangular (d) Gaussian.

Trapezoidal or triangular membership functions are usually used in short-term systems requiring significant dynamic variation. A Gaussian or S-curve membership function is always selected when the device needs very high precision control [58].

3.2.1.2 Knowledge base

The knowledge base is the main part of the fuzzy control system. The knowledge base consists both data base, rule base of the plant. It provides all the necessary definitions for the fuzzification method, such as membership functions, fuzzy set representation of the input-output variables and mapping functions between the real and fuzzy domain [59]. Fuzzy control rules can be generated in four modes. Such four modes are not mutually exclusive and can be combined to achieve an efficient framework [4].

- Expertise and experience in technical control: manual service and Survey questionnaire.
- Based on the control actions of the operators: evaluation of the behavior of the human controller regarding the input-output operating data.
- Based on the Fuzzy Method Model: Complex linguistic analysis process Characteristics.
- Learning based: ability to modify control rules, such as controller self-organization.

The number of basic rules can be specified based on the membership number of the fuzzy set and the inputs. For instance, if the system includes two inputs and each of them has five memberships then the total base rules will be 5* 5= 25 base rule. The

higher number of memberships offers better efficiency of the system, but the system implementation becomes more complex [4].

3.2.1.3 Procedure of fuzzy inference

Fuzzy outputs must be transformed to a scalar output quantity, so that the machine can evaluate the essence of the operation to be performed. Within the process of converting the fuzzy output, there are several techniques for performing the fuzzy reasoning like: Mamdani method, Larsen method, Tsukamoto method, and the Sugeno style inference, or to be more complete, Takagi-Sugeno_Kang (TSK) method [56, 58]. In our study two types of fuzzy inference system will be introduced which are the Mamdani and TSK methods. These two types are the most important and widely employed in fuzzy controllers [55, 60, 61].

3.2.1.3.1 Mamdani approach

Mamdani's method is the most widely used fuzzy interface technique. In 1974, London University's Professor Ebrahim Mamdani designed one of the first fuzzy devices to power a combination of steam engine and boiler. In this method a collection of fuzzy if-then rules was implemented, and these were given by experienced human operators. The Mamdani method's fuzzy interface mechanism can be established in four steps [62, 63].

- Fuzzification.
- Rule evaluation.
- Aggregation of the rule outputs.
- Defuzzification.

A simple two-input one-output problem which includes three rules is examined to explain the Mamdani method's fuzzy interface working process [62].

Rule 1: IF X is A_3 OR Y is B_1 THEN z *is* C_1 (3.1)

Rule 1: IF X is A_2 AND Y is B_1 THEN z *is* C_2 (3.2)

Rule 1: IF X is A_3 THEN z *is* C_3 (3.3)

Step 1: Fuzzification

Fuzzification is the operation which converts a crisp data input x and y, into membership values. The mechanism of transformation of fuzzy values is represented by the membership function. The degree of membership depends on the shape of the membership function applied. According to Figure 3.3, the following equation is obtained [53, 64, 65]:

$$\mu A_1(x)=0.7, \mu A_2(x)=0.4, \mu B_1(y)=0.3, \mu B_2(y)=0.9 \quad (3.4)$$

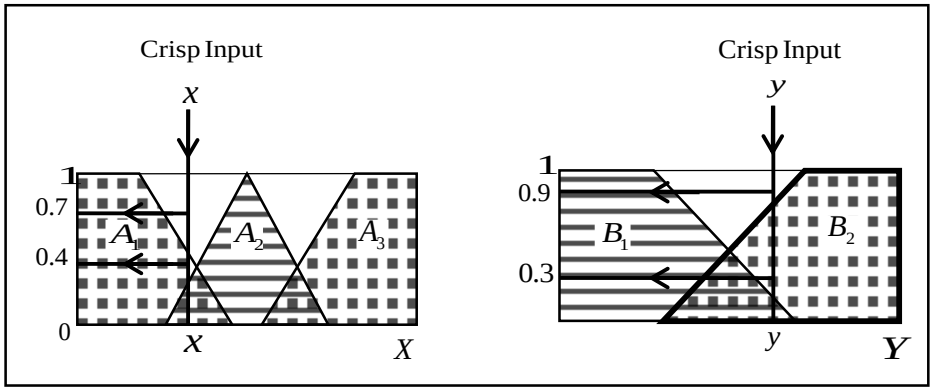

Figure 3.3. Fuzzification

Step 2: Rules evaluation

In the second step, the antecedents of the fuzzy rules apply to the fuzzified inputs. The fuzzy rules turn multiple inputs into single number between 0 and 1 that represents the result of the previous evaluation using the fuzzy operator (AND or OR) [50, 58]. To evaluate the disjunction, the OR fuzzy operation is used thus the classical fuzzy operation union is used. As shown in the equation (3.5), the uses of the union strategy are to get the maximum [54, 62, 65]:

$$\mu_{A\cup B}(x)=\max\{\mu_A(x),\mu_B(x)\} \quad (3.5)$$

Similarly, in order to evaluate the conjunction of the rule antecedents, the AND fuzzy operation is used thus the intersection is applied as in equation (3.6) the uses of the intersection strategy are to get the minimum [54, 62, 65]:

$$\mu_{A\cap B}(x)=\min\{\mu_A(x),\mu_B(x)\} \quad (3.6)$$

The rule evaluations are clearly appearing in Figure 3.4.

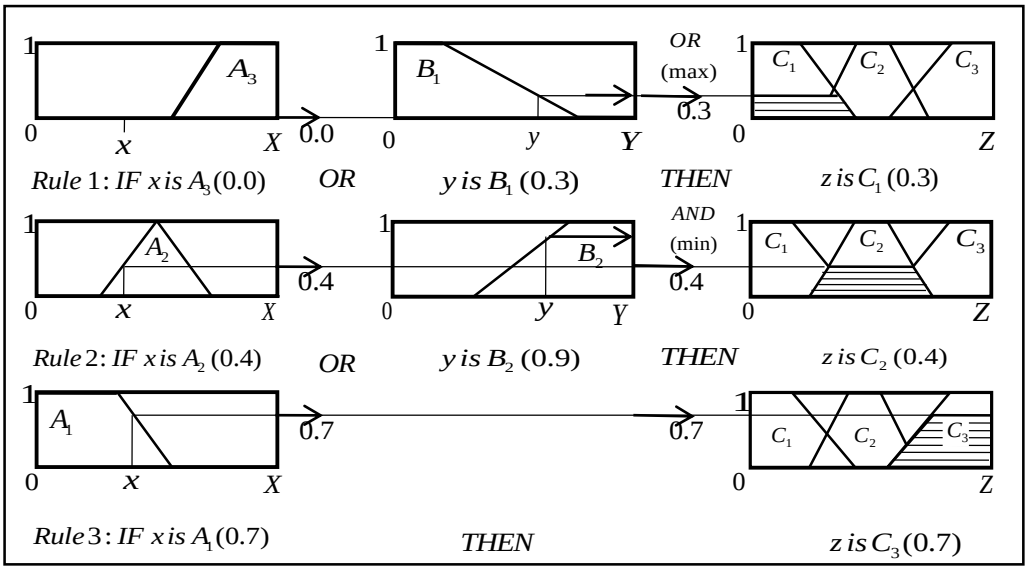

Figure 3.4. Rule evaluation in Mamdani method.

Step 3: Aggregation of the rule outputs

The Aggregation method unifies all rules outputs and gives a single fuzzy set which is the system's fuzzy output. This can be achieved by measuring all outputs to their limit [66, 67].

Figure 3.5 shows the aggregation of the rule outputs.

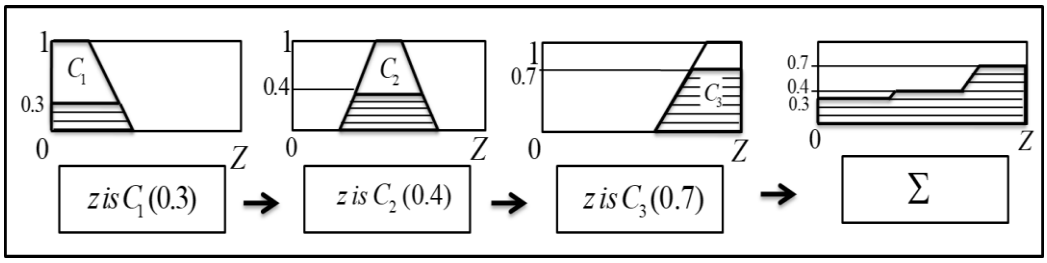

Figure 3.5. Aggregation of the rule outputs.

Step 4: Defuzzification

It is the step at which the fuzzy output is converted into a crisp output. In the literature several methods of defuzzification have been proposed. The most widely used are the center of gravity (COG) method, the mean of maximum method (MOM) and the height method (HM) [53, 54, 64, 66, 67].

- The COG approach determines a fuzzy set's defuzzified value as its fuzzy centroid. The output of COG can be represented by equation(3.7):

$$COG = \frac{\sum_{j=1}^{n} w_j . \mu_z(w_j)}{\sum_{j=1}^{n} \mu_z(w_j)} \tag{3.7}$$

Where, n is the number of quantization levels of the output.

- The MOM approach calculates the defuzzified value as a mean of all values of the discourse universe, with full membership grades, as in the equation(3.8):

$$MOM = \sum_{i=1}^{l} \frac{w_j}{l} \tag{3.8}$$

In equation (3.8), w_j is the support value when the membership function reaches the maximum value $\mu_z(w_j)$, and l is the number of support values.

- The HM is centered on the center of gravity of each rule, weighted according to the corresponding rates of each rule, the control action can be expressed by equation(3.9):

$$Z = \frac{\sum_{j=1}^{n} w_j . \mu(w_j)}{\sum_{j=1}^{n} \mu(w_j)} \tag{3.9}$$

3.2.1.3.2 The Takagi-Sugeno approach

After Mamdani's pioneering work [68] on fuzzy control inspired by the approach of Zadeh to inaccuracy[66].Numerous experiments have been carried out on fuzzy reasoning[70, 69].Many of the fuzzy controls were designed based on the experience of human operators and/or expertise of the control engineers. However, often the case is that an operator cannot linguistically tell what kind of action he is taking in a specific situation. In this respect, the method of modeling control behavior using numerical data is very useful [70]. In 1985, Takagi-Sugeno-Kang introduces a type of a fuzzy system which avoids defuzzification [9].

The basic concept of the T-S fuzzy model is to partition the input space into fuzzy areas and estimate each area by means of a linear model in such a way as to calculate a

global nonlinear model. It is also characterized as a set of IF-THEN rules where linear sub-models describing the dynamic behavior of distinct operating conditions are the consequent part[71].Therefore, the global model is obtained through the interpolation of these various local ones. Using a small number of rules this model can be used to approximate a highly nonlinear function through simple structure. Fuzzy inference in Sugeno-style is very similar to Mamdani method. Sugeno altered only one consequent statute. He used a mathematical function of the input variable, rather than a fuzzy set. The Sugeno-style Fuzzy rule format is [72, 71]:

$$\text{IF } X \text{ is } A \text{ AND } Y \text{ is } B \text{ THEN } Z \text{ is } f(x,y) \qquad (3.10)$$

Where X, Y and Z are linguistic variables; A and B are fuzzy sets on universe of discourses. X, Y, respectively; and $f(x,y)$ is a mathematical function.

The most widely used Sugeno Fuzzy zero-order model applies the following fuzzy rules:

$$\text{IF } X \text{ is } A \text{ AND } Y \text{ is } B \text{ THEN } Z \text{ is } k \qquad (3.11)$$

Where, k is a constant.

In this case, the output is constant for each Fuzzy rule. The singleton spikes represent all the consequent membership functions [72, 71]:

The following Figure 3.6 and Figure3.7 illustrates the idea for TSK which likes Mamdani steps.

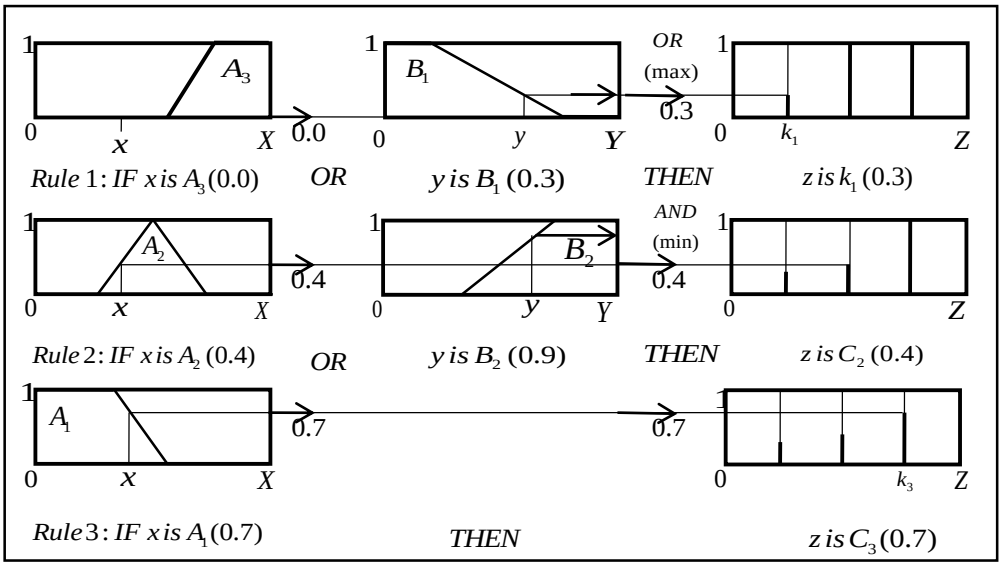

Figure 3.6. Rule evaluation stage in TSK method

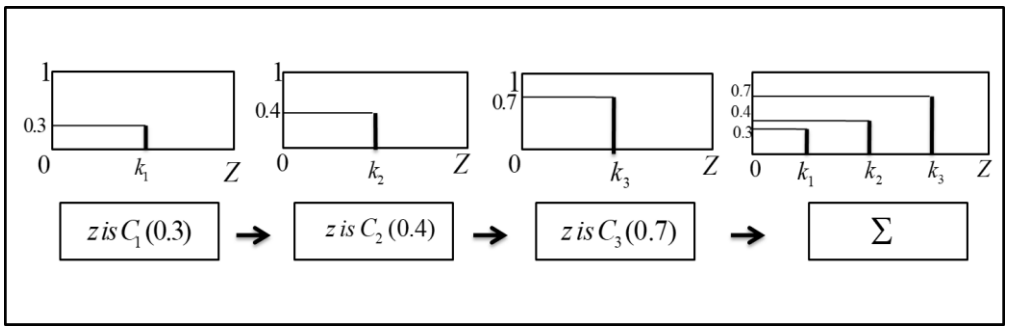

Figure 3.7. Aggregation stage in TSK method

Mamdani method is widely accepted for capturing knowledge from experts. It enables us to describe the expertise more intuitively, in a more human-like way. However, Mamdani-type fuzzy inference involves a significant computational burden. At the other hand, the Sugeno approach is computationally efficient and works well with optimization and adaptive techniques, making it very attractive in control issues, particularly for nonlinear dynamic systems [55, 60, 73].

3.2.1.4 Fuzzy Logic based MPPT Controller

FL is an advanced version of multivalued logic in soft computing, also it can handle non-precision input problems, does not require precise mathematical modeling and is capable of handling nonlinearity [74, 75]. FLC has fast response time and increase system stability [51, 52]. The FLC has two inputs, error ($E_{(n)}$) and change in error ($CE_{(n)}$), as they are computed by the following equation.

$$\begin{cases} E_{(n)} = \dfrac{P_{(n)} - P_{(n-1)}}{V_{(n)} - V_{(n-1)}} \\ CE_{(n)} = E_{(n)} - E_{(n-1)} \end{cases} \quad (3.12)$$

And the output of the FLC is the Duty Cycle (*D*), The value of *D* is given to the Pulse Width Modulation (PWM) block to control the boost converter.

FL control process is divided into three different stages: Fuzzification, inference engine and rule base and defuzzification are shown in Figure 3.8.

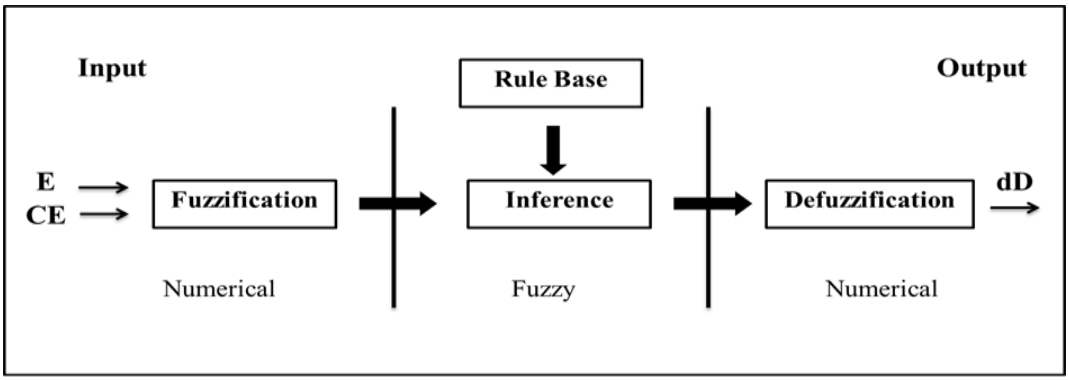

Figure 3.8. Block diagram of FLC

3.2.1.4.1 Fuzzification

Fuzzification is a process that converts the numerical input variables into linguistic variables using fuzzy membership function [74]. These variables are expressed in terms of five linguistic variables using basic fuzzy subsets such as [74, 75].

- **ZE** : zero
- **PB** : positive big
- **PS**: positive small
- **NB**: negative big
- **NS** : negative small

By using the basic fuzzy subsets, Figures 3.9 shows the degrees (or function) of membership of the five basic fuzzy subsets for the input and output variables.

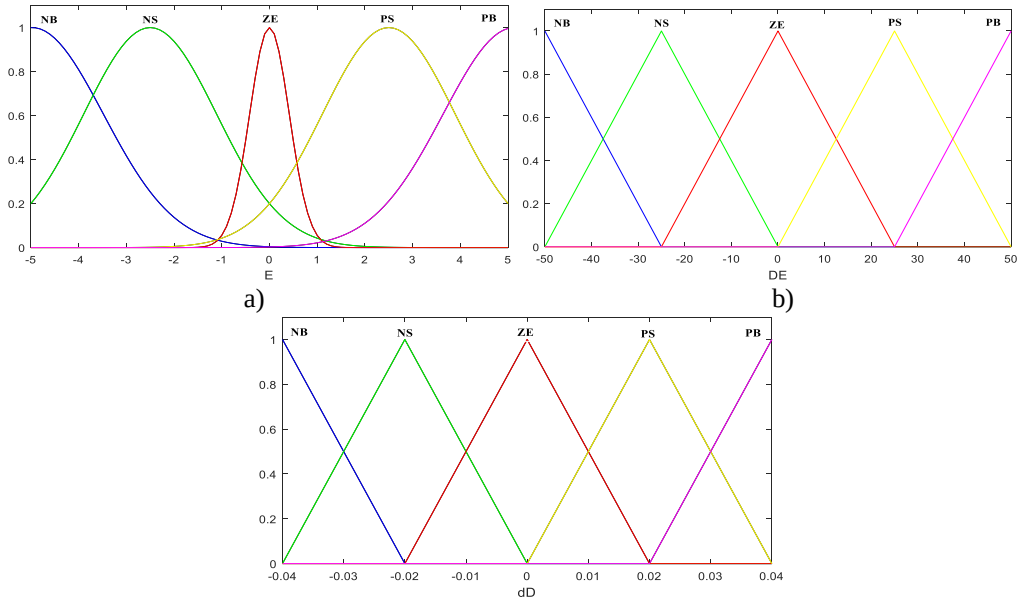

Figure 3.9. Membership functions for: a) input (E), b) input (CE) and c) output (dD) of FLC.

3.2.1.4.2 Inference Engine and Rule Base

The main part of FLC is the Inference System. Inference engine is a rule base program and the rules are placed in the engine block [77, 78]. The fuzzy inference is done with Max-Min operation using Mamdani rule. MIN operation is used for operator "AND" and MAX for operator "OR". Inferential rules are used to control the boost converter so as to achieve maximum PV generator [77, 78, 79].

Table 3.1 shows the rules for the desired relationship between the membership functions of inputs *E*, *CE* and Duty ratio (*D*).

Table 3.1. Twenty-five fuzzy rules for fuzzy MPPT.

		CE				
		NB	NS	ZE	PS	PB
E	NB	ZE	ZE	PB	PB	PB
	NS	ZE	ZE	PS	PS	PS
	ZE	PS	ZE	ZE	ZE	NS
	PS	NS	NS	NS	ZE	ZE
	PB	NB	NB	NB	ZE	ZE

3.2.1.4.3 Defuzzification

The inferential methods provide a function for the resulting membership variable, so the information is fuzzy. Since the DC-DC converter needs an accurate *D* control signal at its input so that defuzzification is necessary[80]. In the Defuzzification process, FLC output is converted from a linguistic variable to a numerical variable still using a membership function, while the FLC output is measured using the Center of Gravity (*CoG*) technique during the defuzzification process to find out the Duty ratio (*D*), its calculated by using the formula (3.13)[51, 81].

$$dD = \frac{\sum_{j=1}^{n} \mu\ D_j\ D_j}{\sum_{j=1}^{n} \mu\ D_j} \tag{3.13}$$

3.2.2 Artificial Neural Network

Analysis concept of artificial neural network (ANN) was developed nearly 50 years ago [82]. However, software for applications has only been developed in the last 20 years to handle practical problems[83, 84].ANN has become popular and expanded with the advancement of soft computing technology in MPP tracking for PV systems [85-86]. ANNs are non-linear mapping systems similar to the role of the human brain, since they mimic the learning mechanism of the human brain [87].

ANNs are collections of small separately connected processing units. Information is passed along interconnections between those units. An incoming link has connected two quantities, an input value and a weight [82, 86, 88]. The unit output is a summed-value function. ANNs are not programmed to perform specific tasks whilst implemented on computers. Alternatively, they are taught with data sets before they learn patterns that are used as inputs. Upon training, they may be presented with new patterns for prediction or classification. An ANN can handle many inputs and produce answers in a designer-suitable form [84, 89, 90, 91].

3.2.2.1 Artificial Neuron Model

3.2.2.1.1 Single-Input Neuron.

ANNs provide a variety of multiprocessor computing systems. It consists of many very basic and highly interconnected processors, called neurons, which correspond to the brain's biological neurons [92]. The simple form of an ANN which has a single-input neuron. The p input is multiplied by the w weight and forms the term wp. This term is then transmitted to the summer, along with a 'dummy' input, 1, multiplied by a bias θ. The summer output n is often called the net input and enters a transfer function F, which generates a neuron output a. That output will be the axon transmitted signal [93, 94]. The Figure 3.10 represents the simplest form of an ANN.

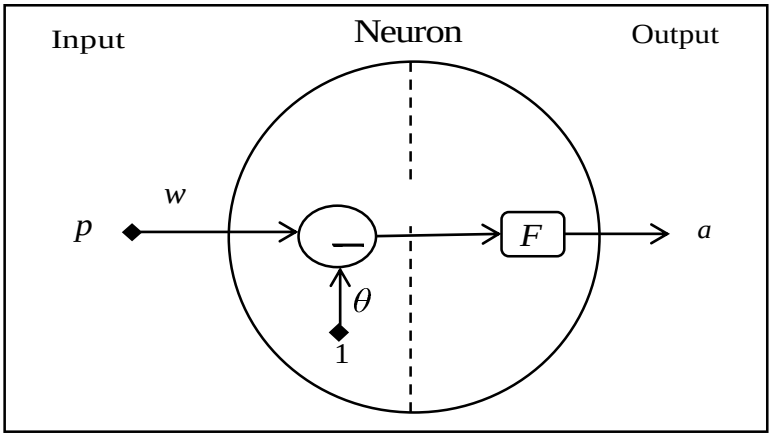

Figure 3.10. Single-input neuron.

The output a, of the neuron is calculated as:

$$a = F\left(w.p + \theta\right) \tag{3.14}$$

3.2.2.1.2 Multiple-Input Neuron.

Usually, a neuron has more than one input. In Figure 3.11, neuron with an S-dimensional input vector is shown. The $p_1, p_2, p_3, ..., p_S$ elements of the input vector p are weighted each time by the corresponding weight vector elements $w_{1,1}, w_{1,2}, w_{1,3}, ..., w_{1,S}$. The neuron has a bias θ that is added with the weighted inputs to form the net input n [93-94].That net input is represented by the equation (3.15).

$$n = p_1.w_{1,1} + p_2.w_{1,2} + p_3.w_{1,3} + ... + p_S w_{1,S} + \theta \quad (3.15)$$

This expression can be rewritten as:

$$n = w.p + \theta \quad (3.16)$$

The neuron output a can be written as:

$$n = F(w.p + \theta) \quad (3.17)$$

Where, F is a transfer function. The weights may also be represented as vectors or matrices, which is a very convenient way of measuring the outputs. In the field of ANNs, the following convention is used in the assignment of indices of weight vector/matrices elements:

- The first index indicates the specific neuron destination for that weight.
- The second index denotes the source of the signal fed to the neuron.

In $w_{1,2}$, the indices therefore state that this weight reflects the relation from source two to neuron first [93].

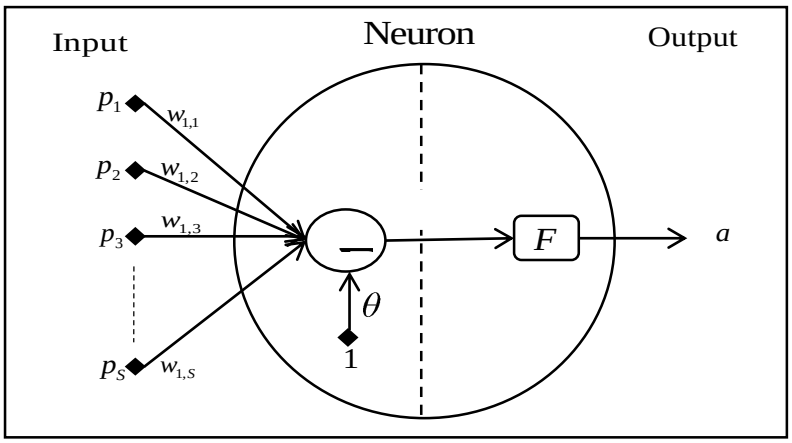

Figure 3.11. Multiple-input neuron.

3.2.2.2 Transfer Function

There are many types of transfer functions used as activation functions, such as sigmoidal (or log-sigmoid), hyperbolic (or tan sigmoid), linear (bipolar), threshold and Gaussian [95, 96]. The Choice of activation function plays an important role in the design of the neural networks. However, the most widely used function among the others is the sigmoidal, hyperbolic, and linear function activations. Examples of linear, sigmoidal and hyperbolic transfer function are shown in Figure.3.12 (a), (b) and (c) respectively [97, 98]. Linear function is described by equation (3.18), sigmoidal function is described by equation (3.19) and hyperbolic tangent sigmoid function is described by equation (3.20).

$$a = F(n) \tag{3.18}$$

$$a = F(n) = \frac{1}{1+e^{-\beta.n}} \tag{3.19}$$

$$a = F(n) = \frac{(1-e^{-\beta.n})}{(1+e^{-\beta.n})} \tag{3.20}$$

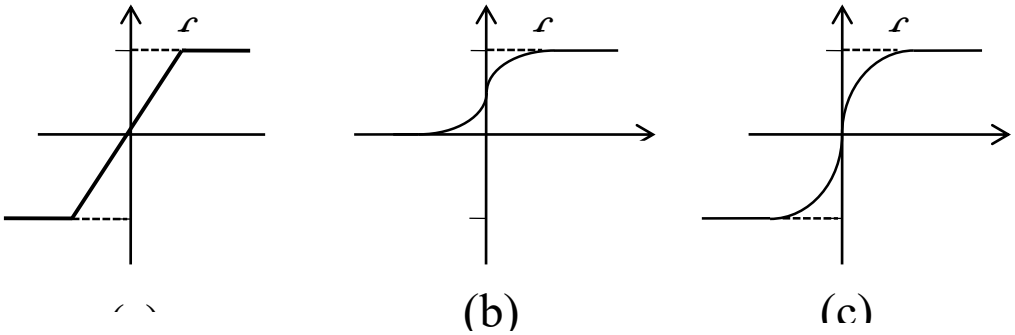

Figure 3.12. Transfer function: (a) linear bipolar, (b) Sigmoidal or log-sigmoid and (c) Hyperbolic tan or tansig.

3.2.2.2.1 A Single Layer of Neurons

In layered neural network, the neurons are arranged in layer form. In the simplest type of layered network, we have an input layer of source nodes projecting onto a neuronal output layer (computation nodes) [93, 99]. In Figure 3.13, a single layer of Q neurons is shown. Each element of the S-dimensional input vector is connected to each neuron and has Q rows and S columns in the weight matrix W. In one layer, all the neurons are of the same form as the single-neuron. Since the layer includes Q neurons, the output vector a, is also Q-dimensional and is calculated as [95, 96]:

$$a = F(W.p + \theta) \tag{3.21}$$

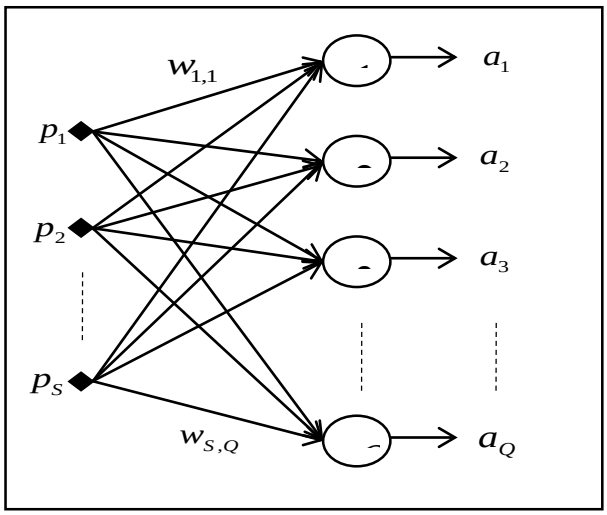

Figure 3.13. Single layer of neurons

Every neuron has a θ_i bias, a summer, a F transfer function and an a_i output. The outputs are taken together and form the output vector a .Typically, the number of inputs to a layer is different from that of neurons $(Q \neq S)$ [99, 100].

3.2.2.2.2 Multiple Layers of Neurons.

Networks with several layers are more powerful than a single layer of neurons. Every layer has its own weight matrix W , vector bias θ and vector output y .To differentiate between those layers, some additional notation should be added. Superscripts are used to identify those layers [101-102]. A three-layer network where this notation is used shown in Figure 3.14. There are S inputs, the first layer has Q neurons, the second layer has R neurons and the third layer has U neurons. The outputs of one layer become the inputs to the next layer, therefore the second layer can be considered as a single layer network with Q inputs, R neurons and a Q×R weight matrix. The method of forwarding one layer's outputs as inputs for the next layer can be written as[93-94]:

$$y^{m+1} = F(W^{m+1}.y^m + \theta^{m+1}) \tag{3.22}$$

For $m = 0,1,....,M-1,$ where M is the number of layers in the network and F is the transfer function.

The neurons of the first layer receive external inputs:

$$y^0 = p \tag{3.23}$$

The outputs of the neurons in the last layer are considered the network outputs:

$$a = y^M \tag{3.24}$$

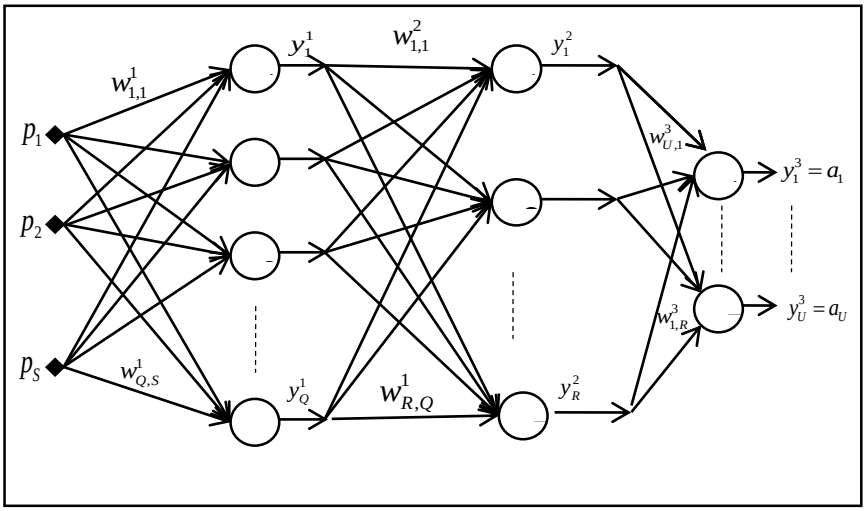

Figure 3.14. Three-layer network

A layer whose output is the output of the network is named output layer. The remaining layers are named hidden layers. The network shown in Figure 3.14 has an output layer (layer three) and two hidden layers (layers one and two) [94, 95].

3.2.2.3 Training Methods

A Training Dataset is used in all prediction methods. The dataset consists of a sub-set of the data we wish to model. The training can be divided into two groups based on the use of performance values during the training cycle [103, 104].Firstly, supervised training, in which the training set includes input features of the system and output results, which have been defined by another process. The supervised training scheme is shown in Figure 3.15. In this technique the learning algorithm aims to find a functional mapping between inputs and outputs by using the training data to determine the prediction technique's parameters (weights and thresholds) [103].

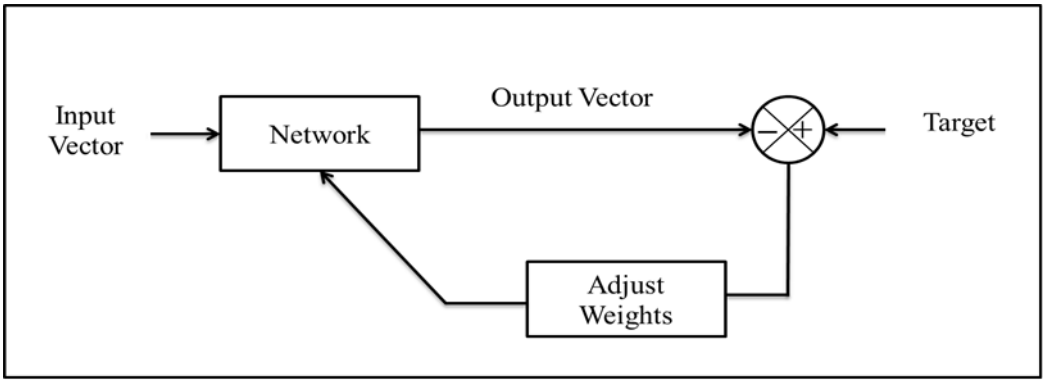

Figure 3.15. Supervise training scheme

During the training phase, the performance of the neural network model is evaluated and monitored through (error or output). This function compares the expected NN output to the actual output. ANN continues to train by iteration until the error value decreases to the desired value. Then, the ANN is tested using new data after the training is completed to determine the ANN's response and quality [104-105].

Secondly, unsupervised learning or self-organized learning, only input training data is required in this form of training. The idea is that similar kind of knowledge often yields to other output types. And the unsupervised methods are also only the initial step of a two-stage or more training cycle, subsequent phases requiring supervised learning, the first stage of training uses an unattended approach to assess the positions and sizes of the basic functions [104-105].The schematic diagram of the unsupervised learning method is shown in Figure 3.16.

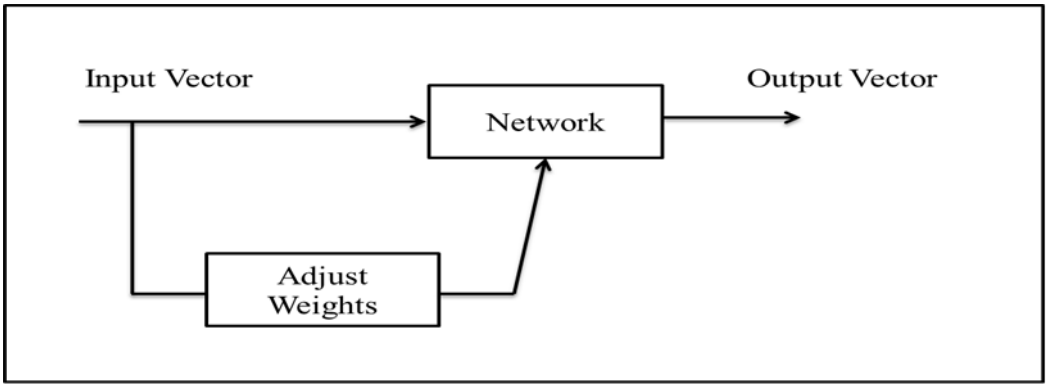

Figure 3.16. Unsupervised training scheme.

There are various types of algorithms are existed to train the ANN, such as back-propagation algorithm, Delta-bar-Delta, Quasi-Newton algorithm, conjugate gradient algorithm, Kohonen training and Levenberg-Marquardt algorithm [106, 107]. The Levenberg-Marquardt method is commonly recommended for training the multilayer feedforward network because of its robustness, and it provides rapid convergence and it is not mandatory for the user to configure any strange design parameters [106].

3.2.2.4 Neural network MPPT controller architecture

The proposed ANN in this study is a feed-forward neural network consisting of three layers, namely the input layer, the hidden layer and the output layers shown in Figure 3.17. The input layer consists the PV array current and voltage, while the output layer is the duty cycle signal that drives the power converter to operate at or close to the MPP based on the hidden layer algorithm. The link between nodes I and j is considered as having a w_{ij} weight in Figure 3.17. The technique for the neural network is based on changing layer weights in order to achieve the target values. During the training process, weights are adjusted to track the target values with minimum error [108, 109].

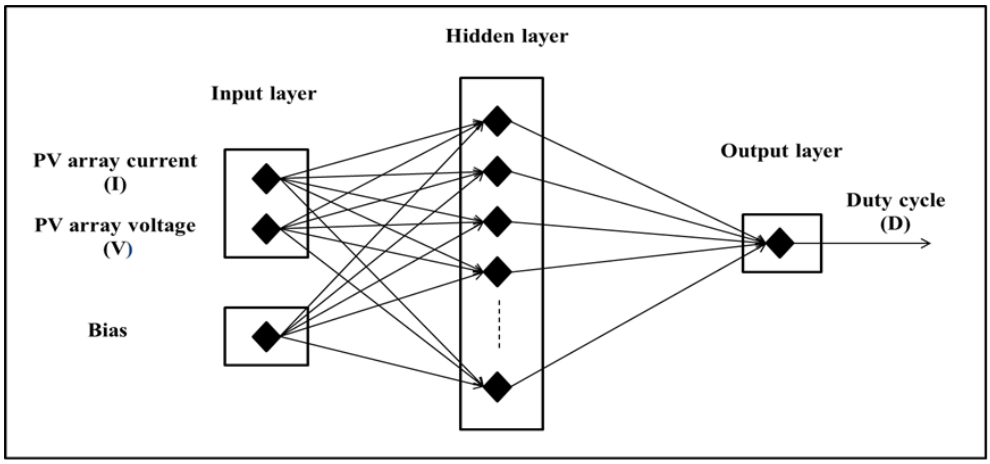

Figure 3.17. Feedforward neural network

However, the main drawback of this approach is that ANN must be trained for the PV array in use and therefore cannot be extended to operate on many forms at the same time unless it is qualified to do so. In addition, the characteristics of the PV array shift over time, which requires the periodic training of the ANN for accurate monitoring of

the MPP. This method requires an expensive microprocessor to be used and is therefore not appropriate for small applications [110, 111].

3.2.2.4.1 Training the network

The training process defines the weights of neural network connections. The method of training used in this work is the supervised approach. Therefore, to accomplish this process a set of input output pairs of the training patterns or training data are required [112].

After setting the number of inputs, the number of hidden layers, and the number of neurons in each hidden layer, we can train the given ANN model during the offline process. First, we need to obtain a range of training patterns (including the measured voltage and current or irradiance and the global maximum power point GMPP obtained via the P–V curve) that will cover potential operating conditions [114, 113].

To perform the training process, a neural network toolbox in MATLAB software has been used, all of the computations are performed offline during the network preparation. In this work the backpropagation algorithm with the optimization method Levenberg-Marquardt is used. Due to its ease of implementation, robustness and stability, this method is considered one of the most commonly used feedforward ANN training algorithms. The network's learning stage is carried out by updating the weights and biases with the Levenberg-Marquardt optimization method using a backpropagation algorithm to minimize a mean squared error output index E given by equation (3.25). The lower the mean square error is, the higher the real-life efficiency and accuracy the network achieves [112, 115].

$$t_{pj}\, E_p = \frac{1}{2}.\sum_j (t_{pj} - o_{pj})^2 \qquad (3.25)$$

Where, p is the index of the output neurons, o_{pj} is the measured output of the outputs and t_{pj} is the desired output of the output neurons.

Multilayer perceptron neural network performance measured as mean square error (MSE) can be calculated by equation (3.26).

$$E = \sum_{p=1}^{m} E_p \tag{3.26}$$

A flowchart, shown in Figure 3.18, presents the methodology of the training process of the ANN for MPPT.

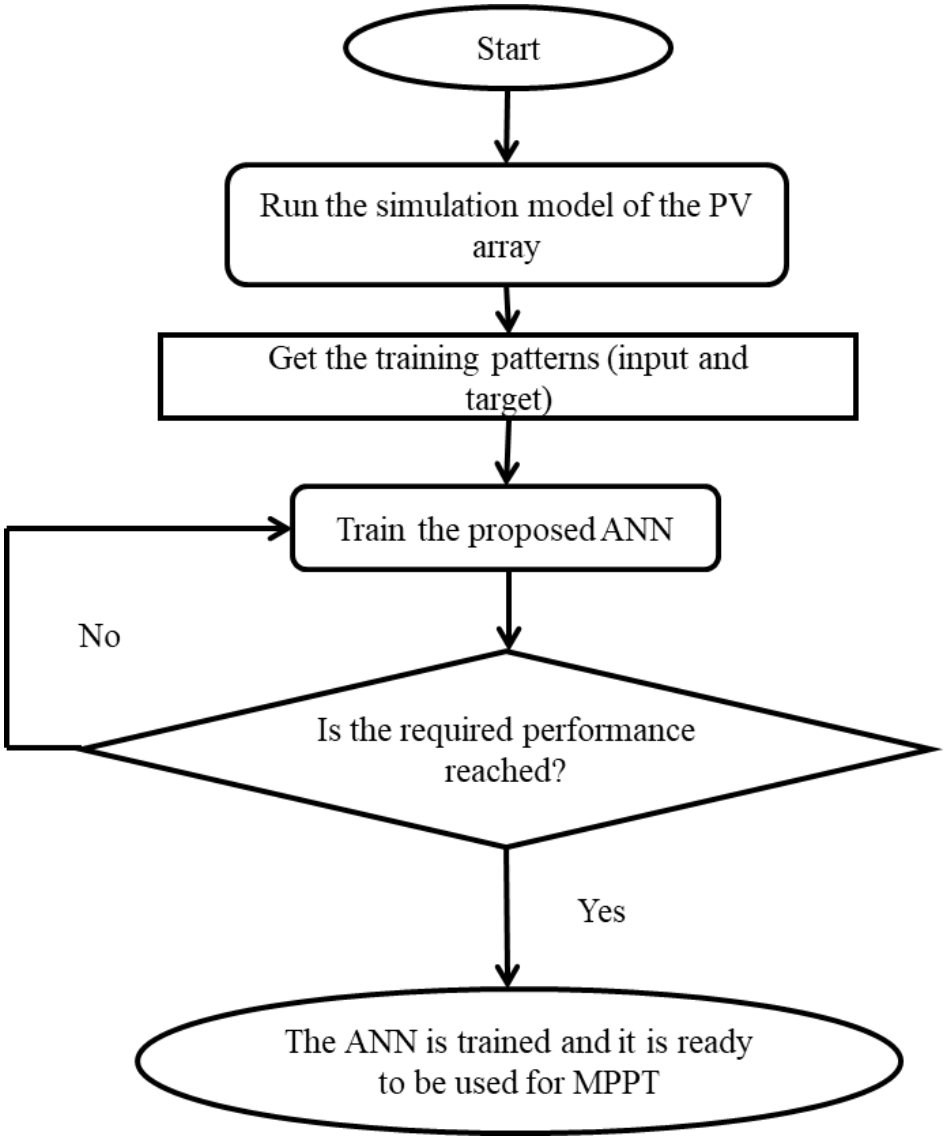

Figure 3.18. Flowchart of the training process of the ANN for MPPT

3.3 Conclusion

This chapter presents a discussion of the selection of the strategy and modelling of the artificial intelligence (AI) systems based MPPT control for the PV array. The chapter begins with a brief introduction of AI systems and the reasons why we use this technology. Then, the control which has the role of maximum power point tracking based on advanced techniques such as fuzzy logic and artificial neural network.

Chapter 04

4 Chapter 4: Hybrid MPPT Techniques

4.1 Introduction

Hybrid MPPT techniques are proposed to improve the tracking performance and to add more accuracy and efficiency to the individual MPPT techniques by incorporating their advantages and eliminating their drawbacks. This method is divided into two stages each one is based on different MPPT technique.

Since P&O MPPT technique has several drawbacks such as the oscillation around MPP and poor tracking performance in the existence of noise, Artificial Intelligence techniques such as Logic controller(FLC) have been introduced to overcome these limitations, this latter proves its efficiency during the tracking process especially in sudden change in the weather conditions, however it exhibits some limitations such as expert knowledge requirement, there Adaptive P&O-Fuzzy Control MPPT comes as a solution to eliminate the drawbacks of P&O and FLC MPPT techniques and integrate their benefits by offering high accuracy, stability, simplicity and fast response even in existence of noise

The Adaptive-Neuro Fuzzy Inference system (ANFIS) based MPPT controller is a hybrid method that combines the benefits of Fuzzy Logic controller (FLC) and Artificial Neural Network (ANN) in treating and learning nonlinear data with high accuracy and efficiency, hence ANFIS controller provides flexibility, fast response and stable steady under various weather conditions.

4.2 Adaptive P&O-Fuzzy Control MPPT

4.2.1 Review on conventional P&O MPPT

Perturb and Observe (P&O) algorithm starts its functionality by sensing the values of the current (I_{PV}) and the voltage (V_{PV}) to calculate the value of PV power (P_{PV}). During every iteration the operating voltage is perturbed (incremented or decremented), then the current values of the PV power and PV voltage are compared with the previous ones until the MPP is reached where the operating point starts the oscillation around the MPP [116, 117, 118, 119, 120].

Despite its simplicity and the ease of implementation, P&O algorithm shows a slow tracking speed when the step size is small, while in the case of a large step size the tracking speed is faster however it leads to high oscillation during steady state, besides it exhibits a low tracking performance during the existence of noise [121, 122].

4.2.2 Review on Fuzzy Logic Controller basest MPPT

Fuzzy logic controller based MPPT is proposed as a solution to overcome the limitations of conventional MPPT controllers and to improve the tracking performance. This technique uses as inputs the error (E) and the change in the error (ΔE), while the output is the duty cycle (D). FLC is divided into three phases, during the first phase which called the fuzzification phase, the crisp inputs are converted into linguistic variables based on membership functions, while in the next stage the output is generated by applying the rule base where Mamdani inference method is used, and in the final stage the fuzzy output is converted back to crisp value [123, 124, 125].

FLC provides a high tracking performance by offering fast convergence and accurate output, however it exhibits some limitations such as the oscillation during low levels of irradiation and the expert knowledge requirement [125, 126].

4.2.3 Adaptive P&O-Fuzzy Control MPPT

Adaptive P&O-Fuzzy Control MPPT is proposed to overcome the drawbacks of FLC and P&O algorithms, and to combine the benefits of both of these methods such as simplicity, fast response, less depending on expert knowledge and good tracking performance in the existence of noise [127, 128]. This technique uses the same inputs of P&O method which are the differential power ΔP and differential voltage ΔV as it is shown in Figure 4.1, however it replaces the comparing and switching methods of P&O technique with fuzzy logic technique where its four categories stay the same with new inputs are used as it is shown in Figure 4.1. Five proposed fuzzy sets for input/output variables are N (Negative), ZE (Zero), PS (Positive small), P (Positive), and PB (Positive big). During its operating process FLC varies the value of according to the values of ΔV and ΔP [123, 126, 129, 33].

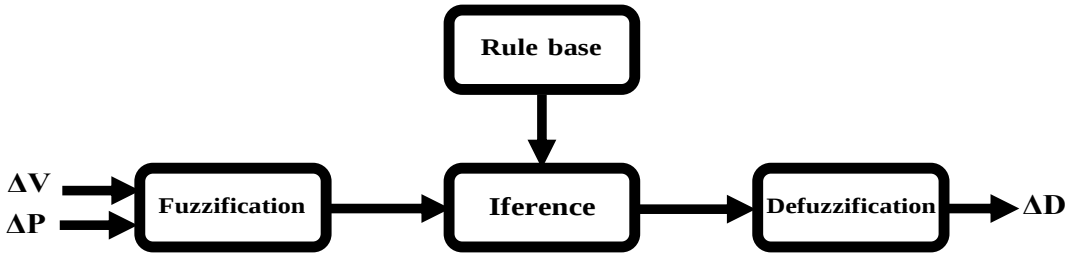

Figure 4.1. Block diagram of FLC MPPT algorithm

The FLC is consists of three major phases as it is describes below:

4.2.3.1 Fuzzification

The inputs ΔP and ΔV which are a numerical values are converted into linguistic values where the membership functions are generated as it is displayed in Figure 4.2 [123, 124, 126, 129, 130].

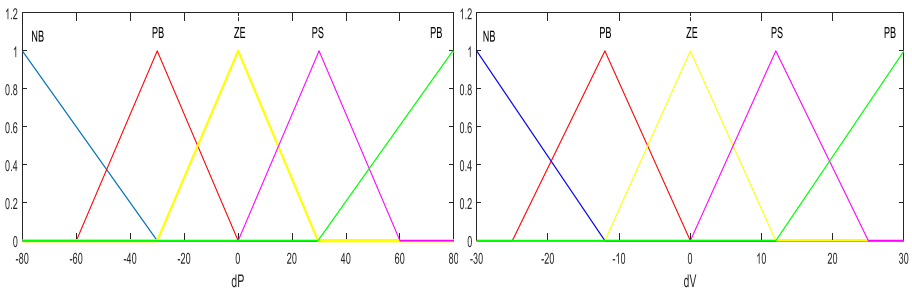

a) b)

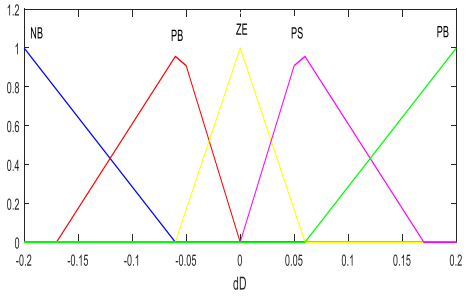

c)

Figure 4.2. Membership functions for (a) input of ΔP, b) input of ΔV and (c) output of ΔD

4.2.3.2 Inference

During inference stage the output ΔD is generated using the rube base given in the Table 1 where Mamdani inference system is used [123, 124, 126, 129, 130].

Table 4.1. Rules Based for Adaptive P&O-Fuzzy MPPT.

ΔP / ΔV	N	ZE	PS	P	PB
N	ZE	PS	P	PB	PB
ZE	ZE	ZE	PS	P	PB
PS	N	ZE	ZE	PS	P
P	N	N	ZE	ZE	PS
PB	N	N	N	ZE	ZE

4.2.3.3 Defuzzification

In the defuzzification stage the outputs of all the rules are aggregated and the common centroid of area (COA) is used to transform the fuzzy output to a crisp value [124, 126, 129].

The Figure.4.3 describes the flowcharts of both P&O and Adaptive P&O-Fuzzy MPPT.

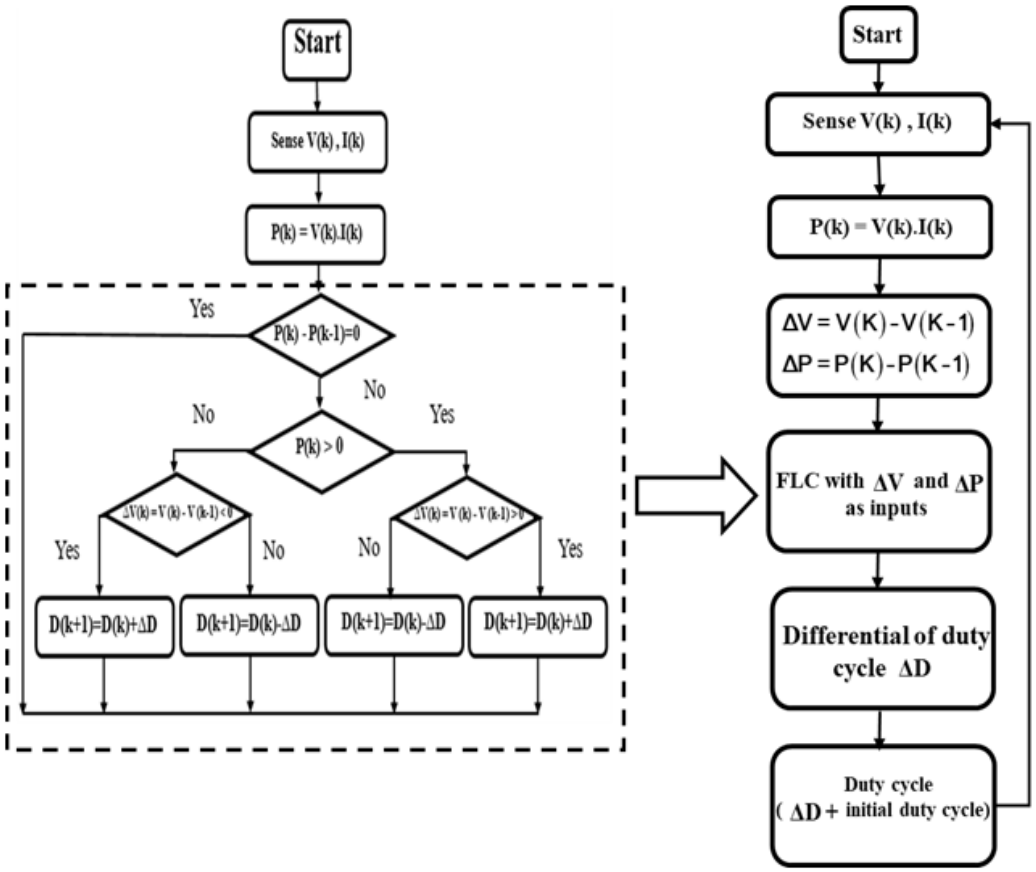

Figure 4.3. Comparison flow chart between P&O and adaptive P&O-fuzzy MPPT.

4.3 Adaptive Neuro Fuzzy Inference System (ANFIS)

4.3.1 Architecture of Adaptive Neuro Fuzzy Inference System (ANFIS)

The Adaptive-Neuro Fuzzy Inference system (ANFIS) is a hybrid method that combines the benefits of two artificial intelligence techniques, Artificial Neural Network (ANN) and Fuzzy Logic (FL) [131, 132, 133, 134]. To construct the mapping relation between the input and output data, this technique uses a hybrid learning method to set the fuzzy if-then rules and tunes the parameters of membership functions.[132, 133, 134, 135, 136, 137].

For simplicity, it is assumed that fuzzy inference system has two inputs (X and y) and one output Z . Moreover the rule base contains two fuzzy if-then rules of Takagi and Surgeon's type where the consequent is given as a function of the antecedent (the output has a linear relation to the input) [132, 135].

Rule 1 : If x is A_1 and y is B_1 , then $f_1 = p_1x + q_1y + r_1$ (1.1)

Rule 2 : If x is A_2 and y is B_2 , then $f_2 = p_2x + q_2y + r_2$ (1.2)

Where $p_1, q_1, r_1, p_2, q_2, r_2$ are the consequent parameters.

A_1 and B_1 are the membership functions for the input x .

A_2 and B_2 are the membership functions for the input y .

The general ANFIS architecture as it shown in Figure.4.4 **i**s consists of five layers as described below.

4.3.1.1 Layer 1: Fuzzification layer

Every node in this layer is an adaptive (square) node with a node function [131, 135, 137, 138, 139, 140, 141, 142].

$$O_i^1 = \mu_{A_i}(x) \quad \text{for} \quad \text{i=1, 2} \tag{1.3}$$

$$O_i^1 = \mu_{B_{i-2}}(y) \quad \text{for} \quad \text{i=3, 4} \tag{1.4}$$

Where:

O_i^1 : Membership value for the crisp value.

μ : Membership function.

1: Indicates the layer number.

i : Indicates the node number.

The membership function μ can be exhibit in several forms, however the bell-shaped is the most widely used shape as it is given in the equation (1.5) [1, 5, 7, 9, 10, 11, 12, 13].

$$\mu_{A_i}(x) = \frac{1}{1 + \left[\left(\frac{x - c_i}{a_i}\right)^2\right]^{b_i}} \tag{1.5}$$

Where $\{a_i, b_i, c_i\}$ are the parameters set.

4.3.1.2 Layer 2 : Product layer

Every node in this layer is a fixed (circle) node labeled $\prod$, where the output is the product of all the incoming signals from the first layer, as given in equation (1.6) [131, 135, 137, 138, 139, 140, 141, 142].

$$O_i^2 = w_i = \mu_{A_i}(x) \times \mu_{B_i}(y) \quad \text{for} \quad \text{i=1, 2} \qquad (1.6)$$

Each node output represents the firing strength of a rule, while the node function in this layer is usually can be computed using T-norm operator that performs AND operator [131, 135, 137, 138, 139, 140, 141, 142].

4.3.2 Layer 3 : Normalized layer

Every node in this layer is a fixed (circle) node labelled norm (N), where the firing strength of each node is normalized by dividing the rule's firing strength by the sum of all rules 'firing strengths, as it is displayed in the following equation [1, 5, 7, 9, 10, 11, 12, 13].

$$O_i^3 = \overline{w}_i = \frac{w_i}{w_1 + w_2} \quad \text{for} \quad \text{i=1, 2} \qquad (1.7)$$

Each node output represents the normalized firing strength of a rule.

4.3.2.1 Layer 4: Defuzzification layer

Every node in this layer is an adaptive node where the node function is shown in the equation (1.8)[131, 135, 137, 138, 139, 140, 141, 142].

$$O_i^4 = \overline{w}_i f = \overline{w}_i (p_i x + q_i y + r_i) \quad \text{for} \quad \text{i=1, 2} \qquad (1.8)$$

Where $\overrightarrow{w_i}$ is the output (normalized firing strength) of layer 3, and $\{p_i, q_i, r_i\}$ are the parameters set which are will be referred to as consequent parameters and required to be optimized during learning process [131, 135, 137, 138, 139, 140, 141, 142].

4.3.2.2 Layer 5: Output layer

The fifth layer contains only one final node which is a fixed node labeled $\sum$. The output of this layer represents the summation of all the incoming signals as it is shown in the following expression [[131, 135, 137, 138, 139, 140, 141, 142].

$$\text{overall output} = O_i^5 = \sum_i \overline{w}_i f_i = \frac{\sum_i w_i f_i}{\sum_i w_i} \tag{1.9}$$

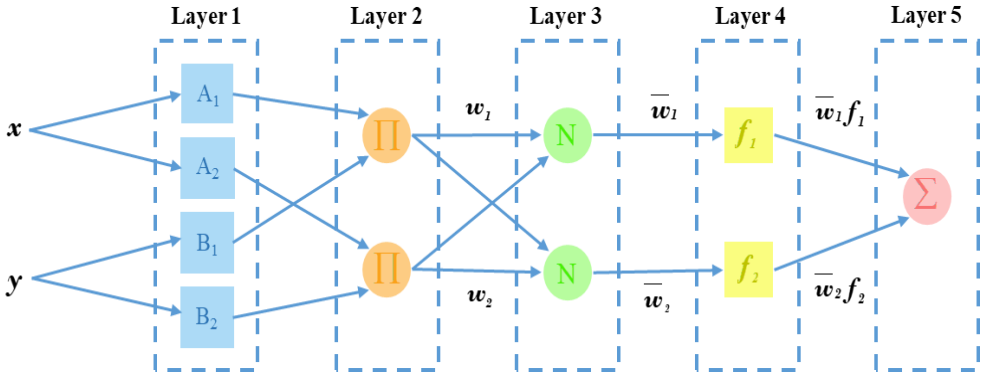

Figure 4.4. ANFIS structure

4.3.3 Hybrid learning method

In order to adjust the parameters of ANFIS approach automatically during every input-output dataset and speed up the learning process, Jang [135] proposed a hybrid learning method that allows to ANFIS to generate the appropriate membership functions with an optimal fuzzy rule set [135, 137, 144, 145, 146]. The hybrid learning algorithm used by ANFIS controller combines back-propagation (BP) method and least square estimation (LSE) during two passes forward pass and backward pass [131, 134, 135, 137, 144].

In forward pass the functional signals propagate forward to compute every node output until the layer 4, where the (LSE) algorithm is used to identify the consequent (linear) parameters [5, 7, 12, 143, 144].

In backward pass the error signals propagate from the output toward the input, where the premise (nonlinear) parameters are updated using gradient descent method [135, 137, 141, 143, 144].

4.3.4 Design and implementation of ANFIS based MPPT

ANFIS based MPPT technique is introduced to control the nonlinear characteristics of the PV system [133, 137], where the current (I_{PV}) and the voltage (V_{PV}) represent the inputs while the duty cycle (D) is taken as output. In order to train ANFIS controller, 1000 Training datasets were collected from previous results obtained from operational experiences using Matlab /Simulink model of conventional MPPT technique [133, 136], these data sets are used as prior knowledge to generate for this case five triangle membership functions for each input and set the appropriate fuzzy If-Then rules to produce the optimal output. During learning process ANFIS controller keep adjusting the parameters of membership functions until the error is reduced, once this phase is done, this controller uses checking data to make sure the produced error is the optimal error [134, 147, 148] .

ANFIS controller proves its flexibility, accuracy, fast convergence and low oscillation under various atmospheric conditions.

The flowchart of the (ANFIS) algorithm is shown in the Figure.5.5.

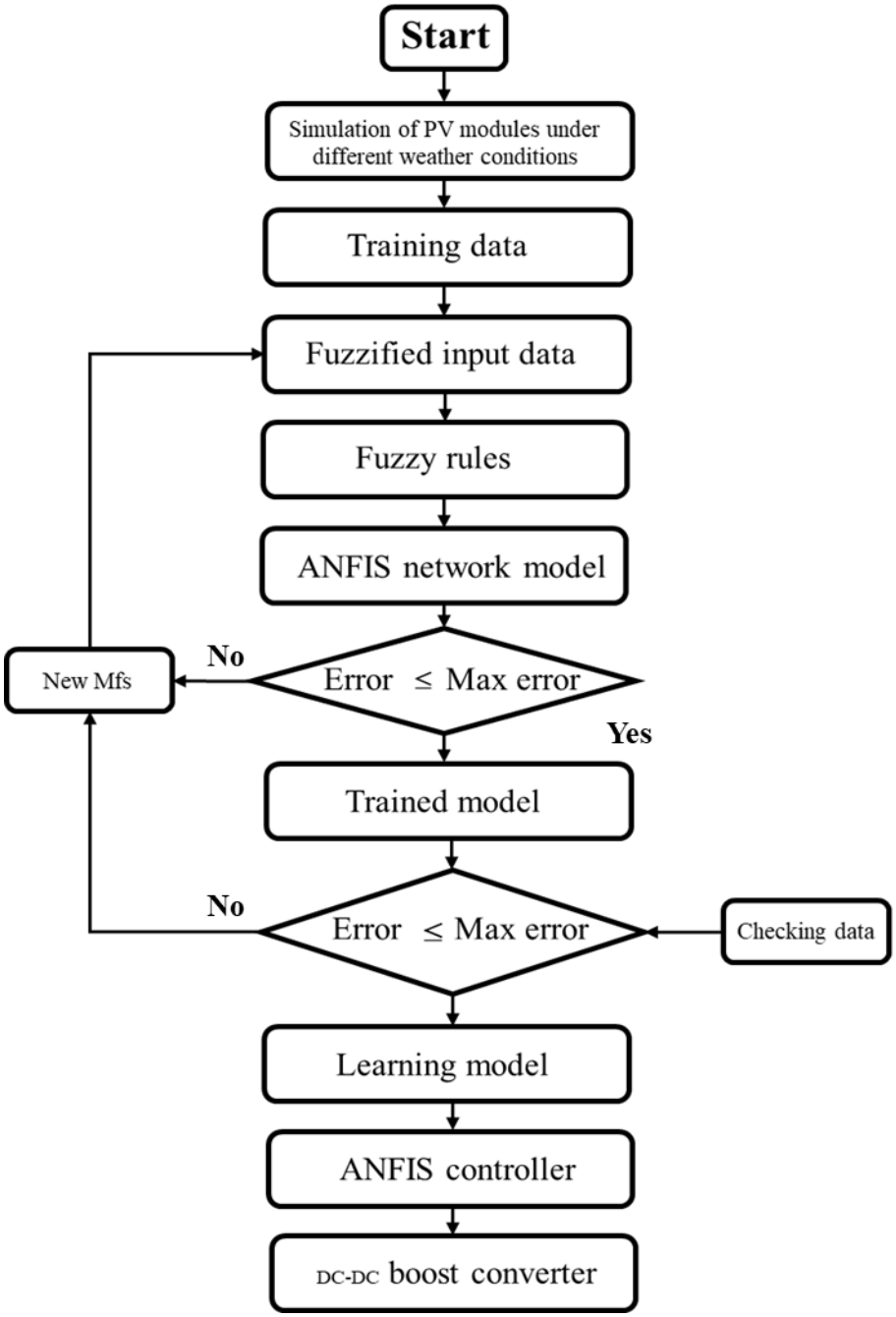

Figure 4.5. ANFIS based MPPT implementation flowchart..

4.4 Conclusion

This chapter discussed two types of hybrid MPPT techniques, ANFIS controller and Adaptive P&O-Fuzzy Control MPPT which combine the benefits of two individual MPPT techniques to form a new efficient controller. These techniques successfully maintained maximum power generated by the PV module by offering fast and accurate response and low oscillation under different weather conditions.

Chapter 05

5 Chapter 05 : Simulation and Results

5.1 Introduction

The use of simulation is a very important step in the study of PV systems, it allows to modify the system parameters very easily (such as irradiance for example) and to test the performance of the optimization methods under different conditions.

This chapter describes how the SIMULINK models of the proposed PV power systems are implemented to test and verify the functionality of the proposed MPPT controls. In this work, different PV systems are implemented in MATLAB/SIMULINK environment. These systems are classified into traditional tracking algorithms (P&O, P&O variable step and INC), artificial intelligence methods (FLC and ANN) and hybrid techniques (ANFIS and Adaptive P&O-Fuzzy).Furthermore, a comparison has been carried out between the proposed controllers by way of simulation results. The simulation is run with variable-step solver for the sake of accuracy. The solver integration method used was the (ode45).

5.2 System Design and Simulation

The designed system was simulated in the MATLAB/SIMULINK environment. The complete SIMULINK model of the proposed system is illustrated in Figure.5.1.The modeled system consists mainly of PV array model, DC/DC boost converter model used to interface PV output to the resistive load and MPPT controller to track the maximum power of the PV array. To perform the tracking of maximum power, a traditional tracking algorithms (P&O, P&O variable step and INC), artificial intelligence methods (FLC and ANN) and hybrid techniques (ANFIS and Adaptive P&O-Fuzzy) have been implemented.

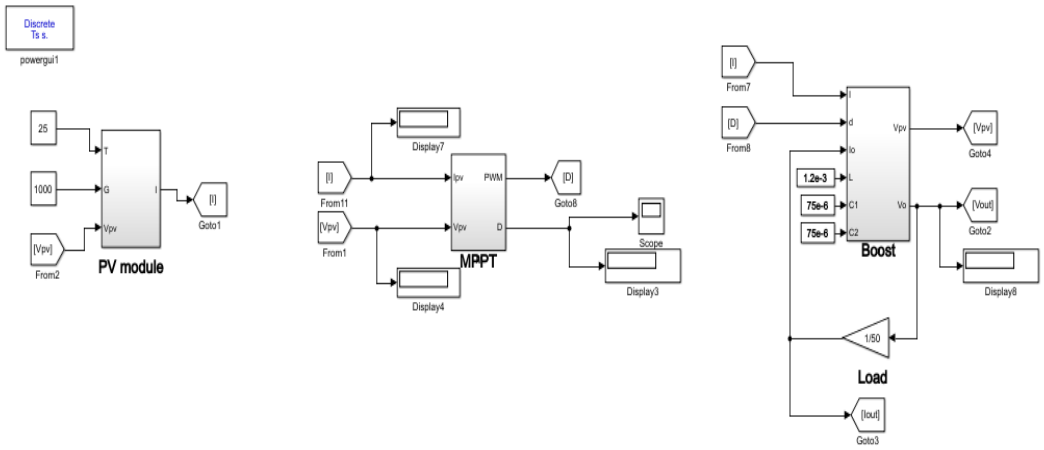

Figure 5.1. SIMULINK model of PV system.

5.2.1 PV Model Simulation and Validation

The simulation of PV model was implemented in MATLAB based on Equation (3.15). The code was electrically designed as a voltage-controlled current source in the Embedded MATLAB Function. The PV voltage V_{pv}, irradiation G and temperature T are fed to the Embedded MATLAB Function and the output is the current produced by the panel.

The PV generator is a module of MSX-60 type, which delivers a maximum of 60Wconnected in 18×2 matrix. To validate the model, usually standard conditions specified at irradiation and temperature ($G = 1000 W/m^2$ and $T = 25°C$).The datasheet of this generator provides the parameters regarding to the characteristic and performance of PV panel under standard test conditions. The parameters of PV panel used in this work are listed in the table 5.1.

Table 5.1. Electrical characteristics data of MSX-60module

PV panel parameters	**Values**
Maximum power, P_{max}	60W
Maximum power voltage, V_{MP}	17.1V
Maximum power current, I_{MP}	3.5A
Short-circuit current, I_{SC}	3.8A
Open-circuit voltage, V_{OC}	21.1V
Voltage/temp. coefficient, K_V	−0.38%/°C
Current/temp. coefficient, K_I	0.065%/°C
The number of cells, N_S	36

The simulated model's output characteristics were compared with the characteristics provided by the manufacture's datasheet as shown in Figure 5.2-a.It was simulated under various temperature ranges to further test the model's accuracy, and results of the I-V characteristics are shown in Figure 5.2-2.The model offers a high degree of accuracy when simulating a PV panel’s behavior.

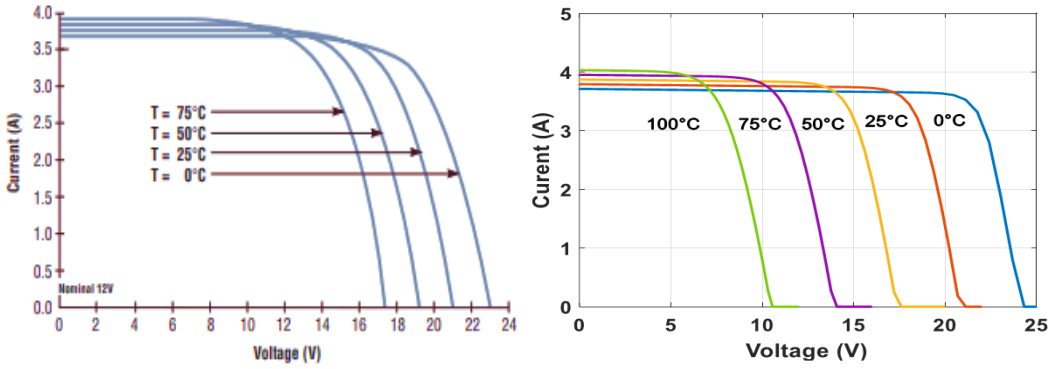

a) **b)**

Figure 5.2. Output characteristic of MSX-60 panel, a) Real production, b) simulated production.

5.3 Boost Converter Design

The approach to mathematical modeling involves a graphical implementation system in which data flow is drawn in SIMULINK platform. Actually, it connects the differential equation to model the boost converter system as shown in Figure 5.3 in a graphical way.

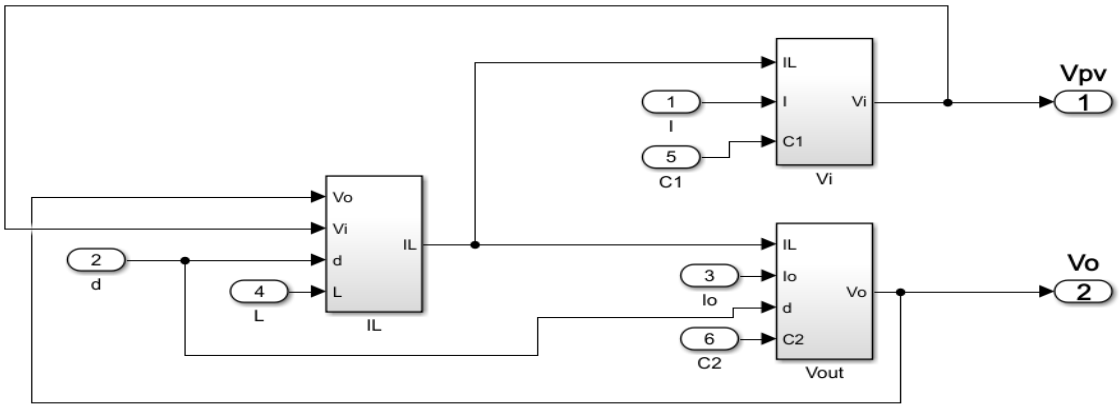

Figure 5.3. Mathematical simulation model of DC-DC boost converter.

There are six inputs and two outputs in the boost converter subsystem block as shown in Figure 5.3. The input terminal *d* represents the gate signal from the Pulse Width Modulation block, I_{pv} and V_{pv} are the input current and input voltage

respectively. I_o and V_o are the output current and output voltage respectively L, C_1 and C_2 are the input inductor, input capacitor and output capacitor respectively.

Table 5.2 lists the parameters of the boost converter components.

Table 5.2. Boost parameters

Parameters	Values
L	1.2 mH
C_{in}	75 μF
C_O	75 μF
F	10 KHz
R	50 Ω
α_{MPP}	0.69

5.4 The MPPT Controllers

5.4.1 Conventional MPPT Techniques

5.4.1.1 The P&O Controller

The Simulation model for P&O technique as implemented in MATLAB/SIMULINK, since it is standalone only DC/DC converter and MPPT module is used to connect load terminals. The MPPT simulation block corresponding to the algorithm is as per in Figure 5.4.

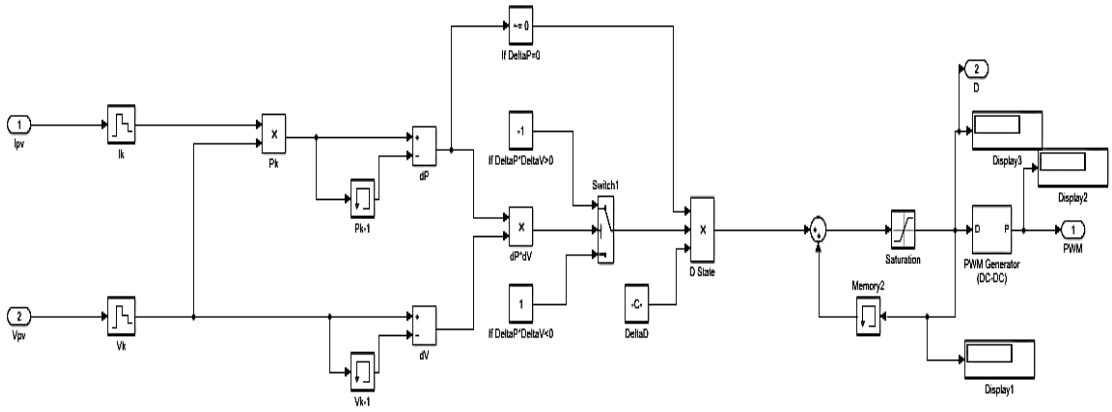

Figure 5.4. *Simulink Block diagram of P&O MPPT Controller.*

5.4.1.2 The INC Controller

The INC algorithm was simulated and performed with a DC-DC boost converter in MATLAB/ SIMULINK. The simulation block corresponding to this algorithm is shown in Figure 5.5.

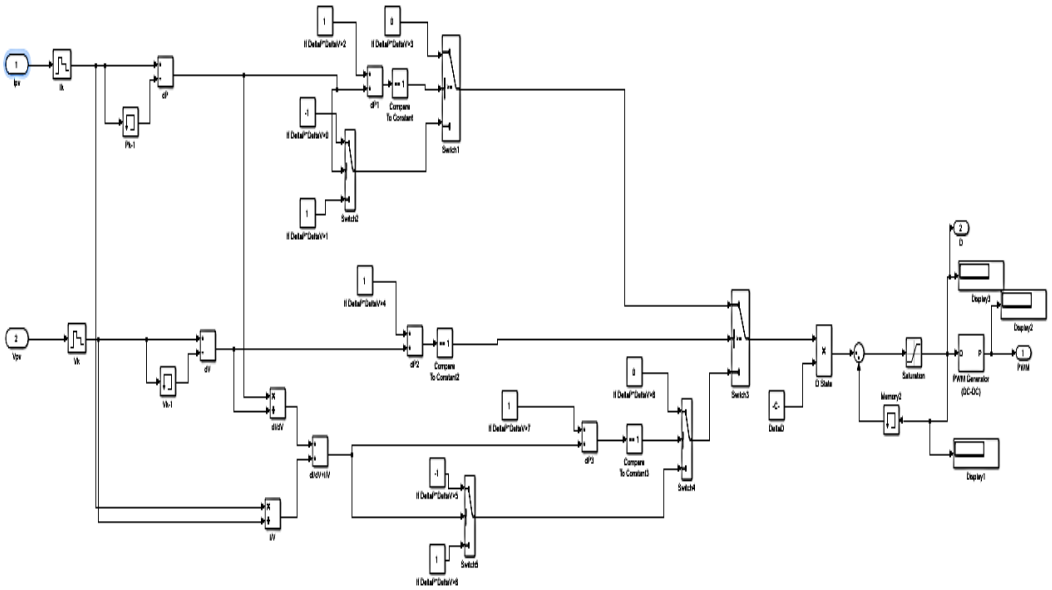

Figure 5.5. Simulink Block diagram of INC MPPT Controller.

5.4.1.3 The Variable Step-Size P&O Controller

The simulations provide a useful opportunity to test the feasibility and efficiency of the proposed variable step-size P&O algorithm. For evaluation and comparison

analysis, the simulation studies were performed under steady-state and dynamic conditions for the proposed variable step-size P&O and conventional P&O by configuring simulations under exactly the same conditions. The variable step-size P&O algorithm was written as M-file code in an embedded MATLAB function.

5.4.2 Artificial Intelligence MPPT Techniques

5.4.2.1 The Fuzzy Logic Controller

Figure 5.6 shows the fuzzy logic diagram as implemented in MATLAB/ SIMULINK.

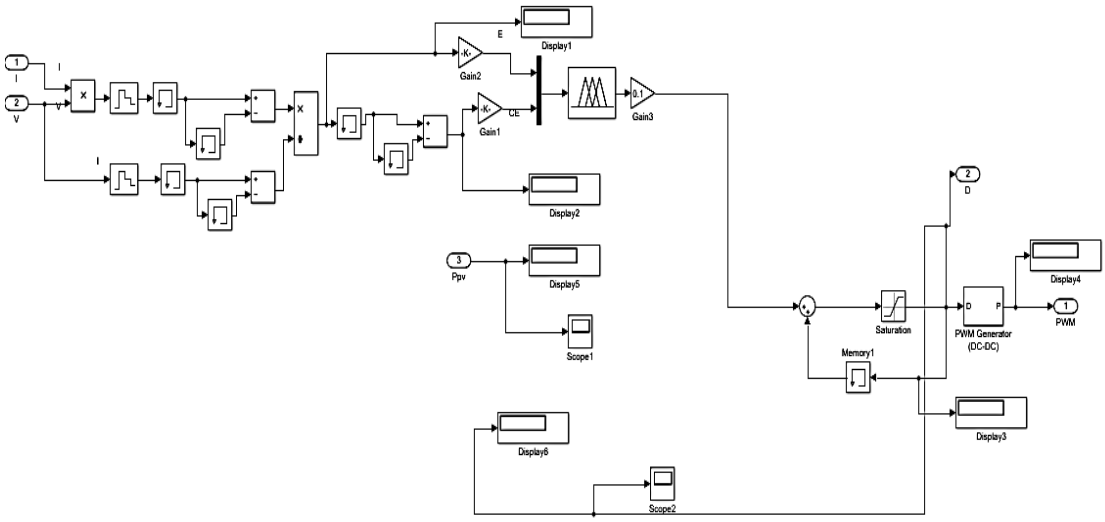

Figure 5.6. Simulink Block diagram of Fuzzy Logic Controller.

In MATLAB/SIMULINK, the FL Controller was implemented using the available Fuzzy Logic Toolbox. The FLC has been designed using a Graphical User Interface (GUI) tool provided by MATLAB/SIMULINK in fuzzy logic toolbox to facilitate the design of the controller.

5.4.2.2 The ANN Controller

To verify the functionality and performance of the proposed ANN based MPPT, the system was implemented in MATLAB/SIMULINK. The training phase is an indispensable task to adjust the parameters of the ANN structure in order to get the best output from NNSTART of MATLAB software is used for ANN training as shown in Figure 5.7.

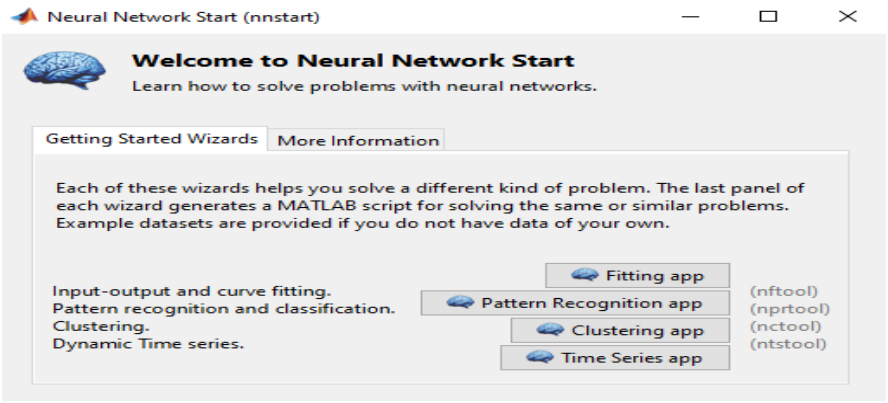

Figure 5.7. ANN training tool NNSTART.

In this work the training data has been divided into three parts, of which 70% is used for training, 15% for validation, and 15% for testing. During the training phase the network weights and biases are adjusted iteratively to reduce the network performance error. The average square error against different epoch for training process is shown in Figure 5.8.

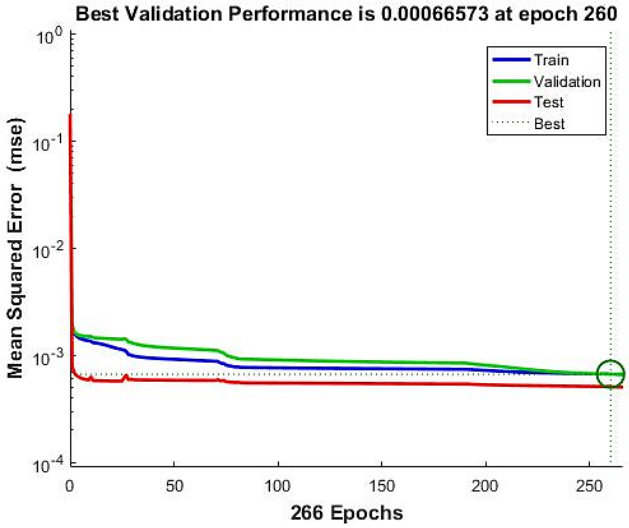

Figure 5.8. Mean squared Error (MSE) performance.

To test the response of network, the test data set are put through the network and will perform a linear regression between the network outputs and the corresponding targets. Then, between the network answer and the corresponding targets, a regression analysis is performed. The output (predicted duty ratio) and the corresponding network targets (calculated duty ratio) are then transferred to the linear regression analysis method. It yields three different parameters as shown in Figure 5.9.

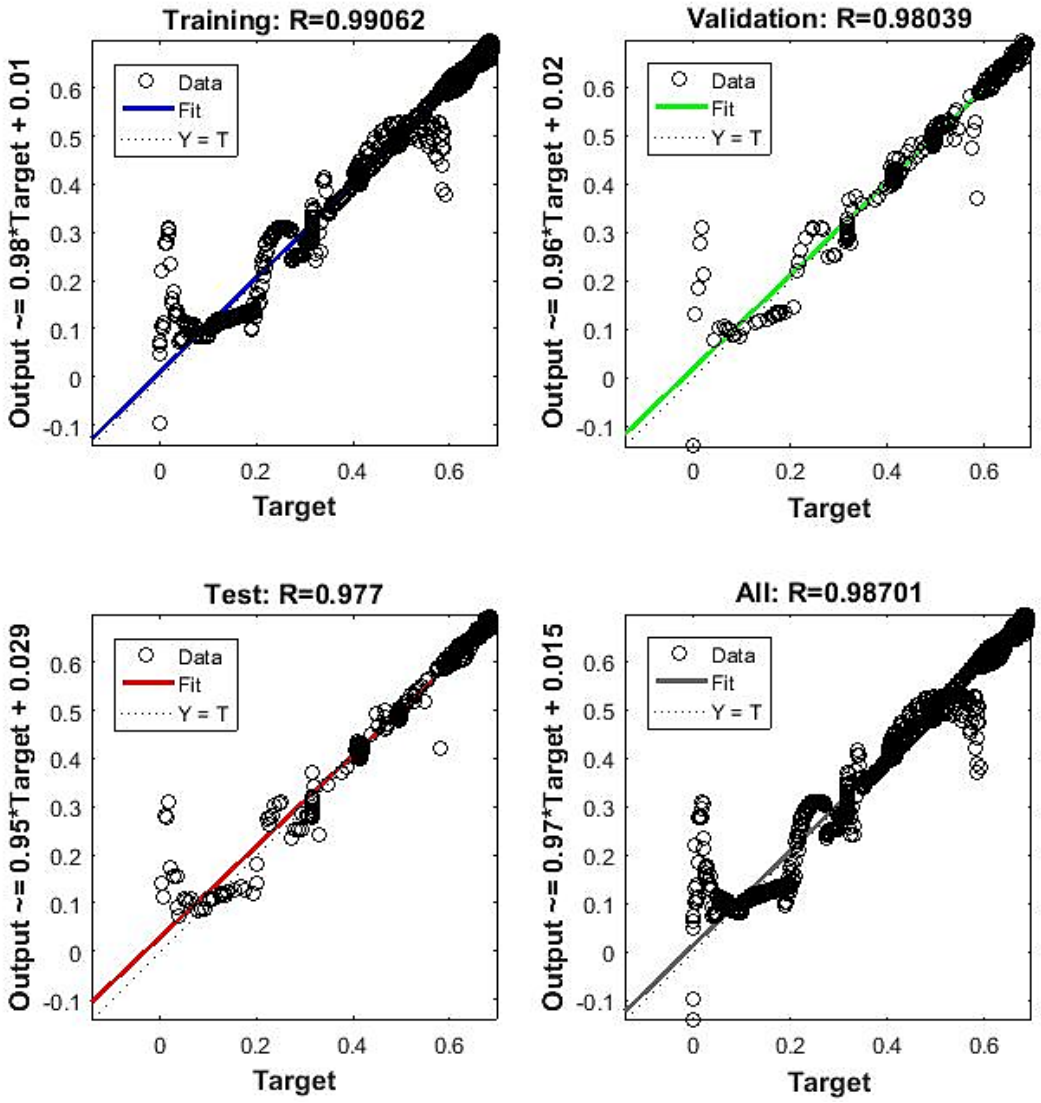

Figure 5.9. Network performance analysis.

5.4.3 Hybrid MPPT Techniques

5.4.3.1 The Adaptive P&O-Fuzzy Controller

The Adaptive P&O-Fuzzy algorithm was implemented in MATLAB/SIMULINK. The algorithm comprises two blokes, the conventional P&O algorithm and FLC. The conventional P&O was written as M-file code in an embedded MATLAB function. The FLC was implemented in a similar manner as mentioned in section5.3.2-a.

5.4.3.2 The ANFIS Controller

To verify the functionality and performance of the proposed ANFIS based MPPT, the system was implemented in MATLAB/SIMULINK. To generate a Sugeno-type

fuzzy inference system (FIS) structure ANFISEDIT is used in MATLAB toolbox to produce a FIS structure as shown in Figure 5.10.

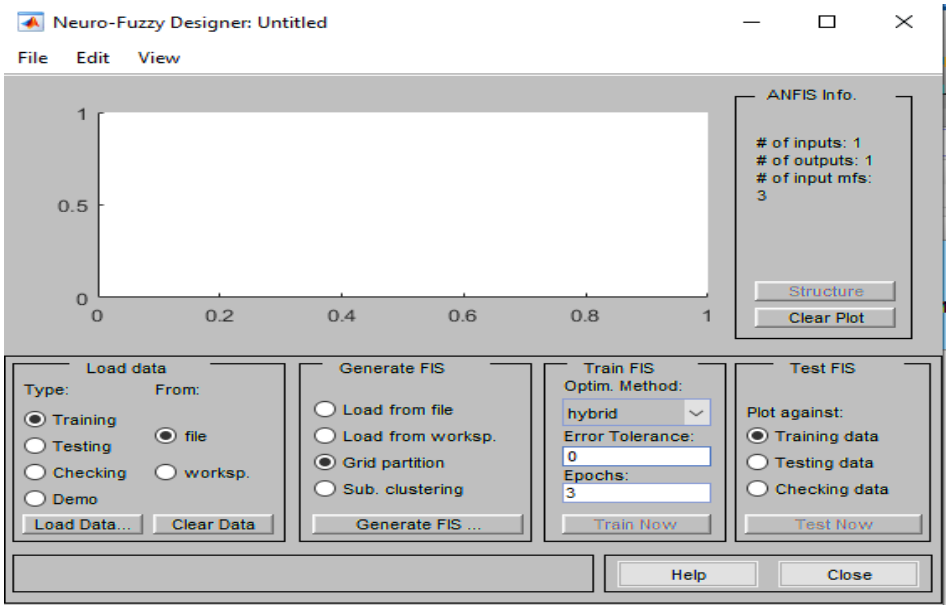

Figure 5.10. Network performance analysis.

The membership function of single output is identified by the Hybrid learning algorithm. The ANFIS reference model is trained on about 100 epochs. The result of training ANFIS network using 5000 data set is shown in Figure 5.11.

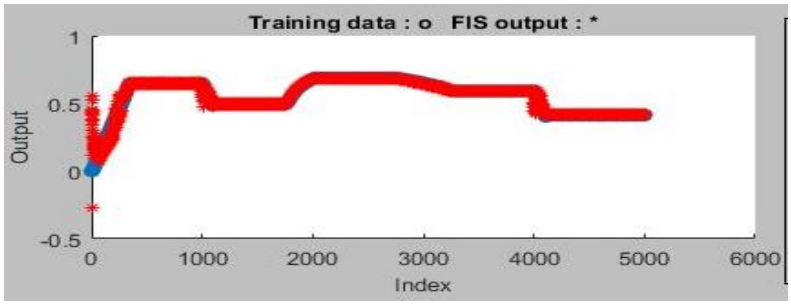

Figure 5.11. Training error versus epochs for the ANFIS.

5.5 Simulation results of the MPPT techniques

5.5.1 Under STC

The first simulation aims to show the ability of the MPPT controller to find and track the maximum power point under standard conditions ($G = 1000 W/m^2$ and $T = 25°C$) using all the previously studied MPPT algorithms as shown in Figure 5.12-17.

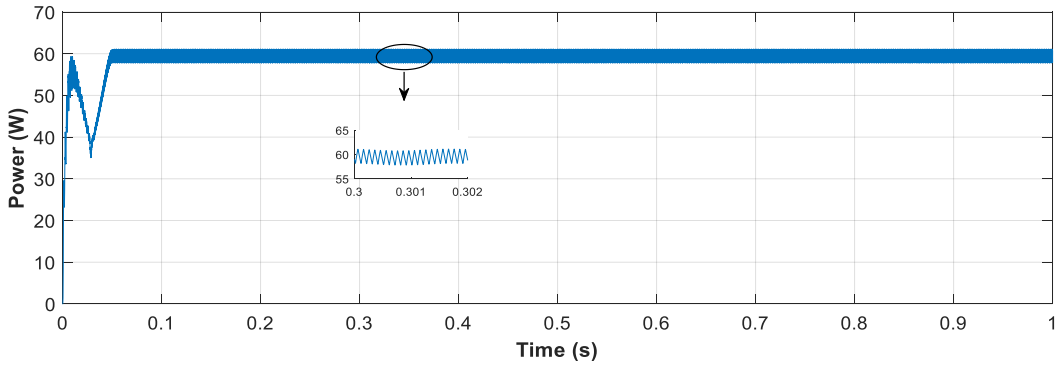

a)

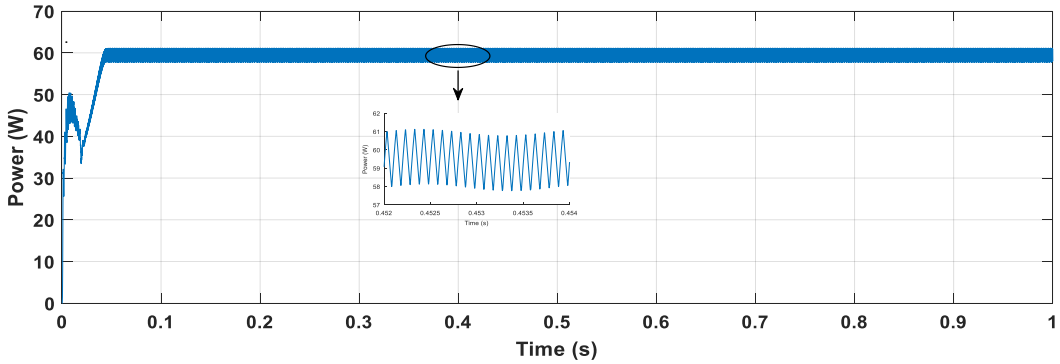

b)

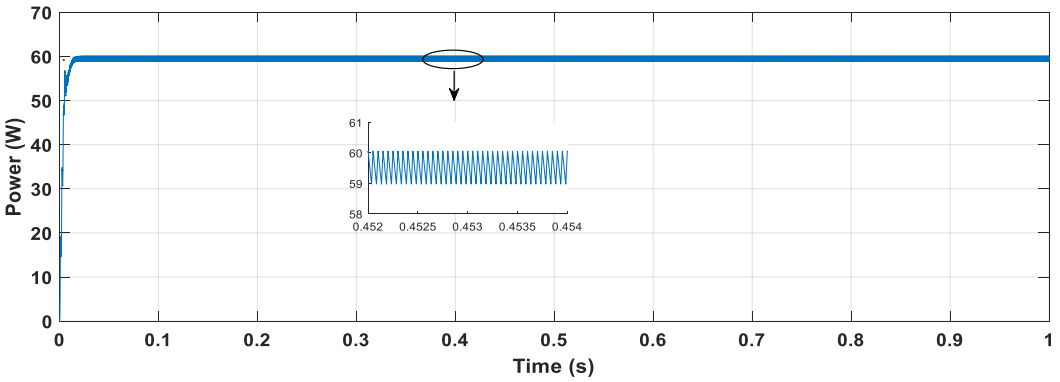

c)

Figure 5.12. PV array output power using: a)P&O algorithm, b) INC algorithm, c) P&O_Variable_step algorithm.

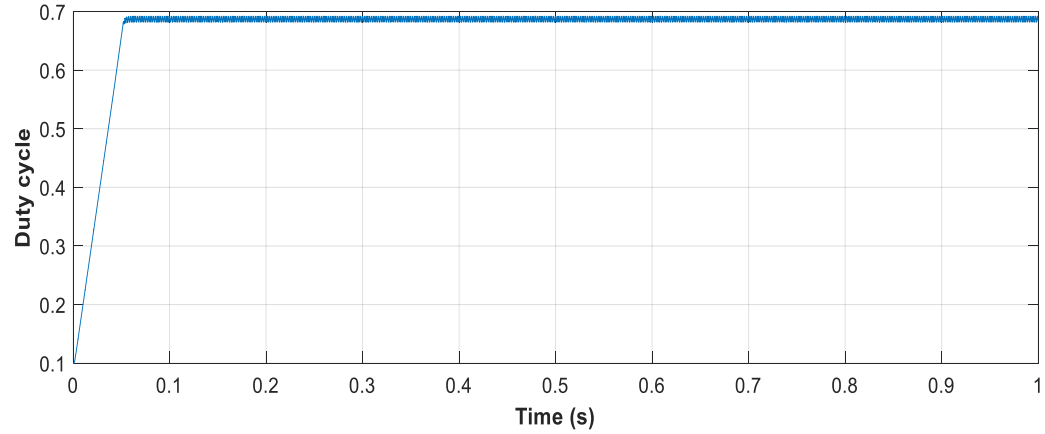

a)

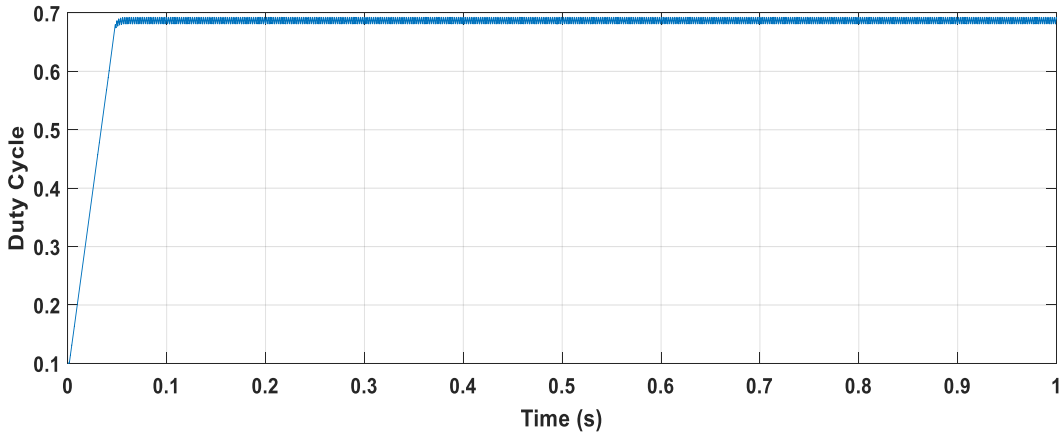

b)

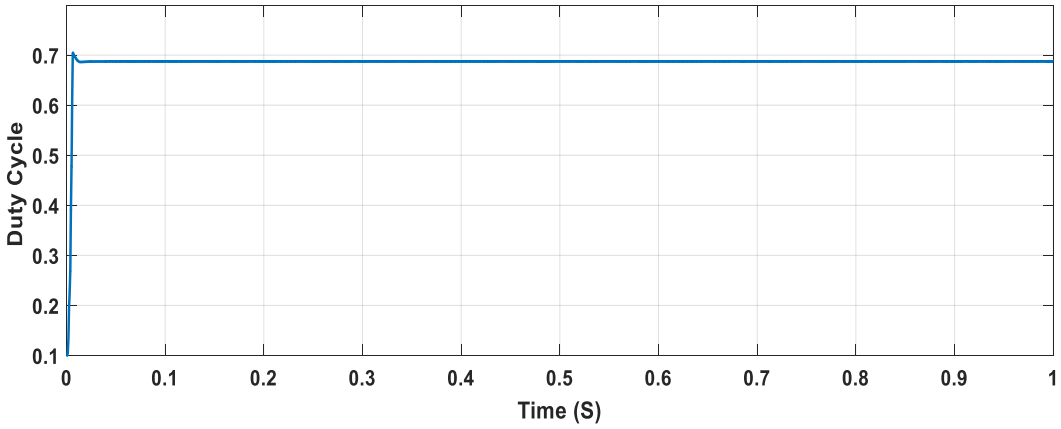

c)

Figure 5.13. Duty ratio waveform of: a) P&O algorithm, b) INC algorithm, c) P&O_Variable_step algorithm.

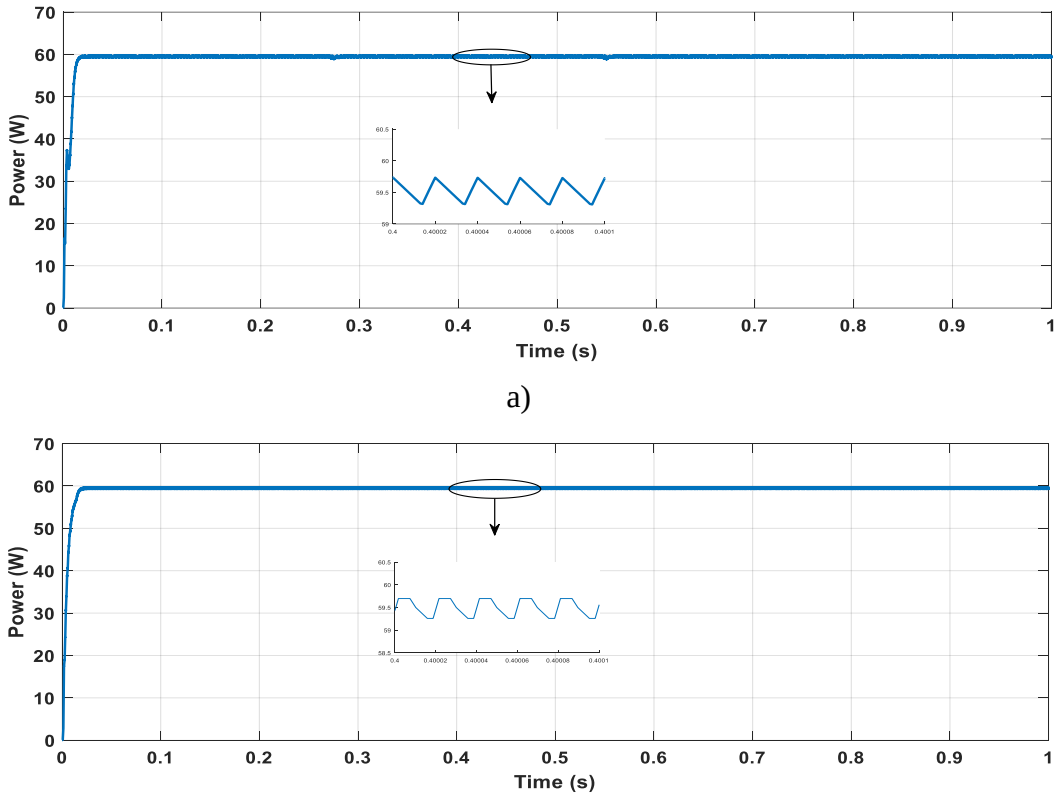

a)

b)

Figure 5.14. PV array output power using: a)FLC algorithm, b) ANN algorithm.

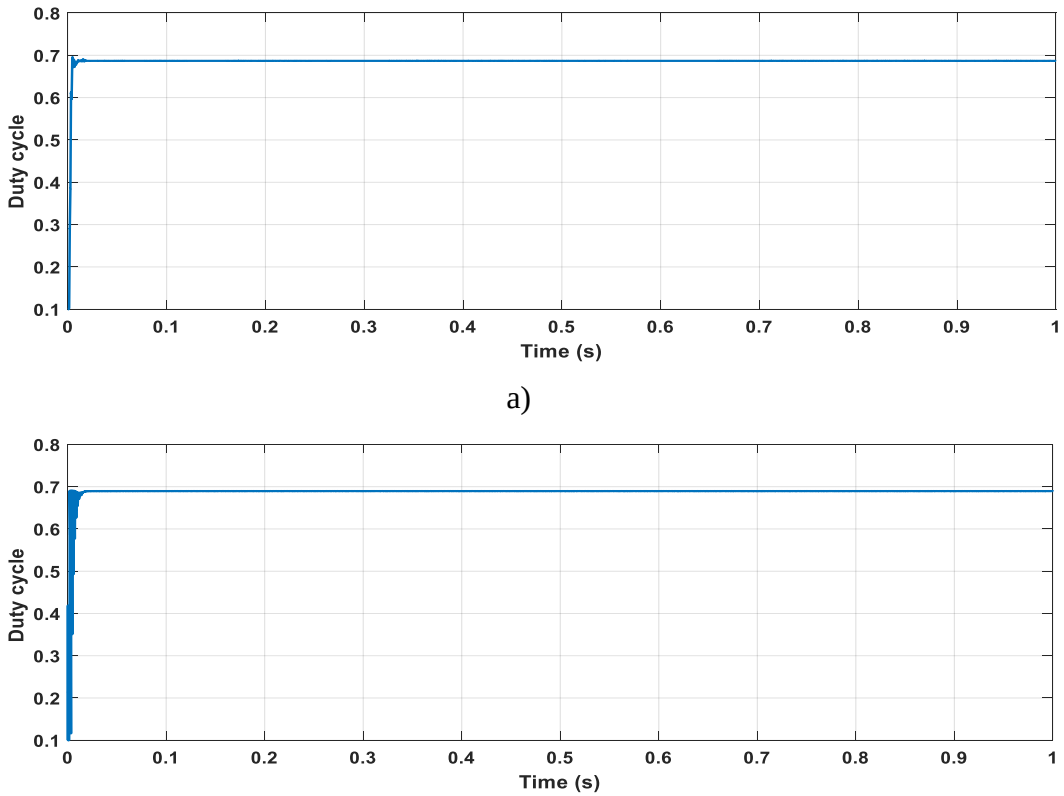

a)

b)

Figure 5.15. Duty ratio waveform of: a) FLC algorithm, b) ANN algorithm.

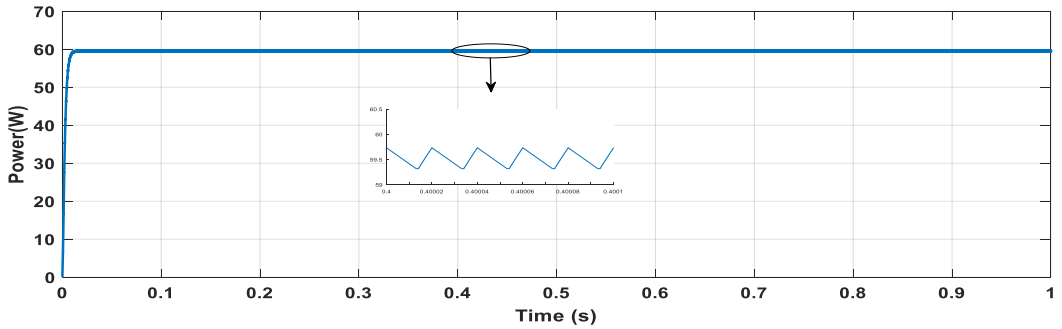

a)

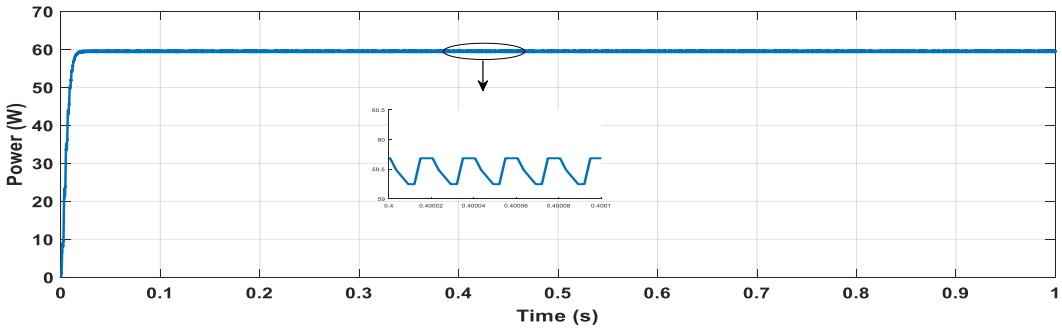

b)

Figure 5.16. PV array output power using: a) ANFIS algorithm, b) FL_P&O algorithm

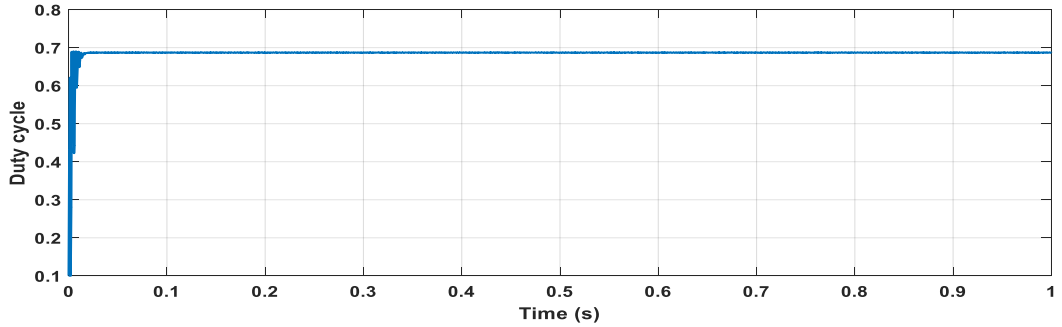

a)

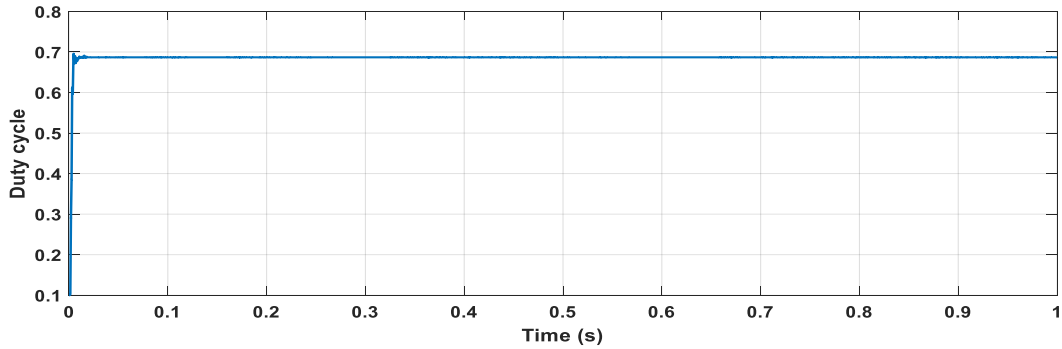

b)

Figure 5.17. PV array output power using: a) ANFIS algorithm, b) FL_P&O algorithm.

5.5.2 Under Variable Irradiation Profile

In this test, the artificial profile of solar irradiation has several changes in level as shown in Figures 5.18.The simulation with this profile is intended to show the ability of the MPPT controller to track the maximum power point during changes in weather conditions as illustrated in Figures 5.19-24.

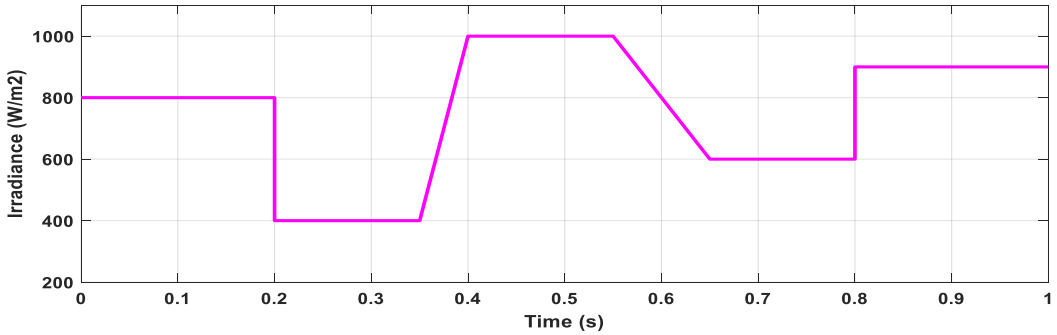

Figure 5.18. Solar irradiance profile for sudden and gradually irradiance changes test.

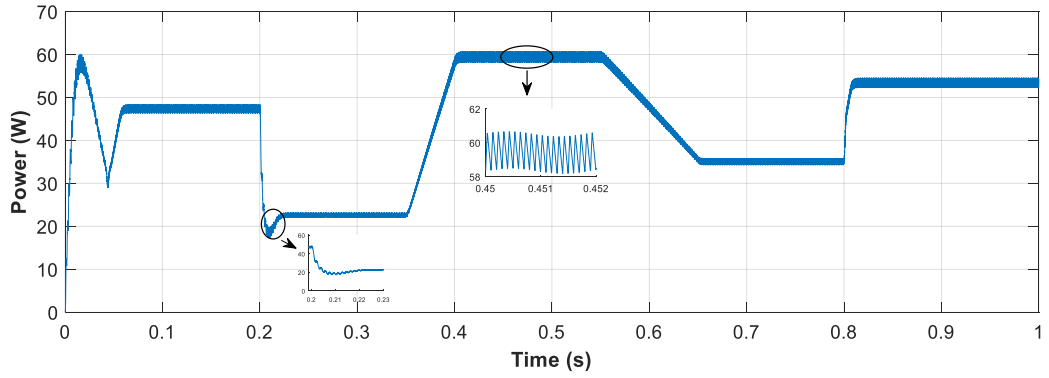

a)

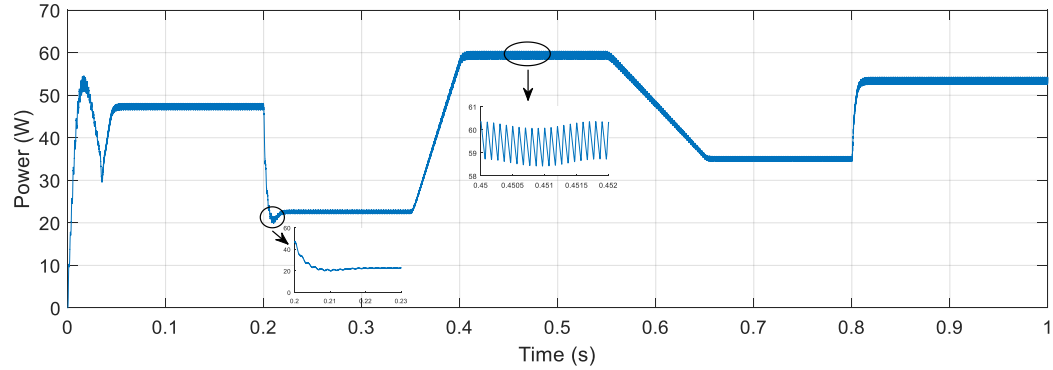

b)

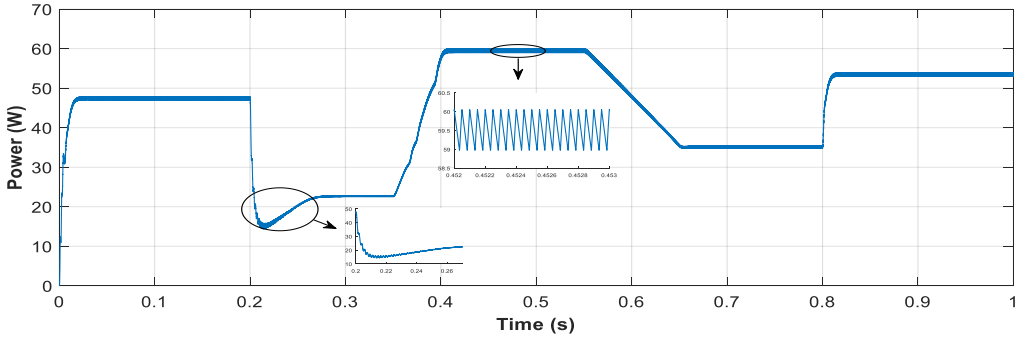

c)

Figure 5.19. PV array output power using: a) P&O algorithm, b) INC algorithm, c)P&O_Variable_step algorithm.

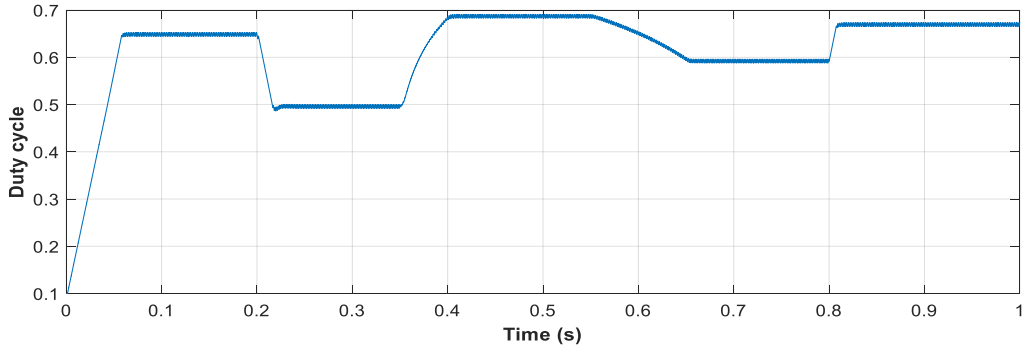

a)

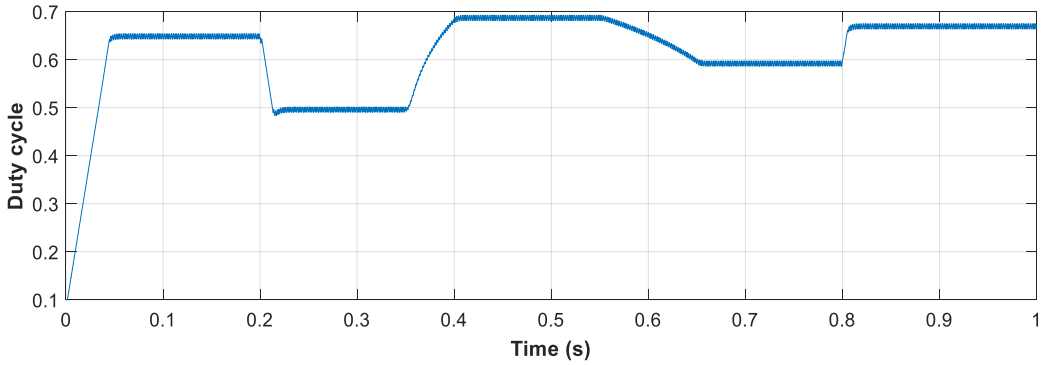

b)

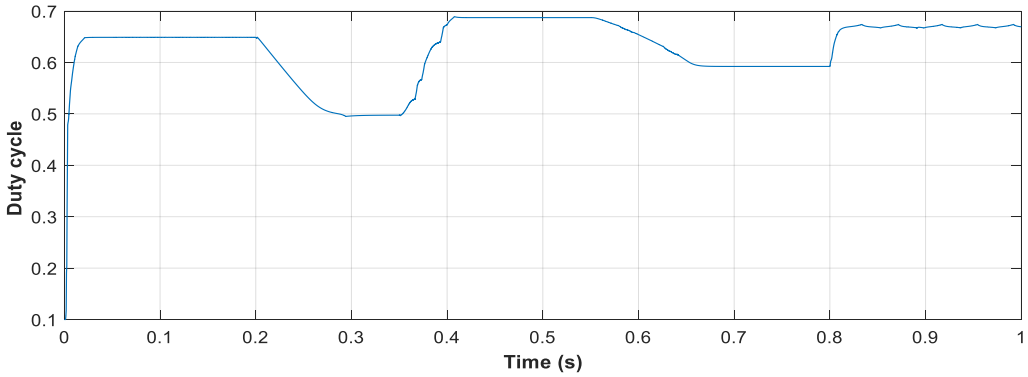

c)

Figure 5.20. Duty ratio waveform of: a) P&O algorithm, b) INC algorithm, c) P&O_Variable_step algorithm.

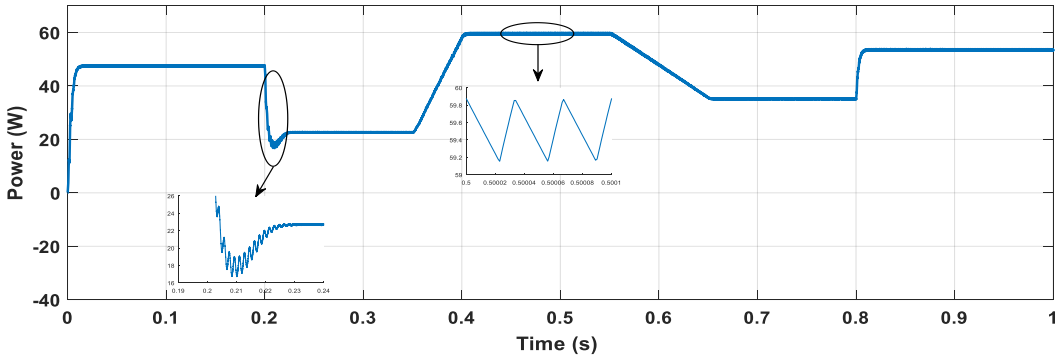

a)

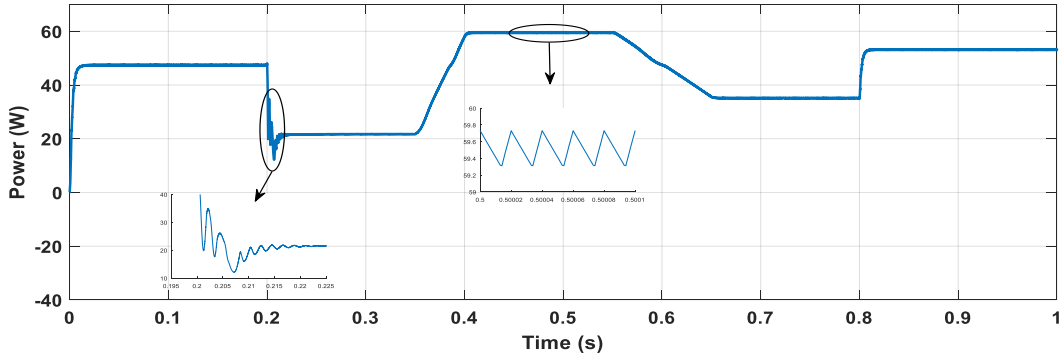

b)

Figure 5.21. PV array output power using: a) FLC algorithm, b) ANNalgorithm.

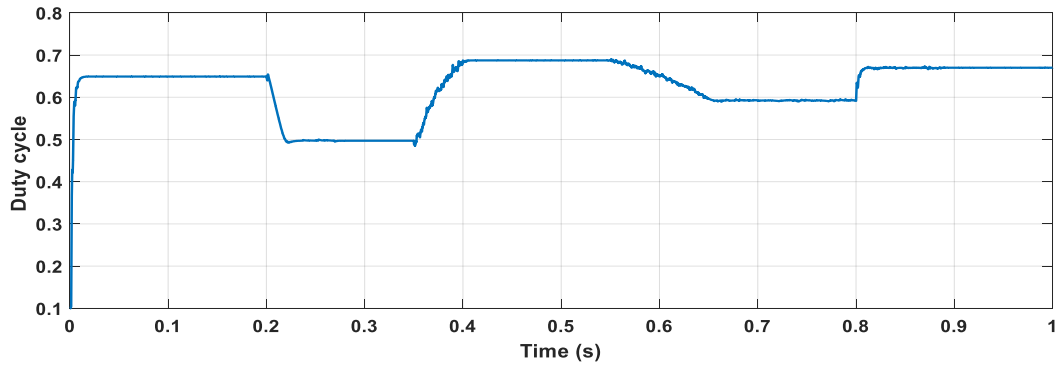

a)

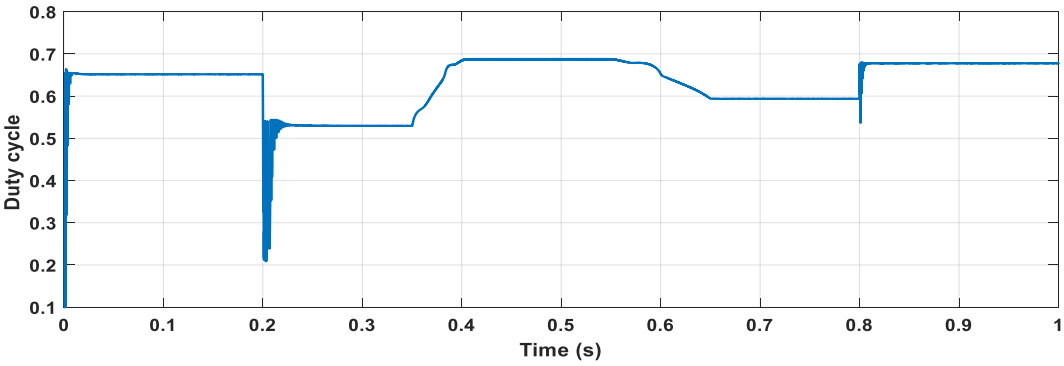

b)

Figure 5.22. Duty ratio waveform of: a) FLC algorithm, b) ANN algorithm.

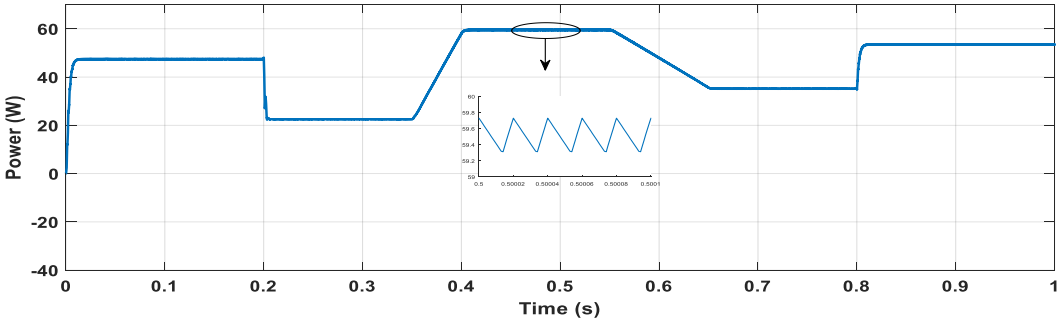

a)

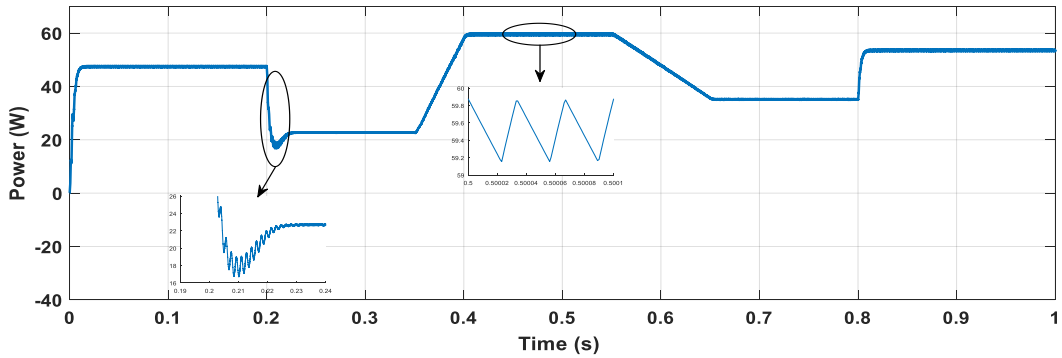

b)

Figure 5.23. PV array output power using: a) ANFIS algorithm, b) FL-P&O algorithm.

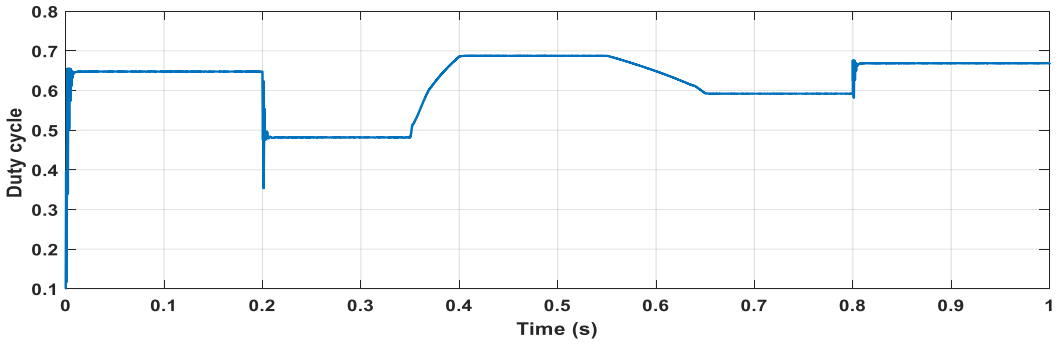

a)

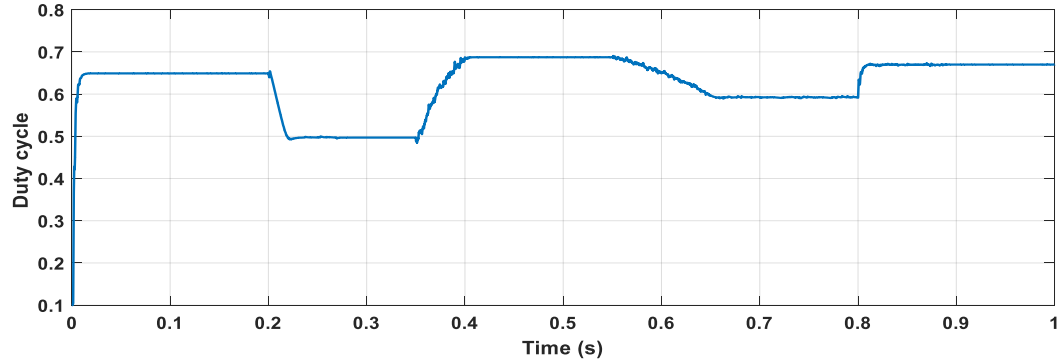

b)

Figure 5.24. Duty ratio waveform of: a) ANFIS algorithm, b) FL-P&O algorithm.

5.5.3 Under Variable Temperature Profile

In these simulations, the irradiation is fixed at $1000W/m^2$ and temperature level variations are created in order to study the response of the system to these variations as well as to perturbations due to temperature variations as shown in Figures 5.25-31.

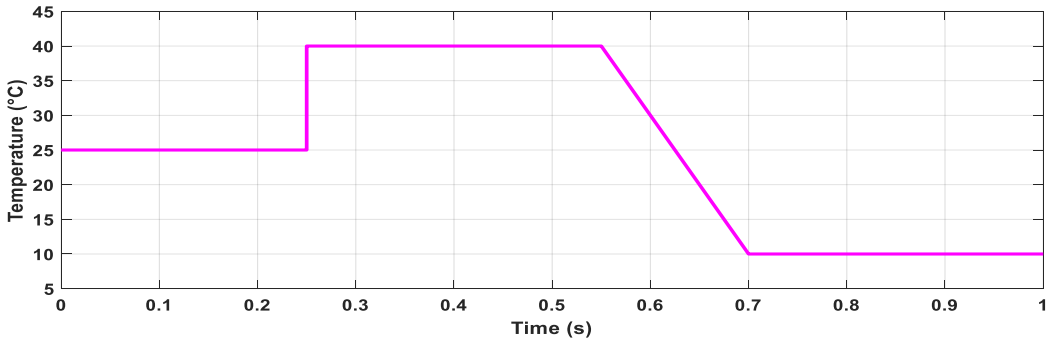

Figure 5.25. Temperature profile for sudden and gradually irradiance changes test.

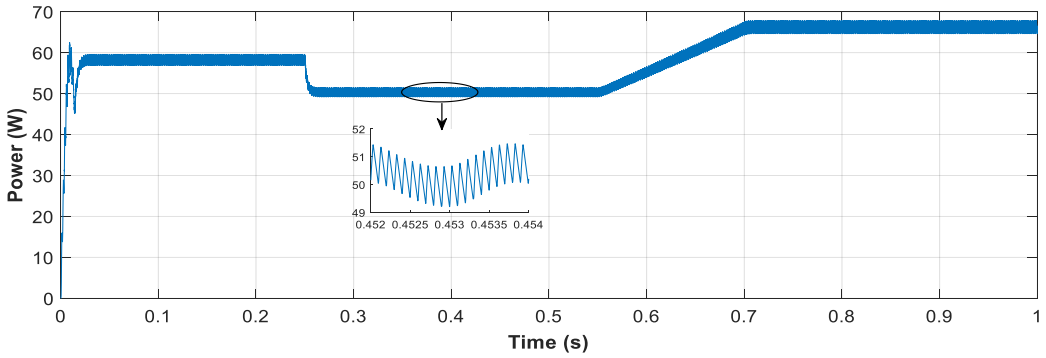

a)

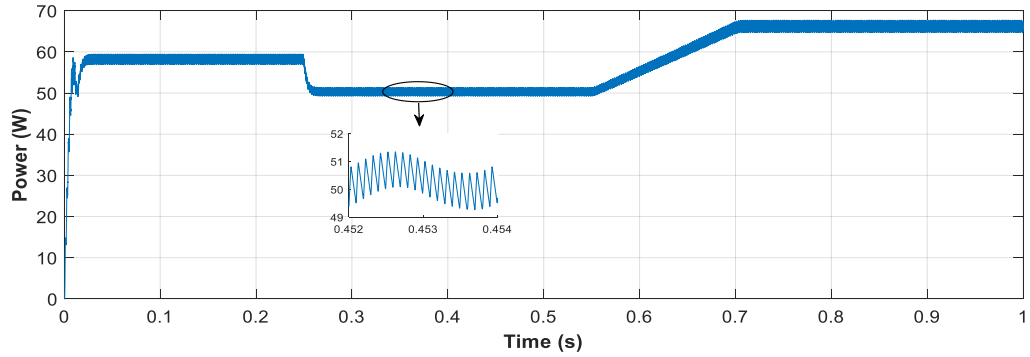

b)

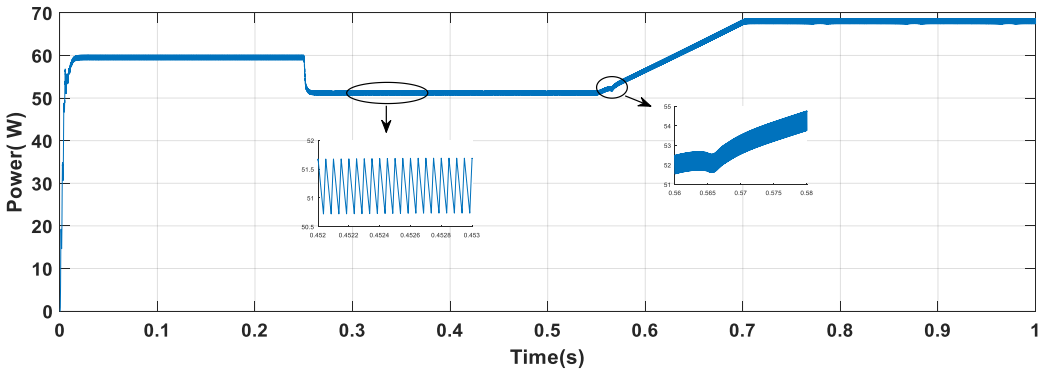

c)

Figure 5.26. PV array output power using: a) P&O, b) INC, c) P&O_Var_step.

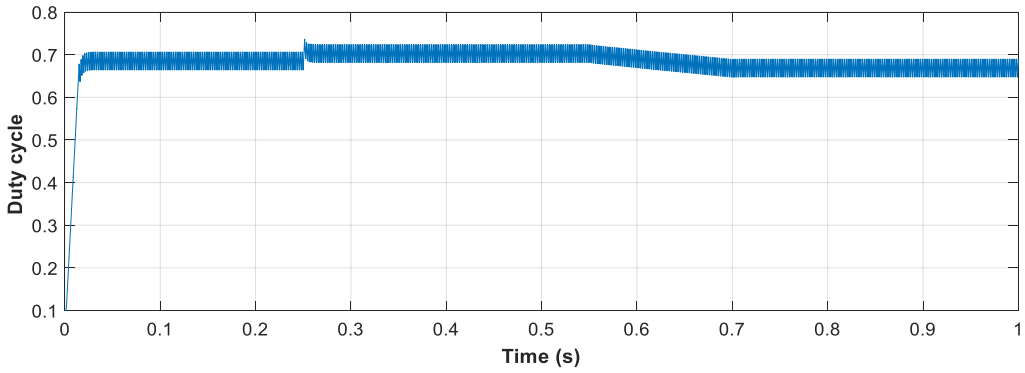

a)

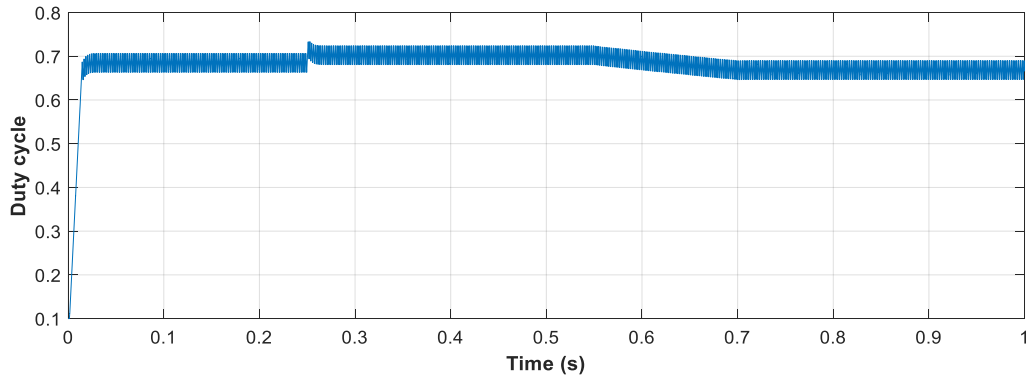

b)

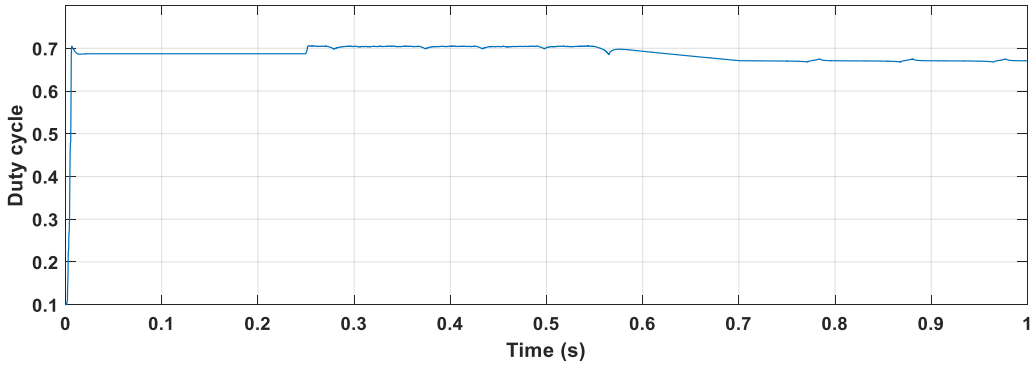

c)

Figure 5.27. Duty ratio waveform of P&O algorithm.

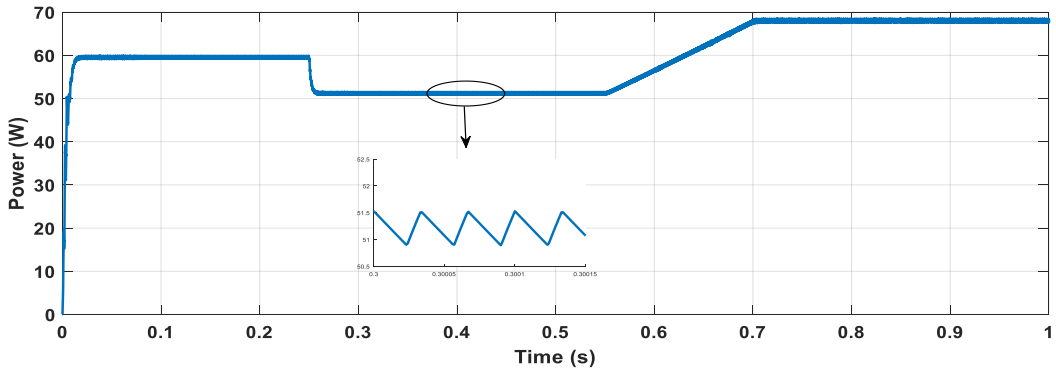

a)

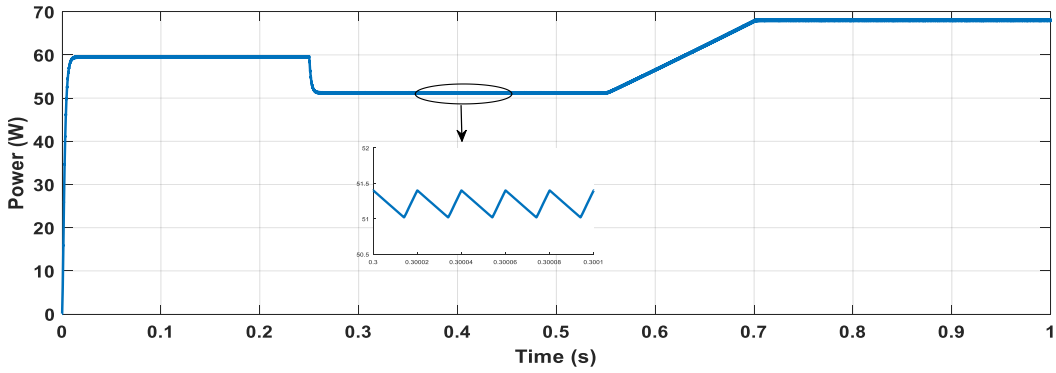

b)

Figure 5.28. PV array output power using: a) FLC algorithm, b) ANNalgorithm.

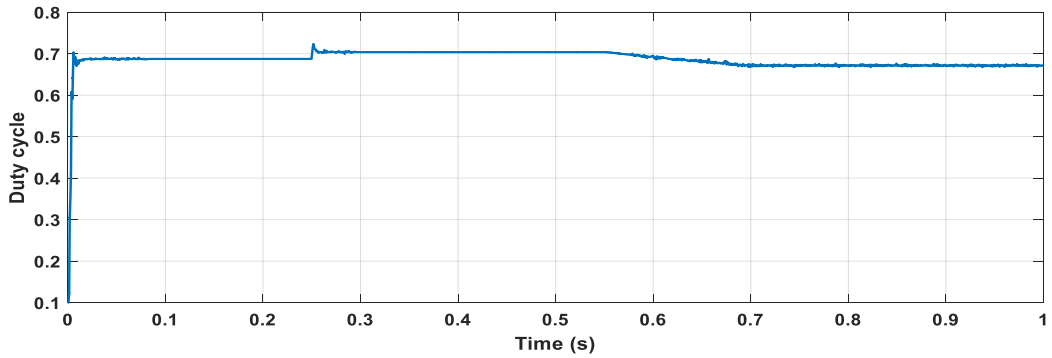

a)

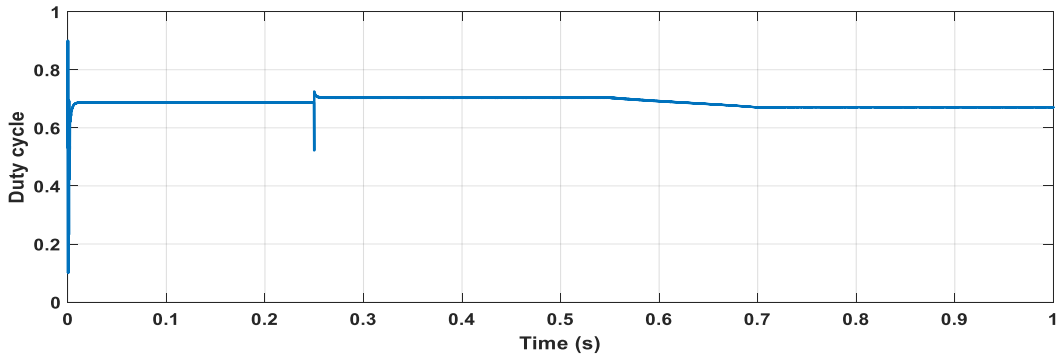

b)

Figure 5.29. Duty ratio waveform of: a) FLC algorithm, b) ANN algorithm

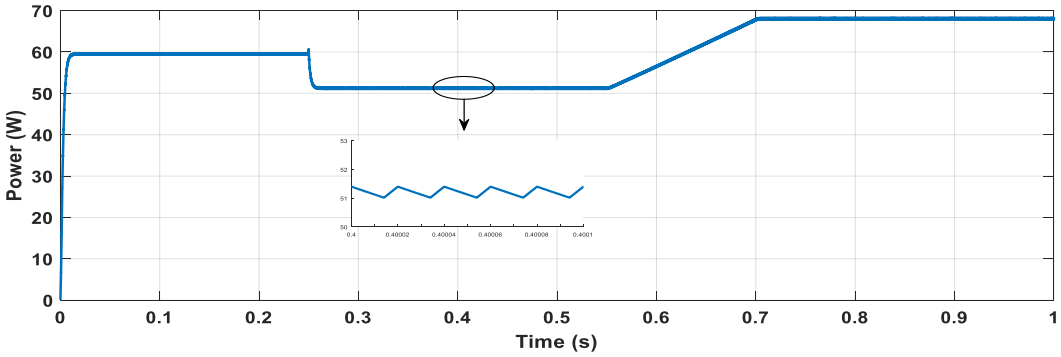

a)

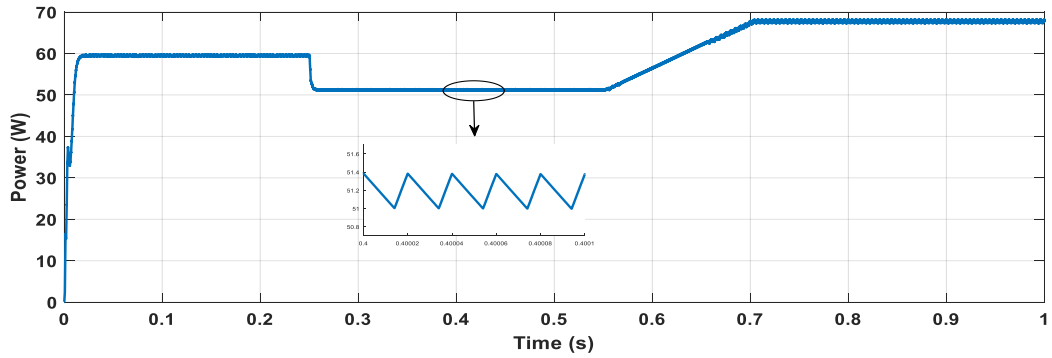

b)

Figure 5.30. PV array output power using: a) ANFIS algorithm, b) FL-P&O algorithm.

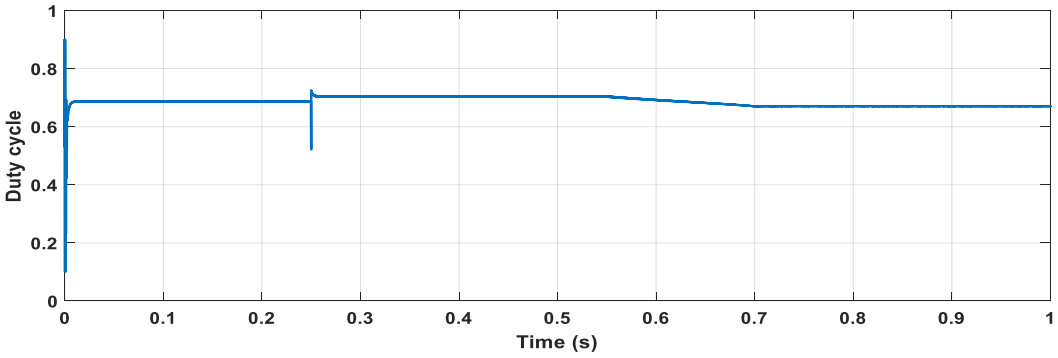

a)

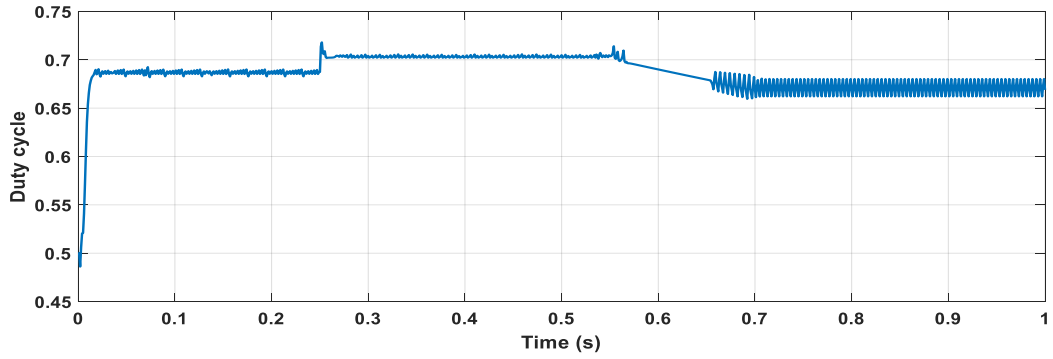

b)

Figure 5.31. Duty ratio waveform of: a) ANFIS algorithm, b) FL-P&O algorithm.

5.6 Tests and results

5.6.1 Comparison between Conventional MPPT Techniques

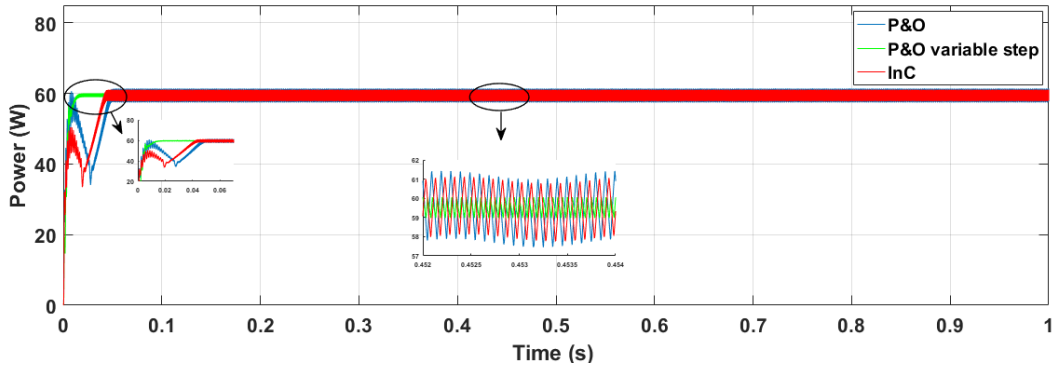

a)

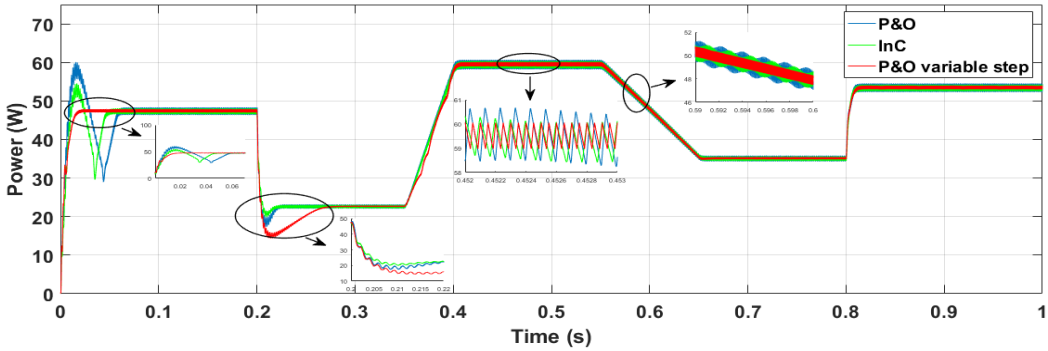

b)

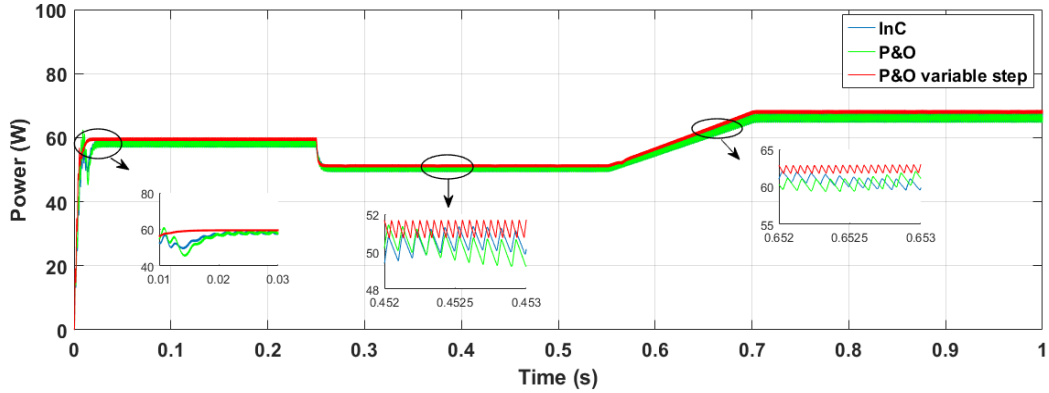

c)

Figure 5.32. Simulation results of the comparison between conventional MPPT Techniques: a) Fixed irradiation, b) variable irradiation, c) variable temperature

The comparison between conventional MPPT algorithms is illustrated in Figure. 5.32. According to this figure the adaptive P&O variable step shows the best

performance in terms of the speed tracking and the power fluctuation compared to the conventional P&O and INC algorithms in the different weather conditions.

- Initially, in STC, the output power of PV generator increases rapidly to a level of 60W where it stabilizes and exhibits a high range of oscillations around maximum power in the case of the P&O controller. On the other hand, less oscillation is observed with INC controller. it is also noted that the latter is faster than the P&O technique in order to reach the MPP as shown in Figure. 5.32-a.
- Next, when compared between P&O and INC, the adaptive P&O variable step shows a good dynamic performance. It can converge faster to the steady-state with less oscillation at 800 W/m² but when an abrupt decrease in solar irradiance occurs (at t=0.2s from 800 W/m² to 200 W/m²), the INC algorithm shows better tracking performance in terms of response time and oscillations. However, at 1000 W/m², the different MPPT algorithms work at the MPP (around 60W) as illustrated in Figure. 5.32-b.
- Finally, according to the Figure. 5.32-c, we notice that the power is inversely proportional to the temperature. This shows the superiority of the INC technique over P&O and adaptive P&O variable step, even for sudden and gradually temperature changes.

The following figure shows the effect of the variation of step size on performance of P&O under standard conditions.

- Compared between P&O MPPT with fixed step-size of 0.0001 and P&O MPPT with fixed step-size of 0.0005 shows a good dynamic performance, it can converge faster to the steady-state with a response time but the oscillation in the steady-state is much higher. The tracking time of P&O MPPT with fixed step-size of 0.0005 under STC is 0.018s to reach the MPP with output power oscillating between 56 to 61.8, while the P&O MPPT with fixed step size of 0.0001 takes 0.055s to track the MPP with power is fluctuating between 58 to 61.8.

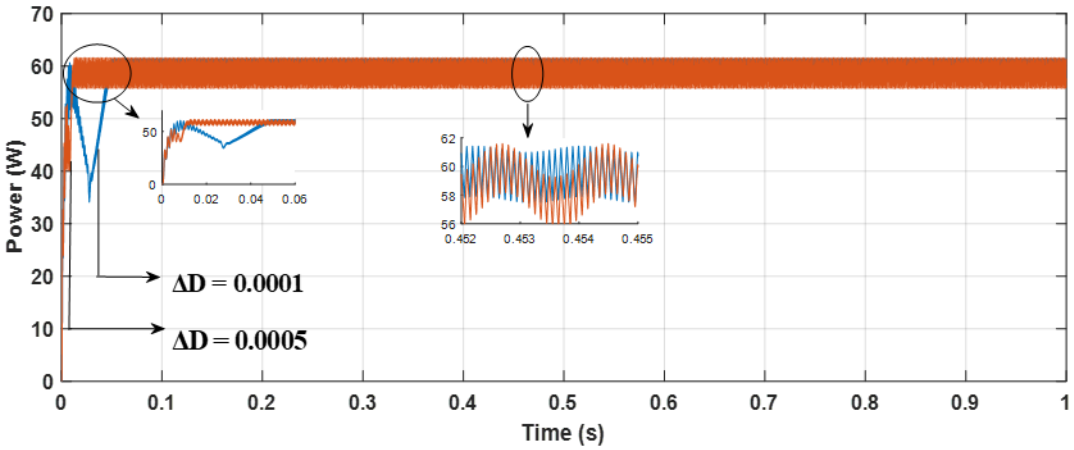

Figure 5.33. Variation of step size effect on P&O performance under standard conditions

5.6.2 Comparison between Artificial Intelligence MPPT Techniques.

Figure 5.34 shows the comparison between artificial intelligence MPPT algorithms.

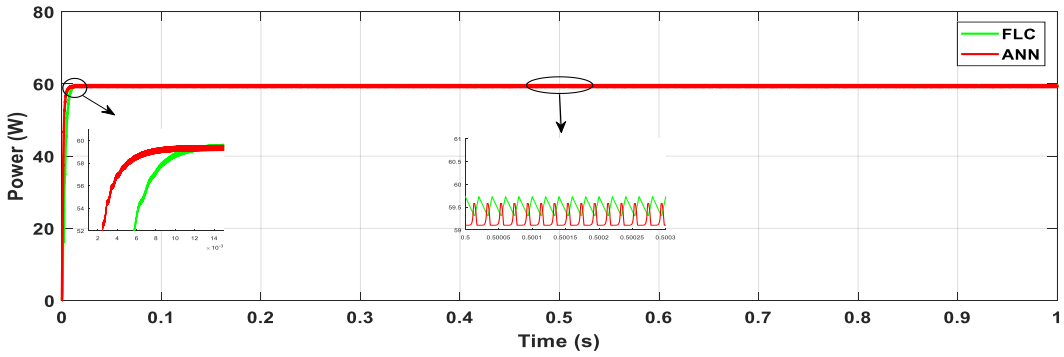

a)

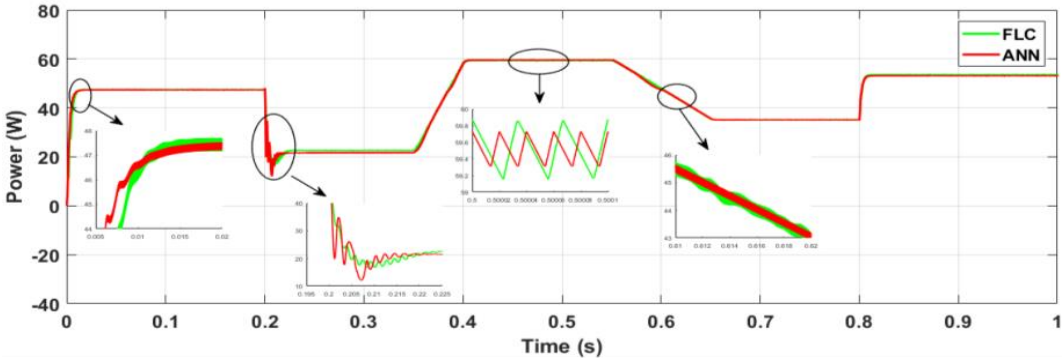

b)

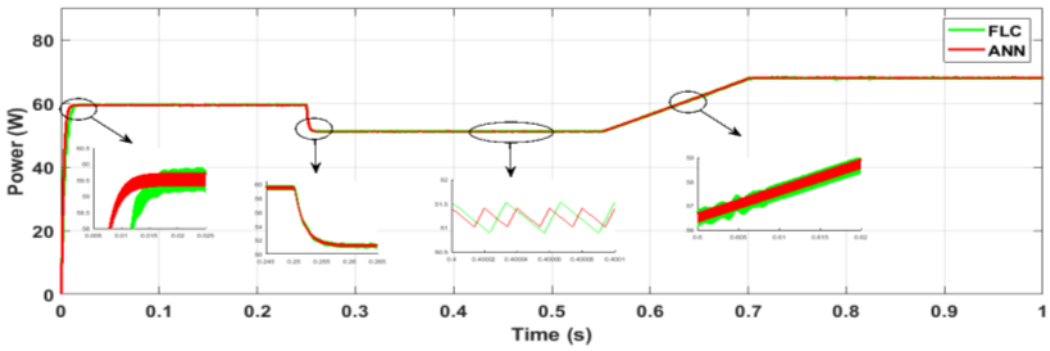

c)

Figure 5.34. Simulation results of the comparison between Artificial Intelligence MPPT Techniques: a) Fixed irradiation, b) variable irradiation, c) variable temperature

- According to Figure 5.34-a, the ANN controller shows the best performance in terms of the speed tracking and the power fluctuation compared to the FLC.
- According to Figure 5.34-b, the ANN controller has better transient characteristics than the fuzzy controller in terms of response time and oscillations during changing solar irradiance.
- According to the Figure 5.34-c, the power is inversely proportional to the temperature. This shows the superiority of the ANN technique over FLC even for sudden and gradually temperature changes.

5.6.3 Comparison between Hybrid MPPT Techniques.

The comparison between hybrid MPPT algorithms is shown in Figure 5.35. The simulation results show good performance of the proposed ANFIS compared to the adaptive fuzzy-P&O in different weather conditions.

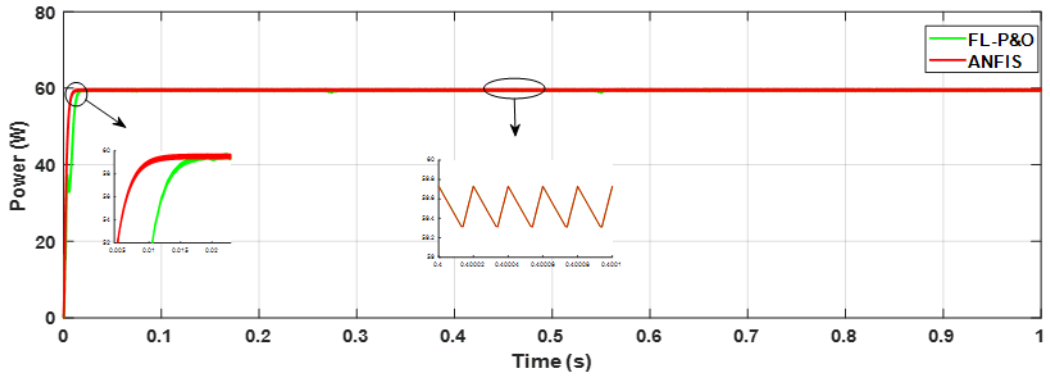

a)

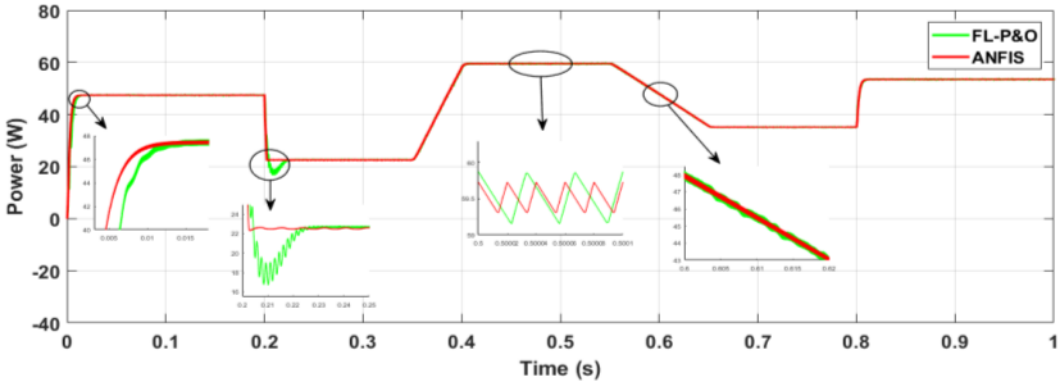

b)

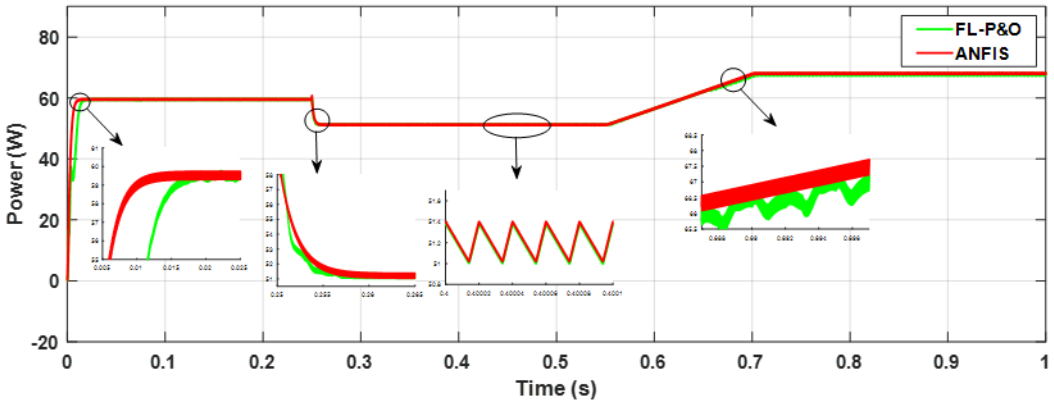

c)

Figure 5.35. Simulation results of the comparison between hybrid MPPT Techniques: a) Fixed irradiation, b) variable irradiation, c) variable temperature

- Under STC, the power increases rapidly to a level of 60W where it stabilizes. The MPPT manages to adjust the duty cycle D very quickly such that stable power is achieved using advanced MPPTs based on ANFIS and Fuzzy-P&O. It is noticeable that the ANFIS technique is faster. At 60 W, the output power does not change since the PV generator operates under constant conditions and does not oscillate around the MPP, which limits power losses as illustrated in Figure 5.35-a.
- Under variable irradiance profile, the dynamic characteristics of the ANFIS technique are better than those of the Fuzzy-P&O technique with a short response time and fewer oscillations as shown in Figure 5.35-b.
- Under variable temperature profile, from Figure 3.35-c, the rise up in temperature leads to lowering in the power. This shows the superiority of the ANFIS technique over Fuzzy-P&O even for sudden and gradually temperature changes.

5.6.4 Comparison between MPPT Techniques

Figure 5.36 shows the simulation result of MPPT controllers based on FLC, ANN and ANFIS tested under different weather conditions.

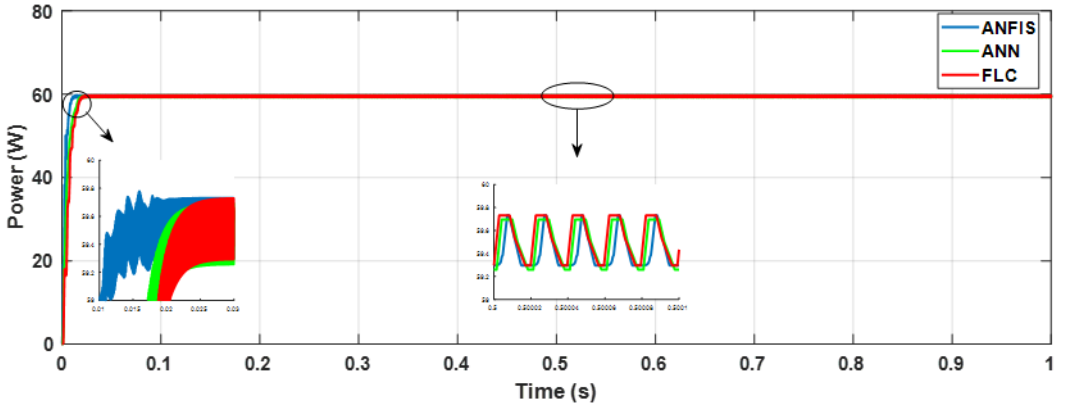

a)

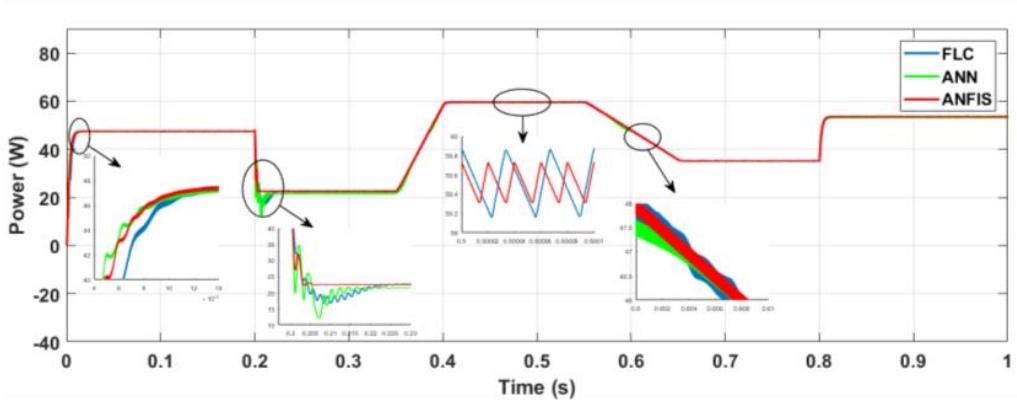

b)

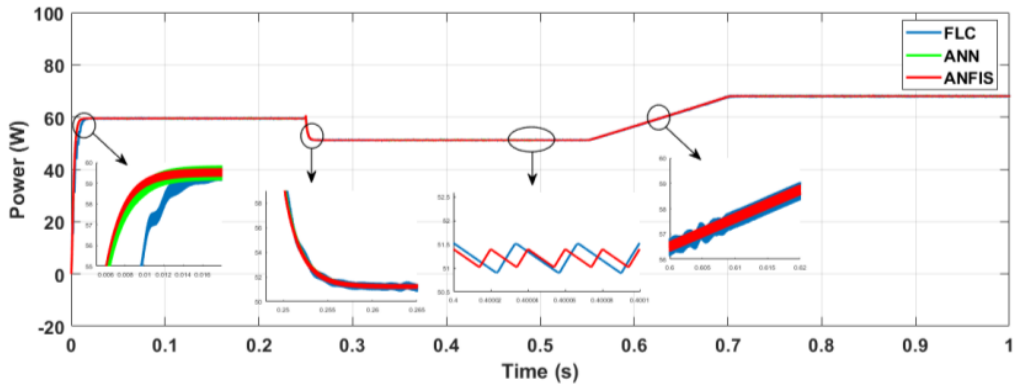

c)

Figure 5.36. Simulation results of the comparison between FLC, ANN and ANFIS based MPPT: a) Fixed irradiation, b) variable irradiation, c) variable temperature

- When compared between ANN and FL controllers, the ANFIS algorithm shows the best performance in term of the speed tracking and the power fluctuation in STC as illustrated in Figure 3.36-a. During an abrupt or gradually change in solar irradiance or temperature, the ANFIS controller shows the best transient characteristics as shown in Figure 3.36-b and c.

Figure 3.37 presents the PV output power for three different controllers P&O, FLC and Fuzzy-P&O respectively performed under different weather conditions.

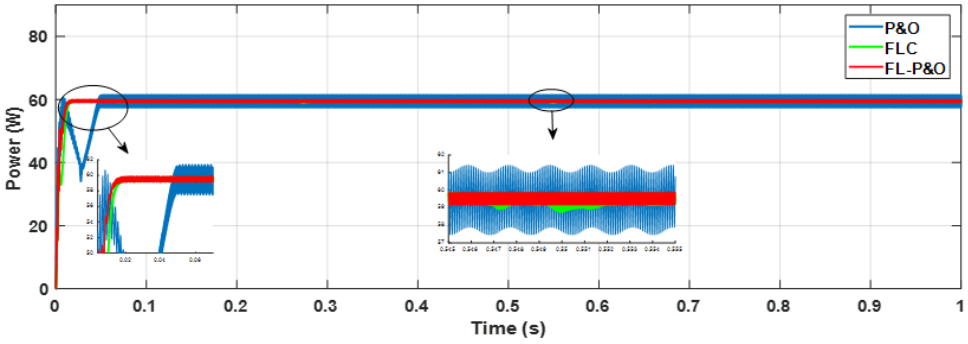

a)

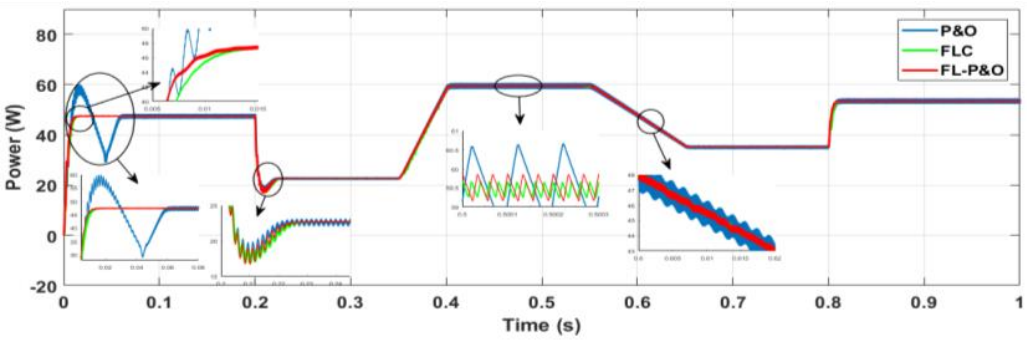

b)

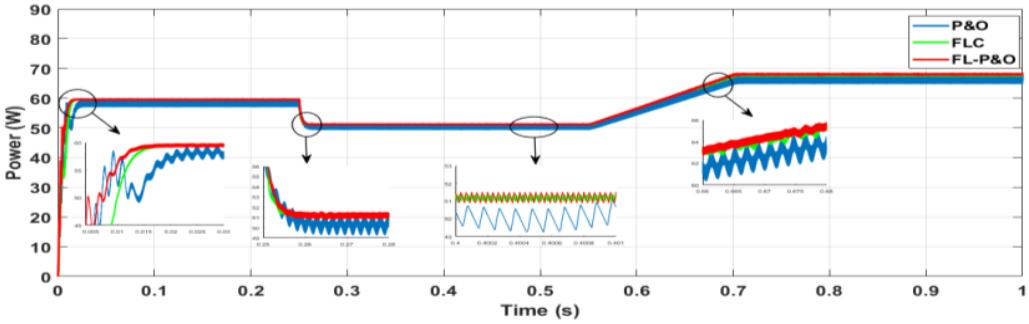

c)

Figure 5.37. Simulation results of the comparison between FLC, ANN and ANFIS based MPPT: a) Fixed irradiation, b) variable irradiation, c) variable temperature

- According to Figure 3.37-a-c the adaptive fuzzy-P&O adapts the tracking performance of FLC and P&O, where it reduces the response time. Moreover, the fuzzy-P&O technique provides less oscillation around the MPP.

A comparative table with the main values obtained in simulation for different MPPT is presented in Table 5.3.

Table 5.3. Summary of simulation results.

MPPT		STC	Irradiation (W/m^2)				Temperature (°C)	
		1000(W/m^2) 25°C	800	400	600	900	25-40	40-10
P&O with step-size = 0.0001	$T_r(s)$	0.055	0.06	0.03	0.0045	0.015	0.0264	0.0032
	η (%)	96.81	98.13	96.31	97.53	98.15	99.026	98.54
	Power oscillation(W)	3.8	1.8	1.77	1.78	2	1	2
P&O with step-size = 0.0005	$T_r(s)$	0.018	None	None	None	None	None	None
	η (%)	95.13	None	None	None	None	None	None
	Power oscillation(W)	5.8	None	None	None	None	None	None
INC	$T_r(s)$	0.048	0.057	0.024	0.0043	0.014	0.0263	0.0031
	η (%)	97.47	98.16	96.46	97.61	98.17	99.15	98.63
	Power oscillation(W)	3	1.77	1.7	1.72	1.98	0.87	1.87
P&O Var_step	$T_r(s)$	0.018	0.02	0.08	0.0042	0.013	0.025	0.0029
	η (%)	99.16	99.06	98.19	98.76	98.98	99.42	99.12
	Power oscillation(W)	1	0.9	0.87	0.89	1.1	0.6	1.2
FLC	$T_r(s)$	0.022	0.016	0.022	0.004	0.01	0.0091	0.0027
	η (%)	99.5	99.31	98.62	99.03	99.84	99.42	99.95
	Power oscillation(W)	0.6	0.66	0.66	0.7	0.174	0.6	0.065
ANN	$T_r(s)$	0.02	0.015	0.0215	0.0035	0.01	0.0058	0.0026
	η (%)	99.66	99.52	99	99.3	99.86	99.8	99.97
	Power oscillation(W)	0.4	0.46	0.48	0.5	0.097	0.2	0.04
ANFIS	$T_r(s)$	0.014	0.012	0.005	0.0033	0.087	0.0058	0.0026
	η (%)	99.66	99.55	99.68	99.34	99.91	99.8	99.97
	Power oscillation(W)	0.4	0.43	0.15	0.47	0.09	0.2	0.04
FL-P&O	$T_r(s)$	0.0218	0.014	0.021	0.0035	0.093	0.0062	0.0024
	η (%)	99.58	99.45	98.93	99.12	99.82	99.16	99.96
	Power oscillation(W)	0.5	0.52	0.517	0.63	0.098	0.43	0.048

Table 5.4 summaries a comparison between the different MPPT methods in terms of tracking speed, power oscillation in steady-state, tracking accuracy and facility of implementation.

Table 5.4. Comparative issues between different MPPT algorithms.

Feature	Conventional MPPT	Artificial Intelligence MPPT	Hybrid MPPT
Tracking speed time	Low	High	High
Steady-state oscillation	Large	small	Very small
Tracking accuracy	Bad	Good	Very good
Implementation complexity	Lower	Moderate	Higher

5.7 Conclusion

This chapter provides the design and MATLAB simulation of the proposed PV system to test the performance of the proposed MPPT techniques and to verify their functionality. The system comprises of PV array, DC-DC boost converter, resistive load and different MPPTs controllers. Each of these components has simulated and masked in an individual subsystem so can be easily controlled and precisely monitored. Then, these subsystems are combined to form the complete system.

Simulation results prove that the conventional techniques have a low tracking speed time and a large steady state oscillation, compared with AI techniques that have high tracking speed time and a small steady state oscillation. However, the hybrid techniques have the best performance in term of tracking speed time and steady state oscillation.

.

General Conclusion

General Conclusion

This work has presented the photovoltaic system, its equivalent circuits and the main factors that affect its curve characteristics and highlighted the DC-DC boost convert and its operating modes. The conventional P&O and InC have been introduced to control the duty cycle of DC-DC boost convert. Since P&O technique with fixed step size exhibits some limitation, a variable step P&O algorithm is introduced for better tracking performance. This work discussed FL and ANN controllers as the most widely used MPPT controllers based on AI techniques which track the MPP rapidly and accurately better than the conventional MPPT controllers. Moreover, two hybrid MPPT controllers are presented which track the MPP effectively better than the individual MPPT methods.

In order to extract I-V and P-V curve characteristics, the PV generator is simulated using MATLAB/SIMULINK software. Also, a mathematical DC-DC boost converter simulator is developed, which generates the terminal voltage associated with the MPP.

The different MPPT methods are developed through MATLAB code and tested under STC and under different weather conditions and different resistive load values to evaluate their performance and functionality. The simulation results are compared to each other based on the response time and the stability of steady-state.

Despite their simplicity and their good tracking performance, InC and P&O techniques show some drawbacks during dynamic weather conditions. Moreover these techniques fail to find a compromise between the steady state oscillation and the convergence time.

The simulation results prove that InC method shows better tracking performance than P&O technique under dynamic weather conditions.

The variable step P&O technique improves the tracking speed of the conventional P&O technique and eliminates the oscillation around the MPP under steady state conditions. This technique shows better tracking performance than the conventional P&O and InC techniques.

The results show that FL and ANN MPPT controllers have a significant improvement compared with the conventional MPPT controllers, where the response

time of FL and ANN methods is reduced to () and () respectively instead of (), () and of P&O, InC and the variable step P&O techniques respectively.

Although the AI-based MPPT methods achieved promising results, there are several limitations involved in using these techniques such as their high cost and complexity. In addition, FLC requires prior knowledge about the PV system and provides some power losses under low radiation levels.

The adaptive fuzzy-P&O and ANFIS hybrid MPPT methods improve the efficiency in steady-state and transient responses of both conventional and AI-based MPPT controllers.

ANFIS technique presents the highest tracking performance in comparison with the previous MPPT methods by offering fast and accurate tracking performance without the need for prior expert knowledge.

References

References

[1] Alajmi, B. N. (2013). Design and control of photovoltaic systems in distributed generation (Doctoral dissertation, University of Strathclyde).

[2] Suthar, M., Singh, G. K., & Saini, R. P. (2013, April). Comparison of mathematical models of photo-voltaic (PV) module and effect of various parameters on its performance. In 2013 International Conference on Energy Efficient Technologies for Sustainability (pp. 1354-1359). IEEE.

[3] Ramos Hernanz, J. A., Campayo Martin, J. J., Zamora Belver, I., LarranagaLesaka, J., Zulueta Guerrero, E., &Puelles Perez, E. (2010, March). Modelling of photovoltaic module. In International conference on renewable energies and power quality (ICREPQ'10) (pp. 23-25).

[4] Aashoor, F. (2015). Maximum power point tracking techniques for photovoltaic water pumping system (Doctoral dissertation, University of Bath).

[5] AFGHOUL, H. (2016). Approche avancée du filtrage actif et du contrôle de puissances dans les installations photovoltaïques interconnectées au réseau (Doctoral dissertation, Université de M'sila).

[6] Ridha, H. M., Heidari, A. A., Wang, M., & Chen, H. (2020). Boosted mutation-based Harris hawks optimizer for parameters identification of single-diode solar cell models. Energy Conversion and Management, 209, 112660..

[7] Tsai, H. L., Tu, C. S., & Su, Y. J. (2008, October). Development of generalized photovoltaic model using MATLAB/SIMULINK. In Proceedings of the world congress on Engineering and computer science (Vol. 2008, pp. 1-6).

[8] Qi, C., & Ming, Z. (2012). Photovoltaic module Simulink model for a stand-alone PV system. physics procedia, 24, 94-100.

[9] Abdulaziz, M., Aldobhani, S., & John, R. (2008). Maximum power point tracking of PV system using ANFIS prediction and fuzzy logic tracking.

[10] Alghuwainem, S. M. (1994). Matching of a dc motor to a photovoltaic generator using a step-up converter with a current-locked loop. IEEE transactions on Energy Conversion, 9(1), 192-198.

[11] Shannan, N. M. A. A., Yahaya, N. Z., & Singh, B. (2013, November). Single-diode model and two-diode model of PV modules: A comparison. In 2013 IEEE

International Conference on Control System, Computing and Engineering (pp. 210-214). IEEE.

[12] Pauls, C. (2014). Optimization approaches for parameter estimation and maximum power point tracking (MPPT) of photovoltaic systems (Doctoral dissertation, University of Liverpool).

[13] Xiao, W., Dunford, W. G., & Capel, A. (2004, June). A novel modeling method for photovoltaic cells. In 2004 IEEE 35th Annual Power Electronics Specialists Conference (IEEE Cat. No. 04CH37551) (Vol. 3, pp. 1950-1956). IEEE.

[14] Chin, V. J., Salam, Z., &Ishaque, K. (2015). Cell modelling and model parameters estimation techniques for photovoltaic simulator application: A review. Applied Energy, 154, 500-519.

[15] Azzouzi, M., Popescu, D., &Bouchahdane, M. (2016). Modeling of electrical characteristics of photovoltaic cell considering single-diode model. Journal of Clean Energy Technologies, 4(6), 414-20.

[16] Chin, V. J., Salam, Z., &Ishaque, K. (2015). Cell modelling and model parameters estimation techniques for photovoltaic simulator application: A review. Applied Energy, 154, 500-519.

[17] Lineykin, S., Averbukh, M., &Kuperman, A. (2012, November). Five-parameter model of photovoltaic cell based on STC data and dimensionless. In 2012 IEEE 27th Convention of Electrical and Electronics Engineers in Israel (pp. 1-5). IEEE.

[18] Hejri, M., Mokhtari, H., Azizian, M. R., Ghandhari, M., &Söder, L. (2014). On the parameter extraction of a five-parameter double-diode model of photovoltaic cells and modules. IEEE Journal of Photovoltaics, 4(3), 915-923.

[19] Yahya-Khotbehsara, A., &Shahhoseini, A. (2018). A fast modeling of the double-diode model for PV modules using combined analytical and numerical approach. Solar Energy, 162, 403-409.

[20] Azzouzi, M., Mazzouz, L., & Popescu, D. (2014, July). Matlab-simulink of photovoltaic system based on a two-diode model. In Proceedings of the World Congress on Engineering 2014 (Vol. 1, pp. 2-4).

[21] Suthar, M., Singh, G. K., & Saini, R. P. (2013, April). Comparison of mathematical models of photo-voltaic (PV) module and effect of various parameters on its performance. In 2013 International Conference on Energy Efficient Technologies for Sustainability (pp. 1354-1359). IEEE.

[22] Van Dyk, E. E., & Meyer, E. L. (2004). Analysis of the effect of parasitic resistances on the performance of photovoltaic modules. Renewableenergy, 29(3), 333-344.

[23] Feroz Mirza, A., Mansoor, M., Ling, Q., Khan, M. I., & Aldossary, O. M. (2020). Advanced Variable Step Size Incremental Conductance MPPT for a Standalone PV System Utilizing a GA-Tuned PID Controller. Energies, 13(16), 4153.

[24] Gousiopoulos, A. (2016). The efficiency of photovoltaic systems (Doctoral dissertation, University of Southampton).

[25] Nanjannavar, V., Gandhi, P., & Patel, N. (2013, November). LabVIEW based PV cell characterization and MPPT under varying temperature and irradiance conditions. In 2013 Nirma University International Conference on Engineering (NUiCONE) (pp. 1-6). IEEE.

[26] Taghvaee, M. H., Radzi, M. A. M., Moosavain, S. M., Hizam, H., &Marhaban, M. H. (2013). A current and future study on non-isolated DC–DC converters for photovoltaic applications. Renewable and sustainable energy reviews, 17, 216-227.

[27] Singh, S. N. (2017). Selection of non-isolated DC-DC converters for solar photovoltaic system. Renewable and Sustainable Energy Reviews, 76, 1230-1247.

[28] Alsumiri, M. (2015). Sliding mode control of renewable energy generation systems (Doctoral dissertation, University of Liverpool).

[29] Hadji, S. (2018). Optimisation de la conversion énergétique pour les systèmes à énergie Photovoltaïque (Doctoral dissertation).

[30] Hua, C., & Shen, C. (1998, May). Study of maximum power tracking techniques and control of DC/DC converters for photovoltaic power system. In PESC 98 Record. 29th Annual IEEE Power Electronics Specialists Conference (Cat. No. 98CH36196) (Vol. 1, pp. 86-93). IEEE.

[31] Sokolov, M. (2013). Small-signal modelling of maximum power point tracking for photovoltaic systems (Doctoral dissertation, Imperial College London).

[32] Selmi, T., Abdul-Niby, M., Devis, L., & Davis, A. (2014, March). P&omppt implementation using matlab/simulink. In 2014 Ninth International Conference on Ecological Vehicles and Renewable Energies (EVER) (pp. 1-4). IEEE.

[33] Dhaouadi, G. U. I. Z. A., Djamel, O. U. N. N. A. S., Youcef, S. O. U. F. I., & Salah, C. H. E. N. I. K. H. E. (2019, September). Implementation of Incremental Conductance Based MPPT Algorithm for Photovoltaic System. In 2019 4th International Conference on Power Electronics and their Applications (ICPEA) (pp. 1-5). IEEE.

[34] Lakshmi, D., & Rashmi, M. R. (2017, December). A modified incremental conductance algorithm for partially shaded PV array. In 2017 International Conference on Technological Advancements in Power and Energy (TAP Energy) (pp. 1-6). IEEE.

[35] Chauhan, U., Rani, A., & Kumar, B. (2020, February). A Modified Incremental Conductance Maximum Power Point Technique for Standalone PV System. In 2020 7th International Conference on Signal Processing and Integrated Networks (SPIN) (pp. 61-64). IEEE..

[36] Jusoh, A., Alik, R., Guan, T. K., &Sutikno, T. (2017). MPPT for PV system based on variable step size p&o algorithm. Telkomnika, 15(1), 79.

[37] Jiandong, D., Ma, X., &Tuo, S. (2018, September). A variable step size P&O MPPT algorithm for three-phase grid-connected PV systems. In 2018 China International Conference on Electricity Distribution (CICED) (pp. 1997-2001). IEEE.

[38] Yang, Q., & Wang, Q. (2013, August). An Improving Control Method of CTV+ P&O on Photovoltaic Power Generation Maximum Power Point Tracking. In 2013 5th International Conference on Intelligent Human-Machine Systems and Cybernetics (Vol. 1, pp. 285-288). IEEE.

[39] Mohapatra, A., Nayak, B., & Mohanty, K. B. (2014, December). Current based novel adaptive P&O MPPT algorithm for photovoltaic system considering sudden change in the irradiance. In 2014 IEEE International Conference on Power Electronics, Drives and Energy Systems (PEDES) (pp. 1-4). IEEE.

[40] Dahbi, S., Aziz, A., Benazzi, N., Elhafyani, M., &Benahmed, N. (2016). Advanced MPPT controller based on P&O algorithm with variable step size and acceleration mechanism for solar photovoltaic system. In Proceedings of the Mediterranean Conference on Information & Communication Technologies 2015 (pp. 57-67). Springer, Cham.

[41] Al-Diab, A., &Sourkounis, C. (2010, May). Variable step size P&O MPPT algorithm for PV systems. In 2010 12th International Conference on Optimization of Electrical and Electronic Equipment (pp. 1097-1102). IEEE.

[42] Serrano-Guerrero, X., González-Romero, J., Cárdenas-Carangui, X., &Escrivá-Escrivá, G. (2016, September). Improved variable step size P&O MPPT algorithm for PV systems. In 2016 51st International Universities Power Engineering Conference (UPEC) (pp. 1-6). IEEE.

[43] Barr, A., &Feigenbaum, E. A. (1981). The Handbook of Artificial Intelligence. William Kaufmann. Inc., Los Altos, CA, 163-171.

[44] Rumelhart, D. E., Hinton, G. E., & Williams, R. J. (1986). Learning Internal Representations by Error Propagation," Parallel Distributed Processing (PDP): Exploration in the Microstructure of Cognition, Vol. 1, Chapter 8.

[45] Zadeh, L. A. (1972). A fuzzy-set-theoretic interpretation of linguistic hedges.

[46] Zadeh, L. A. (1973). Outline of a new approach to the analysis of complex systems and decision processes. IEEE Transactions on systems, Man, and Cybernetics, (1), 28-

[47] Mamdani, E. H., &Assilian, S. (1975). An experiment in linguistic synthesis with a fuzzy logic controller. International journal of man-machine studies, 7(1), 1-13.

[48] Togai, M., & Watanabe, H. (1986, December). Expert system on a chip: An engine for real-time approximate reasoning. In Proceedings of the ACM SIGART international symposium on Methodologies for intelligent systems (pp. 147-154).

[49] Dutta, S. (1993). Fuzzy logic applications: Technological and strategic issues. IEEE Transactions on Engineering Management, 40(3), 237-254.

[50] Veerachary, M., Senjyu, T., &Uezato, K. (2002). Feedforward maximum power point tracking of PV systems using fuzzy controller. IEEE Transactions on Aerospace and Electronic Systems, 38(3), 969-981.

[51] Hohm, D. P., &Ropp, M. E. (2000, September). Comparative study of maximum power point tracking algorithms using an experimental, programmable, maximum power point tracking test bed. In Conference Record of the Twenty-Eighth IEEE Photovoltaic Specialists Conference-2000 (Cat. No. 00CH37036) (pp. 1699-1702). IEEE.

[52] Chin, C. S., Neelakantan, P., Yoong, H. P., & Teo, K. T. K. (2011). Optimisation of fuzzy based maximum power point tracking in PV system for rapidly changing solar irradiance. Transaction on Solar Energy and Planning, 2, 130-137.

[53] Yager, R. R., &Filev, D. P. (1994). Essentials of fuzzy modeling and control. New York, 388, 22-23.

[54] Yen, J., &Langari, R. (1999). Fuzzy logic: intelligence, control, and information (Vol. 1). Upper Saddle River, NJ: Prentice Hall.

[55] YİĞİT, Ş., BÜYÜKÖZKAN, K., SÖNMEZ, F., & ÇUHADAROĞLU, B. HVAC SİSTEMLERİNDE AÇ-KAPA ve BULANIK MANTIK KONTROLÜN KIYASLAMALI OLARAK İNCELENMESİ.

[56] Jang, J. S. (1993). ANFIS: adaptive-network-based fuzzy inference system. IEEE transactions on systems, man, and cybernetics, 23(3), 665-685.

[57] Cirstea, M. N., Dinu, A., Khor, J. G., & McCormick, M. (2002). Neural and fuzzy logic control of drives and power systems, Newnes. An imprint of Elsevier Science First published, 412.

[58] Bai, Y., Zhuang, H., & Wang, D. (Eds.). (2007). Advanced fuzzy logic technologies in industrial applications. Springer Science & Business Media.

[59] Cirstea, M. N., Dinu, A., Khor, J. G., & McCormick, M. (2002). Neural and fuzzy logic control of drives and power systems, Newnes. An imprint of Elsevier Science First published, 412.

[60] Jang, J. S. R., Sun, C. T., &Mizutani, E. (1997). Neuro-fuzzy and soft computing-a computational approach to learning and machine intelligence [Book Review]. IEEE Transactions on automatic control, 42(10), 1482-1484.

[61] Driankov, D., Hellendoorn, H., &Reinfrank, M. (1993). Stability of fuzzy control systems. In An Introduction to fuzzy control (pp. 245-292). Springer, Berlin, Heidelberg.

[62] Iancu, I. (2012). A Mamdani type fuzzy logic controller. Fuzzy Logic: Controls, Concepts, Theories and Applications, 325-350.

[63] Mamdani, E. H. (1974, December). Application of fuzzy algorithms for control of simple dynamic plant. In Proceedings of the institution of electrical engineers (Vol. 121, No. 12, pp. 1585-1588). IET.

[64] Mendel, J. M. (1995). Fuzzy logic systems for engineering: a tutorial. Proceedings of the IEEE, 83(3), 345-377.

[65] Dadios, E. (Ed.). (2012). Fuzzy logic: controls, concepts, theories and applications. BoD–Books on Demand.

[66] Thomas, D. E., & Armstrong-Helouvry, B. (1995). Fuzzy logic control-a taxonomy of demonstrated benefits. Proceedings of the IEEE, 83(3), 407-421.

[67] Lee, C. C. (1990). Fuzzy logic in control systems: fuzzy logic controller. I. IEEE Transactions on systems, man, and cybernetics, 20(2), 404-418.

[68] Ma, Q., Tan, X., Kong, D., & Xi, H. (2008, June). A novel approach to network vulnerabilities quantitative evaluation based on Mamdani-Style fuzzy logic. In 2008 7th World Congress on Intelligent Control and Automation (pp. 3327-3330). IEEE.

[69] Unde, M., Deokar, K., Hans, M., & Kawthe, S. (2020, January). Closed-Loop Design of Fuzzy Logic Controller in Solar Power Generation. In 2020 Fourth International Conference on Inventive Systems and Control (ICISC) (pp. 215-219). IEEE.

[70] Shaheen, O., El-Nagar, A. M., El-Bardini, M., & El-Rabaie, N. M. (2020). Stable adaptive probabilistic Takagi–Sugeno–Kang fuzzy controller for dynamic systems with uncertainties. ISA transactions, 98, 271-283.

[71] Cavallaro, F. (2015). A Takagi-Sugeno fuzzy inference system for developing a sustainability index of biomass. Sustainability, 7(9), 12359-12371.

[72] Sivanandam, S. N., Sumathi, S., & Deepa, S. N. (2007). Introduction to fuzzy logic using MATLAB (Vol. 1). Berlin: Springer.

[73] Hamam, A., &Georganas, N. D. (2008, October). A comparison of Mamdani and Sugeno fuzzy inference systems for evaluating the quality of experience of Hapto-Audio-Visual applications. In 2008 IEEE International Workshop on Haptic Audio visual Environments and Games (pp. 87-92). IEEE.

[74] Raj, M. P., & Joshua, A. M. (2017, September). Design, implementation and performance analysis of a LabVIEW based fuzzy logic MPPT controller for stand-alone PV systems. In 2017 IEEE International Conference on Power, Control, Signals and Instrumentation Engineering (ICPCSI) (pp. 1012-1017). IEEE.

[75] Al Nabulsi, A., &Dhaouadi, R. (2012). Efficiency optimization of a DSP-based standalone PV system using fuzzy logic and dual-MPPT control. IEEE Transactions on Industrial informatics, 8(3), 573-584.

[76] Canny, D., &Yusivar, F. (2018, August). Maximum Power Point Tracking (MPPT) Algorithm Simulation Based on Fuzzy Logic Controller on Solar Cell with Boost Converter. In 2018 2nd International Conference on Smart Grid and Smart Cities (ICSGSC) (pp. 117-121). IEEE.

[77] De Brito, M. A., Sampaio, L. P., Luigi, G., e Melo, G. A., &Canesin, C. A. (2011, June). Comparative analysis of MPPT techniques for PV applications. In 2011 International Conference on Clean Electrical Power (ICCEP) (pp. 99-104). IEEE.

[78] Kish, G. J., Lee, J. J., & Lehn, P. W. (2012). Modelling and control of photovoltaic panels utilising the incremental conductance method for maximum power point tracking. IET Renewable Power Generation, 6(4), 259-266.

[79] Roy, R. B., Basher, E., Yasmin, R., &Rokonuzzaman, M. (2014, December). Fuzzy logic based MPPT approach in a grid connected photovoltaic system. In The 8th International Conference on Software, Knowledge, Information Management and Applications (SKIMA 2014) (pp. 1-6). IEEE.

[80] Prasad, C. B., Sonam, S. K., Reddy, B. R. G., & Harika, P. (2017, June). A fuzzy logic based MPPT method for solar power generation. In 2017 International Conference on Intelligent Computing and Control Systems (ICICCS) (pp. 1182-1186). IEEE.

[81] Mohammadian, M. (2020). Modelling, control and prediction using hierarchical fuzzy logic systems: design and development. In Robotic Systems: Concepts, Methodologies, Tools, and Applications (pp. 187-207). IGI Global

[82] .Nannariello, J., & Fricke, F. R. (2001). Introduction to neural network analysis and its application to building services engineering. Building Services Engineering Research and Technology, 22(1), 58-68.

[83] Elgharbi, A., Mezghani, D., & Mami, A. (2012). A maximum power point tracking method based on artificial neural network for a pv system. International Journal of Advances in Engineering & Technology, 5(1), 130.

[84] Kalogirou, S. A. (2003). Artificial intelligence for the modeling and control of combustion processes: a review. Progress in energy and combustion science, 29(6), 515-566.

[85] Lin, W. M., Hong, C. M., & Chen, C. H. (2011). Neural-network-based MPPT control of a stand-alone hybrid power generation system. IEEE transactions on power electronics, 26(12), 3571-3581.

[86] Rizzo, S. A., &Scelba, G. (2015). ANN based MPPT method for rapidly variable shading conditions. Applied Energy, 145, 124-132.

[87] Paul, S. (2013). Comparison of MPPT using GA-Optimized ANN employing PI controller with GA-Optimized ANN employing fuzzy controller for PV system.

[88] Liu, Y. H., Liu, C. L., Huang, J. W., & Chen, J. H. (2013). Neural-network-based maximum power point tracking methods for photovoltaic systems operating under fast changing environments. Solar energy, 89, 42-53.

[89] Rumelhart, D. E., & Hinton, G. E. (1986). R. J. Williams, “Learning Internal Representations by Error Propagation,” in Parallel Distributed Processing, The MIT Press: Cambridge, Massachusetts.

[90] Badai, J., Bu, Q., & Zhang, L. (2020). Review of Artificial Intelligence Applications and Algorithms for Brain Organoid Research. Interdisciplinary Sciences: Computational Life Sciences, 1-12.

[91] Punitha, K., Devaraj, D., &Sakthivel, S. (2013). Artificial neural network based modified incremental conductance algorithm for maximum power point tracking in photovoltaic system under partial shading conditions. Energy, 62, 330-340.

[92] Jang, J. S. R., Sun, C. T., &Mizutani, E. (1997). Neuro-fuzzy and soft computing-a computational approach to learning and machine intelligence [Book Review]. IEEE Transactions on automatic control, 42(10), 1482-1484.

[93] Kazemi, K., Moradi, S., &Asoodeh, M. (2013). A neural network based model for prediction of saturation pressure from molecular components of crude oil. Energy sources, Part A: Recovery, utilization, and environmental effects, 35(11), 1039-1045.

[94] Sharma, K., & Kang, H. (2013). Backpropagaton in Hl7 in Medical Informatics to Analysis Speed of Sending Data. Global Journal of Computer Science and Technology.

[95] Ladst, F., &Garrosa, E. (2008). Prediction of Burnout. Diplomica Verlag.

[96] Bose, B. K. (2007). Neural network applications in power electronics and motor drives—An introduction and perspective. IEEE Transactions on Industrial Electronics, 54(1), 14-33.

[97] Veerachary, M., &Yadaiah, N. (2000). ANN based peak power tracking for PV supplied DC motors. Solar energy, 69(4), 343-350.

[98] Kalman, B. L., &Kwasny, S. C. (1992, June). Why tanh: choosing a sigmoidal function. In [Proceedings 1992] IJCNN International Joint Conference on Neural Networks (Vol. 4, pp. 578-581). IEEE.

[99] Manry, M. T., Chandrasekaran, H., Hsieh, C. H., Hu, Y. H., & Hwang, J. N. (2001). Signal processing applications of the multilayer perceptron. In Handbook on Neural Network Signal Processing. CRC Press.

[100] Mellit, A., &Kalogirou, S. A. (2008). Artificial intelligence techniques for photovoltaic applications: A review. Progress in energy and combustion science, 34(5), 574-632.

[101] Hornik, K., Stinchcombe, M., & White, H. (1989). Multilayer feedforward networks are universal approximators. Neural networks, 2(5), 359-366.

[102] Cybenko, G. (1989). Approximation by superpositions of a sigmoidal function. Mathematics of control, signals and systems, 2(4), 303-314.

[103] Hutchinson, A. (1994). Algorithmic learning. Oxford University Press, Inc.

[104] Scott, D. (2008). The discovery of new functional oxides using combinatorial techniques and advanced data mining algorithms (Doctoral dissertation, UCL (University College London)).

[105] Beale, M. H., Hagan, M. T., & Demuth, H. B. (1992). Neural network toolbox user's guide. The Mathworks Inc.

[106] Arif, A., Wang, Z., Wang, J., Mather, B., Bashualdo, H., & Zhao, D. (2017). Load modeling—A review. IEEE Transactions on Smart Grid, 9(6), 5986-5999.

[107] Haque, R. (2006). Transmission loss allocation using artificial neural networks (Doctoral dissertation).

[108] Jyothy, L. P., & Sindhu, M. R. (2018, February). An artificial neural network based MPPT algorithm for solar PV system. In 2018 4th International Conference on Electrical Energy Systems (ICEES) (pp. 375-380). IEEE.

[109] Mutwali, B. H. A., & El-Hawary, M. E. (2013, August). Oil barrel price forecasting: A case study of Saudi Arabia. In 2013 IEEE Electrical Power & Energy Conference (pp. 1-3). IEEE.

[110] Chaouachi, A., Kamel, R. M., &Nagasaka, K. (2010). A novel multi-model neuro-fuzzy-based MPPT for three-phase grid-connected photovoltaic system. Solar energy, 84(12), 2219-2229.

[111] Chikh, A., & Chandra, A. (2015). An optimal maximum power point tracking algorithm for PV systems with climatic parameters estimation. IEEE Transactions on Sustainable Energy, 6(2), 644-652.

[112] Yong, Z., Hong, L., Liqun, L., &XiaoFeng, G. (2012, August). The MPPT control method by using BP neural networks in PV generating system. In 2012 International Conference on Industrial Control and Electronics Engineering (pp. 1639-1642). IEEE.

[113] Chen, L., & Wang, X. (2019). Enhanced MPPT method based on ANN-assisted sequential Monte–Carlo and quickest change detection. IET Smart Grid, 2(4), 635-644.

[114] Rizzo, S. A., &Scelba, G. (2015). ANN based MPPT method for rapidly variable shading conditions. Applied Energy, 145, 124-132.

[115] Mellit, A., Kalogirou, S. A., Hontoria, L., &Shaari, S. (2009). Artificial intelligence techniques for sizing photovoltaic systems: A review. Renewable and Sustainable Energy Reviews, 13(2), 406-419.

[116] Wong, Y. J., Arumugasamy, S. K., Chung, C. H., Selvarajoo, A., & Sethu, V. (2020). Comparative study of artificial neural network (ANN), adaptive neuro-fuzzy inference system (ANFIS) and multiple linear regression (MLR) for modeling of Cu (II) adsorption from aqueous solution using biochar derived from rambutan (Nephelium lappaceum) peel. Environmental monitoring and assessment, 192(7), 1-20.

[117] Blange, R., Mahanta, C., &Gogoi, A. K. (2015, June). MPPT of solar photovoltaic cell using perturb & observe and fuzzy logic controller algorithm for buck-boost DC-DC converter. In 2015 International Conference on Energy, Power and Environment: Towards Sustainable Growth (ICEPE) (pp. 1-5). IEEE.

[118] Al-Majidi, S. D., Abbod, M. F., & Al-Raweshidy, H. S. (2018). A novel maximum power point tracking technique based on fuzzy logic for photovoltaic systems. International Journal of Hydrogen Energy, 43(31), 14158-14171.

[119] Zainuri, M. A. A. M., Radzi, M. A. M., Soh, A. C., &Abd Rahim, N. (2013). Development of adaptive perturb and observe-fuzzy control maximum power point tracking for photovoltaic boost dc–dc converter. IET Renewable Power Generation, 8(2), 183-194.

[120] Boukenoui, R., Bradai, R., Mellit, A., Ghanes, M., &Salhi, H. (2015, November). Comparative analysis of P&O, modified hill climbing-FLC, and adaptive P&O-FLC MPPTs for microgrid standalone PV system. In 2015 international conference on renewable energy research and applications (ICRERA) (pp. 1095-1099). IEEE.

[121] Abdelsalam, A. K., Massoud, A. M., Ahmed, S., &Enjeti, P. N. (2011). High-performance adaptive perturb and observe MPPT technique for photovoltaic-based microgrids. IEEE Transactions on power electronics, 26(4), 1010-1021.

[122] Saravanan, S., &Babu, N. R. (2016). Maximum power point tracking algorithms for photovoltaic system–A review. Renewable and Sustainable Energy Reviews, 57, 192-204.

[123] Zainuri, M. A. A. M., Radzi, M. A. M., & Rahman, N. F. A. (2019). Photovoltaic boost DC/DC converter for power led with adaptive P&O-fuzzy maximum power point tracking. In 10th international conference on robotics, vision, signal processing and power applications (pp. 245-251). Springer, Singapore.

[124] Triki, Y., Bechouche, A., Seddiki, H., & Abdeslam, D. O. (2020). Unity Efficiency and Zero-Oscillations Based MPPT for Photovoltaic Systems. Applied Solar Energy, 56(2), 75-84.

[125] El Khateb, A. H., Abd Rahim, N., & Selvaraj, J. (2013). Fuzzy logic control approach of a maximum power point employing SEPIC converter for standalone photovoltaic system. Procedia Environmental Sciences, 17, 529-536.

[126] Zainuri, M. M., Radzi, M. M., Soh, A. C., & Rahim, N. A. (2012, December). Adaptive P&O-fuzzy control MPPT for PV boost dc-dc converter. In 2012 IEEE International Conference on Power and Energy (PECon) (pp. 524-529). IEEE.

[127] Priya, T. H., &Parimi, A. M. (2016, November). Design of adaptive perturb and observe-fuzzy MPPT controller for high voltage gain multilevel boost converter. In 2016 IEEE 7th Power India International Conference (PIICON) (pp. 1-6). IEEE.

[128] Boukenoui, R., Bradai, R., Mellit, A., Ghanes, M., &Salhi, H. (2015, November). Comparative analysis of P&O, modified hill climbing-FLC, and adaptive P&O-FLC MPPTs for microgrid standalone PV system. In 2015 international conference on renewable energy research and applications (ICRERA) (pp. 1095-1099). IEEE.

[129] Priya, T. H., &Parimi, A. M. (2016, November). Design of adaptive perturb and observe-fuzzy MPPT controller for high voltage gain multilevel boost converter. In 2016 IEEE 7th Power India International Conference (PIICON) (pp. 1-6). IEEE.

[130] Aredes, M. A., França, B. W., &Aredes, M. (2014). Fuzzy adaptive P&O control for MPPT of a photovoltaic module. Journal of Power and Energy Engineering, 2(04), 120.

[131] Aldair, A. A., Obed, A. A., &Halihal, A. F. (2018). Design and implementation of ANFIS-reference model controller based MPPT using FPGA for photovoltaic system. Renewable and Sustainable Energy Reviews, 82, 2202-2217.

[132] Afghoul, H., &Krim, F. (2012, September). Intelligent energy management in a photovoltaic installation using neuro-fuzzy technique. In 2012 IEEE International Energy Conference and Exhibition (ENERGYCON) (pp. 20-25). IEEE.

[133] Naci, G. E. N. C., & Haji, D. (2020). Dynamic Behavior Analysis of ANFIS Based MPPT Controller for Standalone Photovoltaic Systems. International Journal of Renewable Energy Research (IJRER), 10(1), 101-108.

[134] Mlakić, D., &Nikolovski, S. (2016, May). ANFIS as a method for determinating MPPT in the photovoltaic system simulated in MATLAB/Simulink. In 2016 39th International Convention on Information and Communication Technology, Electronics and Microelectronics (MIPRO) (pp. 1082-1086). IEEE.

[135] Jang, J. S. (1993). ANFIS: adaptive-network-based fuzzy inference system. IEEE transactions on systems, man, and cybernetics, 23(3), 665-685.

[136] Khosrojerdi, F., Taheri, S., &Cretu, A. M. (2016, October). An adaptive neuro-fuzzy inference system-based MPPT controller for photovoltaic arrays. In 2016 IEEE Electrical Power and Energy Conference (EPEC) (pp. 1-6). IEEE.

[137] Abido, M. A., Khalid, M. S., &Worku, M. Y. (2015). An efficient ANFIS-based PI controller for maximum power point tracking of PV systems. Arabian Journal for Science and Engineering, 40(9), 2641-2651.

[138] Raj, A., &Lekhaj, P. (2018, May). An ANFIS Based MPPT Controller for Fuel Cell Powered Induction Motor Drive. In 2018 International Conference on Smart Grid and Clean Energy Technologies (ICSGCE) (pp. 201-205). IEEE.

[139] Al-Majidi, S. D., Abbod, M. F., & Al-Raweshidy, H. S. (2019). Design of an Efficient Maximum Power Point Tracker Based on ANFIS Using an Experimental Photovoltaic System Data. Electronics, 8(8), 858.

[140] Shabaan, S., El-Sebah, M. I. A., &Bekhit, P. (2018). Maximum power point tracking for photovoltaic solar pump based on ANFIS tuning system. Journal of Electrical Systems and Information Technology, 5(1), 11-22.

[141] Natarajan, U., Palani, S., &Anandampilai, B. (2012). Prediction of surface roughness in milling by machine vision using ANFIS. Computer-Aided Design and Applications, 9(3), 269-288.

[142] Reddy, K. J., & Sudhakar, N. (2019). ANFIS-MPPT control algorithm for a PEMFC system used in electric vehicle applications. International Journal of Hydrogen Energy, 44(29), 15355-15369.

[143] Chaouachi, A., Kamel, R. M., &Nagasaka, K. (2010). A novel multi-model neuro-fuzzy-based MPPT for three-phase grid-connected photovoltaic system. Solar energy, 84(12), 2219-2229.

[144] Loganathan, C., &Girija, K. V. (2014). Investigations on hybrid learning in ANFIS. Int. J. Eng. Res. Appl, 4(10), 31-37.

[145] Shoorehdeli, M. A., Teshnehlab, M., &Sedigh, A. K. (2009). Training ANFIS as an identifier with intelligent hybrid stable learning algorithm based on particle swarm optimization and extended Kalman filter. Fuzzy Sets and Systems, 160(7), 922-948.

[146] Teshnehlab, M., Shoorehdeli, M. A., &Sedigh, A. K. (2008, April). Novel hybrid learning algorithms for tuning ANFIS parameters as an identifier using fuzzy PSO. In 2008 IEEE International Conference on Networking, Sensing and Control (pp. 111-116). IEEE.

[147] Belhachat, F., &Larbes, C. (2017). Global maximum power point tracking based on ANFIS approach for PV array configurations under partial shading conditions. Renewable and Sustainable Energy Reviews, 77, 875-889.

[148] Mlakić, D., &Nikolovski, S. (2016, May). ANFIS as a method for determinating MPPT in the photovoltaic system simulated in MATLAB/Simulink. In 2016 39th International Convention on Information and Communication Technology, Electronics and Microelectronics (MIPRO) (pp. 1082-1086). IEEE.